Published for SISSA by Springer

Received: *March 7, 2024*
Revised: *July 15, 2024*
Accepted: *August 4, 2024*
Published: *August 28, 2024*

Differential cross-sections for events with missing transverse momentum and jets measured with the ATLAS detector in 13 TeV proton-proton collisions

The ATLAS collaboration

E-mail: atlas.publications@cern.ch

Abstract: Measurements of inclusive, differential cross-sections for the production of events with missing transverse momentum in association with jets in proton-proton collisions at $\sqrt{s} = 13\,\text{TeV}$ are presented. The measurements are made with the ATLAS detector using an integrated luminosity of $140\,\text{fb}^{-1}$ and include measurements of dijet distributions in a region in which vector-boson fusion processes are enhanced. They are unfolded to correct for detector resolution and efficiency within the fiducial acceptance, and are designed to allow robust comparisons with a wide range of theoretical predictions. A measurement of differential cross sections for the $Z \to \nu\nu$ process is made. The measurements are generally well-described by Standard Model predictions except for the dijet invariant mass distribution. Auxiliary measurements of the hadronic system recoiling against isolated leptons, and photons, are also made in the same phase space. Ratios between the measured distributions are then derived, to take advantage of cancellations in modelling effects and some of the major systematic uncertainties. These measurements are sensitive to new phenomena, and provide a mechanism to easily set constraints on phenomenological models. To illustrate the robustness of the approach, these ratios are compared with two common Dark Matter models, where the constraints derived from the measurement are comparable to those set by dedicated detector-level searches.

Keywords: Hadron-Hadron Scattering , Jets, Vector Boson Production

ArXiv ePrint: 2403.02793

https://doi.org/10.1007/JHEP08(2024)223

JHEP08(2024)223

Contents

1 Introduction

A high priority goal of experiments at the Large Hadron Collider (LHC) is to establish to what extent the Standard Model (SM) remains valid at the accessible energies above

JHEP08(2024)223

the electroweak symmetry-breaking scale. If the measured data agree with the SM, it is important to both quantify that agreement and to interpret it in terms of limits on physics beyond the SM (BSM). If the data are inconsistent with SM predictions, this could constitute evidence for BSM physics.

One key reason to suspect BSM physics exists is the astrophysical and cosmological evidence for the existence of Dark Matter (DM) [1–3]. Many BSM theories postulate a DM particle that may be produced at the LHC, giving rise to missing transverse momentum ($p_{\mathrm{T}}^{\mathrm{miss}}$) in proton-proton ($pp$) collision events, over and above that expected from SM processes producing neutrinos. Searches have exploited this signature to set limits on DM models [4, 5]. In addition, the cross-section for the principal SM process producing large $p_{\mathrm{T}}^{\mathrm{miss}}$, in which a Z boson decaying to neutrinos recoils against jets, has recently been measured by the CMS collaboration [6]. The ATLAS collaboration has also recently produced a measurement of the Z-boson invisible width which exploits this signature [7].

The main purpose of this analysis is to make precise, detector-corrected measurements of $p_{\mathrm{T}}^{\mathrm{miss}}$ produced in association with jets, inclusively and with as little model dependence as possible. This is the first such measurement made using the full $140\,\mathrm{fb}^{-1}$ of integrated luminosity collected by the ATLAS detector in Run 2 of the LHC. The results are presented alongside auxiliary measurements, made in the same phase space, of the transverse momentum of the hadronic system, $p_{\mathrm{T}}^{\mathrm{recoil}}$, recoiling against isolated leptons, and photons. This allows modelling effects and major uncertainties to cancel when a ratio of cross-sections is taken. This complements and extends the approach of taking ratios presented in a previous study [8]. The results are compared quantitatively to state-of-the-art SM predictions.

The measurements also serve another purpose. Contributions from DM production would typically *not* cancel out in the cross-section ratios, making them sensitive to DM and other BSM signatures. A secondary objective of the paper is therefore to demonstrate that the measurements can be used for searches and setting constraints, with only a minor penalty in sensitivity, and without the need to repeat complex and time-consuming detector simulation. This means they can be readily reinterpreted to gain information about models, and model parameter points, beyond those considered here.

Cross-sections differential in $p_{\mathrm{T}}^{\mathrm{miss}}$ and $p_{\mathrm{T}}^{\mathrm{recoil}}$, and in several jet observables, are defined in fiducial phase spaces designed to probe different aspects of the SM. The dominant SM contribution to the $p_{\mathrm{T}}^{\mathrm{miss}}$-plus-jets final state comes from Z bosons produced in association with jets and decaying into neutrinos, $Z(\to \nu\nu)$ + jets; other contributions come from leptonic W boson decays where the lepton does not enter the fiducial phase space. Diboson and triboson production can also provide small contributions. All relevant kinematic selections are included in the fiducial phase space definition, and detector effects, including instrumental sources of $p_{\mathrm{T}}^{\mathrm{miss}}$, are corrected for using an unfolding procedure. Motivated by ease of comparison to SM predictions, and to validate the consistency of the approach, a measurement of $Z \to \nu\nu$ production is also made, where the contributions from other SM processes are treated as backgrounds and subtracted before unfolding.

For the BSM interpretation, two example models are chosen to illustrate the constraints that can be extracted from the measurements. First, a common simplified DM model [9], which was searched for previously in this final state by ATLAS [4] using the same data sample as the current analysis, and by CMS [5]. Second, a more complicated model that introduces an additional Higgs doublet and a pseudoscalar that couples to DM [10, 11] and has also been searched for previously [12, 13] is considered.

The paper is structured as follows. After a brief description of the experimental apparatus in section 2, the cross-sections and observables to be measured are defined in section 3. The theoretical predictions, Monte Carlo event generation, and detector simulation are discussed in section 4. The details of the event selection and object reconstruction are given in section 5, and the treatment of backgrounds is described in section 6. The correction for detection effects, and the associated systematic uncertainties, are described in section 7. Results are reported in section 8, and interpreted in terms of SM and BSM calculations in section 9. Finally, the conclusions are summarised.

2 ATLAS detector

The ATLAS experiment [14] at the LHC is a multipurpose particle detector with a forward-backward symmetric cylindrical geometry and a near 4π coverage in solid angle.[1] It consists of an inner tracking detector surrounded by a thin superconducting solenoid providing a 2 T axial magnetic field, electromagnetic and hadronic calorimeters, and a muon spectrometer. The inner tracking detector covers the pseudorapidity range $|\eta| < 2.5$. It consists of silicon pixel, silicon microstrip, and transition radiation tracking detectors. Lead/liquid-argon (LAr) sampling calorimeters provide electromagnetic (EM) energy measurements with high granularity within the region $|\eta| < 3.2$. A steel/scintillator-tile hadronic calorimeter covers the central pseudorapidity range ($|\eta| < 1.7$). The endcap and forward regions are instrumented with LAr calorimeters for EM and hadronic energy measurements up to $|\eta| = 4.9$. The muon spectrometer surrounds the calorimeters and is based on three large superconducting air-core toroidal magnets with eight coils each. The field integral of the toroids ranges between 2.0 and 6.0 T m across most of the detector. The muon spectrometer includes a system of precision tracking chambers up to $|\eta| = 2.7$ and fast detectors for triggering up to $|\eta| = 2.4$. The luminosity is measured mainly by the LUCID-2 [15] detector, which is located close to the beampipe. A two-level trigger system is used to select events [16]. The first-level trigger is implemented in hardware and uses a subset of the detector information to accept events at a rate below 100 kHz. This is followed by a software-based trigger that reduces the accepted event rate to 1 kHz on average depending on the data-taking conditions. A software suite [17] is used in data simulation, in the reconstruction and analysis of real and simulated data, in detector operations, and in the trigger and data acquisition systems of the experiment.

3 Measured observables and fiducial phase spaces

The differential cross-sections to be measured are defined within a fiducial phase space, specified in terms of requirements applied to final state particles. These requirements are

[1] ATLAS uses a right-handed coordinate system with its origin at the nominal interaction point (IP) in the centre of the detector and the z-axis along the beam pipe. The x-axis points from the IP to the centre of the LHC ring, and the y-axis points upwards. Polar coordinates (r, ϕ) are used in the transverse plane, ϕ being the azimuthal angle around the z-axis. The pseudorapidity is defined in terms of the polar angle θ as $\eta = -\ln\tan(\theta/2)$. Angular distance is measured in units of $\Delta R \equiv \sqrt{(\Delta\eta)^2 + (\Delta\phi)^2}$.

JHEP08(2024)223

chosen to closely reflect the acceptance of the detector, thus reducing the need for theory-based extrapolations. For the dilepton regions, the leptons are required have the same flavour and opposite charge.

3.1 Particle-level objects

At particle-level, the following objects are defined. Charged leptons (electrons or muons) are required to be prompt, in that they do not originate from the decay of a hadron. Leptons from the decay of prompt τ-leptons are allowed. The four-momenta of prompt photons within a cone of $\Delta R = 0.1$ is added to the four-momentum of the lepton to produce a 'dressed' lepton.

Photons are required to be prompt and isolated. The photon isolation is chosen such that it mimics the isolation requirement at the detector level, requiring that the transverse energy in a cone of $\Delta R = 0.4$ around the photon be less than $(2.45\,\text{GeV} + 0.044 \times p_\text{T})$ where p_T is the transverse momentum of the photon in GeV.

For the inclusive p_T^miss measurement, the particle-level p_T^miss is defined as the magnitude of a vector, which is the negative two-momentum (x, y components) sum of all visible final-state particles with $|\eta| < 5$, excluding muons with $|\eta| > 2.5$ or $p_\text{T} < 7\,\text{GeV}$. The p_T^recoil observable is defined in a similar way, but the identified charged dressed leptons, and isolated photons, are excluded from the sum. Thus, for the inclusive p_T^miss measurements, $p_\text{T}^\text{recoil} \equiv p_\text{T}^\text{miss}$. For the measurement of $Z \to \nu\nu$, the particle-level p_T^miss is defined as the summed p_T of the neutrinos from the decayed boson.

Jets are defined using the anti-k_t jet algorithm [18, 19] with a radius parameter of 0.4. All stable final-state particles are used as input to the jet algorithm, except that for the inclusive p_T^miss measurement neutrinos and other invisible particles as well as muons are excluded, while for the $Z \to \nu\nu$ measurement invisible particles as well as the boson decay products are excluded. Any jets that contain a hadron coming from the decay of a prompt τ-lepton are classified as hadronically decaying τ-leptons.

Jets are removed if the jet momentum direction is closer than $\Delta R < 0.2$ to any lepton. Next, all leptons that are within $\Delta R = 0.4$ of a jet are discarded. If no leptons remain, jets are removed if the jet momentum direction is closer than $\Delta R < 0.2$ to any photon. These conditions mirror closely the overlap removal of reconstructed objects described in section 5.2.

3.2 Phase-space regions

Measurements are made in six regions defined in terms of the number and flavour of leptons or the presence of a photon: p_T^miss+jets, e+jets, $2e$+jets, μ+jets, 2μ+jets and γ+jets. The first of these is the primary measurement, while the others are auxiliary measurements with similar topologies to the primary, which constrain the uncertainties through correlations across the regions. The similarity in topologies is ensured by using the same event selection, and by the fact that in the main p_T^miss measurement region, $p_\text{T}^\text{recoil} \equiv p_\text{T}^\text{miss}$. Table 1 summarises the selections that define these regions. The differences between the pseudorapidity requirements between electrons and muons arise from their different experimental acceptance, and the desire to minimise extrapolation during the unfolding procedure.

For each of these regions, two sub-regions are defined by further selection on the jet content of the hadronic recoil system, the ≥ 1 jet and vector boson fusion (VBF) regions.

JHEP08(2024)223

Attribute	p_T^{miss}+jets	e+jets	$2e$+jets	μ+jets	2μ+jets	γ+jets
Lepton or photon rapidity	—	$\lvert y\rvert \leq 1.37$ or $1.52 \leq \lvert y\rvert \leq 2.47$		$\lvert y\rvert \leq 2.5$		$\lvert y\rvert \leq 1.37$ or $1.52 \leq \lvert y\rvert \leq 2.47$
Leading lepton or photon p_T [GeV]	—	> 30	> 80	> 7	> 80	> 160
Sub-leading lepton p_T [GeV]	—	—	> 7	—	> 7	—
Dilepton mass, $m_{\ell\ell}$ [GeV]	—	—	$m_{\ell\ell} \in (66, 116)$	—	$m_{\ell\ell} \in (66, 116)$	—
(Additional) muons	None with $p_T > 7\,\text{GeV}$, $\lvert\eta\rvert < 2.5$					
(Additional) electrons	None with $p_T > 7\,\text{GeV}$, $\lvert\eta\rvert < 1.37$ or $1.52 < \lvert\eta\rvert < 2.47$					
m_T [GeV]	—	$m_T \in (30, 100)$	—	—	—	—
p_T^{miss} [GeV]	> 200	> 60	—	—	—	—
p_T^{recoil} [GeV]	> 200	> 200	> 200	> 200	> 200	> 200

Table 1. Requirements defining the six principal phase-space regions of the measurement. For the inclusive p_T^{miss} measurement, $p_T^{miss} \equiv p_T^{recoil}$. In the $Z \to \nu\nu$ measurement, it corresponds to the p_T of the Z boson. Transverse mass, m_T, is defined as $\sqrt{2 p_T p_T^{recoil} (1 - \cos(\phi))}$ where p_T is the lepton transverse momentum and ϕ is the azimuthal angle between the lepton and p_T^{recoil}. For the dilepton regions, the leptons are required have the smae flavour and opposite charge.

These are designed to enhance the sensitivity to particular classes of BSM physics involving DM, such as those that are studied in section 9. Table 2 summarises the selections that define these sub-regions.

3.3 Measured observables

Differential cross-sections as a function of several observables are measured in the regions defined in section 3.2. The distribution of p_T^{recoil}, defined in section 3.1, is measured for all selections in all regions. It is sensitive both to the SM processes involving neutrinos (predominantly $Z \to \nu\nu$) and to potential contributions from BSM invisible particles. In addition, in the VBF phase-space region the m_{jj} and $\Delta\phi_{jj}$ distributions are also measured, where m_{jj} is the invariant mass of the two leading jets and $\Delta\phi_{jj} = \phi_1 - \phi_2$ is the signed difference in azimuthal angle between the jets ordered in their rapidities such that $y_1 > y_2$. This observable probes the CP structure of the VBF interaction [20]. The m_{jj} distribution is sensitive to the presence of potential new particles decaying into jets. All these distributions are available from HEPData [21] and implemented in Rivet [22].

4 Theoretical predictions and simulation

Monte Carlo (MC) event generators capable of simulating the complete final state of collision events are used as input to a detailed GEANT4 [23, 24] simulation of the ATLAS detector [25].

JHEP08(2024)223

Attribute	≥ 1 jet	VBF
$\Delta\phi\,(\text{jet}, p_{\text{T}}^{\text{miss}})$	> 0.4 for four leading p_{T} jets	
Hadronic τ-lepton	None with $p_{\text{T}} > 20\,\text{GeV}$, $\lvert\eta\rvert < 1.37$ or $1.52 < \lvert\eta\rvert < 2.47$	
Leading jet p_{T} [GeV]	> 120	> 80
Sub-leading jet p_{T} [GeV]	—	> 50
Leading jet $\lvert y\rvert$	< 2.4	< 4.4
Sub-leading jet $\lvert y\rvert$	—	< 4.4
Dijet invariant mass m_{jj} [GeV]	—	> 200
$\lvert\Delta y_{jj}\rvert$	—	> 1
In-gap jets	—	None with $p_{\text{T}} > 30\,\text{GeV}$

Table 2. A summary of the fiducial selections applied to the hadronic recoil system to define the subregions of the measurement. The veto on 'in-gap jets' is applied to jets with a rapidity lying between the rapidities of the leading and the sub-leading jets.

The output from this is passed through the same reconstruction and analysis chain as the data, to evaluate efficiencies and the migration matrix used to unfold for detector effects, and to make measurements at particle level. Given the inclusive nature of the measurement, several important processes contribute, requiring a wide range of sophisticated configurations for the event generators. The generated samples are also reweighted as appropriate to improve their modelling of the data (with a negligible effect on the unfolded results).

Event generator predictions are also used for comparison with the final particle-level results. Since the data are corrected for detector effects, new predictions can be used directly for the comparisons, without the full detector simulation. For this reason, the predictions used for the final comparison are in some cases improved versions that embody the most accurate and precise predictions available at the time of publication. The samples employed for each use case are described in turn below.

4.1 Fully simulated Standard Model samples

Events containing a single W or Z/γ^* boson in association with jets (V+jets), as well as prompt single-photon production, were simulated with the SHERPA 2.2.1 [26] event generator. In this set-up, the OPENLOOPS [27, 28] and COMIX [29] libraries provided matrix elements with next-to-leading-order (NLO) virtual quantum chromodynamics (QCD) corrections for up to two jets, and matrix elements accurate to leading-order (LO) for up to four jets. The default SHERPA parton shower [30] based on Catani-Seymour dipoles and the cluster hadronisation model [31] was used. This used the parameters developed by the SHERPA authors for this version based on the NNPDF3.0NNLO parton distribution function (PDF) set [32]. The NLO matrix elements of a given jet multiplicity were matched to the parton shower using a colour-exact variant of the MC@NLO algorithm [33]. Different jet multiplicities were then merged into an inclusive sample using an improved CKKW matching procedure [34, 35] that was extended to NLO accuracy using the MEPS@NLO prescription [33–36]. The merging scale was set to $Q_{\text{cut}} = 20\,\text{GeV}$. For single-photon production a dynamic merging scale [37] of 20 GeV was used, and photons were required to be isolated according to a smooth-cone isolation criterion [38]. In all cases, matrix elements were matched with the SHERPA parton shower [30] using the MEPS@NLO prescription.

Electroweak (EW) production of two forward jets in association with a W or Z/γ^* boson and up to one additional parton emission at LO accuracy was simulated using SHERPA 2.2.11 [39]. These predictions are labelled 'EWK' in the comparisons to data. The Catani-Seymour dipole-based parton shower was used, matched with the matrix element using the MEPS@LO prescription, and a cluster hadronisation model was employed. Diagrams arising from semileptonic diboson production, with one boson decaying hadronically, were removed in a gauge-invariant manner by requiring a colour-singlet exchange in the t-channel, also known as the 'VBF approximation'.

Samples of leptonically decaying dibosons were simulated with SHERPA 2.2.2 [26], with a similar set-up to the V+jets samples [40]. The QCD corrections to matrix elements at NLO accuracy were provided by the OPENLOOPS library [27, 28]. The parameters and PDFs were the same as for the V+jets samples. Triboson production was simulated with the same set-up as the fully leptonically decaying diboson samples. Semileptonically decaying diboson samples were simulated with almost the identical set-up to the fully leptonic ones, except that the SHERPA 2.2.1 [26] generator was used. These predictions together are labelled 'diboson' in the comparisons to data.

The production of on-shell $t\bar{t}$ events was modelled using the POWHEG BOX [41–44] v2 generator at NLO with the NNPDF3.0NLO [32] PDF set and the h_{damp} parameter[2] set to 1.5 m_t [45]. The events were interfaced to PYTHIA 8.230 [46] using the A14 set of tuned parameters (tune) [47] and the NNPDF2.3LO PDF set [48]. The NLO $t\bar{t}$ inclusive production cross-section was corrected to the theory prediction at next-to-next-to-leading order (NNLO) in QCD including the resummation of next-to-next-to-leading logarithmic (NNLL) soft-gluon terms calculated using TOP++2.0 [49–55].

Single-top tW associated production was modelled using the POWHEG BOX [42–44, 56] v2 generator at NLO in QCD in the five flavour scheme with the NNPDF3.0NLO [32] PDF set. The diagram removal scheme [57] was used to treat the overlap with top-quark pair production [45]. Single-top t-channel and s-channel production were modelled using the POWHEG BOX [42–44, 58, 59] v2 generator at NLO in QCD in the four- and five-flavour schemes with the corresponding NNPDF3.0NLO [32] PDF sets respectively. The matrix element generators were interfaced to PYTHIA 8.230 [46] using the A14 tune [47] and the NNPDF2.3LO PDF set. The inclusive cross-sections were corrected to the theory prediction calculated at NLO in QCD with HATHOR v2.1 [60, 61].

Additional pile-up collisions were overlaid, based on soft QCD processes simulated with PYTHIA 8.186 using the NNPDF2.3LO PDF set and the A3 tune [62] over the original hard-scattering events. Additional weighting factors are applied to the fully simulated samples

[2] The h_{damp} parameter controls the transverse momentum p_{T} of the first additional emission beyond the leading-order Feynman diagram in the parton shower and therefore regulates the high-p_{T} emission against which the $t\bar{t}$ system recoils.

to improve the modelling, including a factor to reproduce the distribution of the average number of interactions per bunch crossing observed in the data.

4.2 Standard Model predictions

For the particle-level predictions, no data-driven scale factors are applied, and pile-up events are not added. The settings described above are also valid for the SM predictions used for comparison with the final result, with the following exceptions.

A particle-level prediction for top-quark pair production was produced with SHERPA 2.2.11, using NLO-accurate matrix elements for up to one additional parton, and LO-accurate matrix elements for up to four additional partons calculated with the Comix [29] and OPENLOOPS 2 [27, 28, 63, 64] libraries. They were matched with the SHERPA parton shower [30] using the MEPS@NLO prescription [33–36].

The diboson and single EW boson MC samples were also replaced with calculations produced with SHERPA 2.2.11 and OPENLOOPS 2 [27, 28, 63, 64]. In the case of V+jets production, the matrix-element-level description of additional emissions was extended up to five jets at LO. The PDF4LHC PDF set [65] was used, supplemented with quantum electrodynamics (QED) effects from LUXQED [66]. To improve the description of W+jets and Z+jets processes, these MC predictions were then reweighted to account for higher-order EW corrections. The reweighting procedure was based on parton-level predictions for W/Z+jets production from ref. [67], and included NLO EW corrections [68–71] supplemented by Sudakov logarithms at two loops [72–75].

In the ≥ 1 jet region, an alternative prediction was obtained by extending the reweighting procedure to include NNLO QCD corrections [76–79] from ref. [67]. These corrections were provided separately for W+jets, $Z(\rightarrow \ell\ell)$ + jets (where $\ell = e$ or μ) and $Z(\rightarrow \nu\nu)$ + jets processes, as a function of the vector-boson p_{T}, to improve the description of the measured Z boson p_{T} distribution [80]. The reweighting procedure took into account the difference between the intrinsic perturbative accuracy of the generated MC samples and the provided parton-level calculations. In addition, the reweighting was extended in the VBF region to include NLO EW corrections [81] for Vjj production, which were provided separately for each decay channel as a function of dijet invariant mass and azimuthal difference between the tagging jets.

In the VBF region, an alternative prediction for V+jets was obtained using the high energy jets (HEJ) framework [82, 83]. HEJ calculates the tower of leading logarithmic QCD corrections in the ratio of the partonic centre-of-mass energy and transverse momentum squared, s/p_{T}^2, to all orders in the strong coupling α_{s}, for all relevant SM processes. These corrections are relevant in regions of phase space where jets span a large range of rapidity or where pairs of jets have a large invariant mass. The framework includes the matching of these corrections to both tree-level high-multiplicity matrix elements point-by-point in phase space, and to NLO corrections for distributions. The framework was implemented in a partonic event generator [84]. These predictions are only available for the leptonic measurements.

4.3 Standard Model theory uncertainties

The uncertainties in the SM predictions are estimated following the prescription developed in ref. [67]. Uncertainties on pure QCD higher-order corrections in the SM processes are

JHEP08(2024)223

estimated by varying the renormalisation and factorisation scales by factors of 0.5 and 2. The difference between the nominal prediction and the envelope of the seven possible versions (the cases where both the renormalisation and factorisation scales vary upwards or downward at the same time are excluded) is assigned as an uncertainty, denoted by $\delta^{(1)}K_{\rm (N)NLO}$. To account for possible differences in the shape of the $p_{\rm T}^V$ and m_{jj} spectra between low and high scales in the V+jets channels, additional uncertainties $\delta^{(2)}K_{\rm (N)NLO}$ and $\delta^{(4)}K_{\rm (N)NLO}$ are constructed from conservative shape distortions of the nominal scale-uncertainty band as a function of $p_{\rm T}^V$ and m_{jj}, respectively. The distortion is given by $(x^2 - x_0^2)/(x^2 + x_0^2)$ where x_0 is the midpoint of the observable of interest in logarithmic space, namely 650 GeV and 1300 GeV for $p_{\rm T}^V$ and m_{jj}, respectively. As discussed in ref. [67], this shape uncertainty increases the scale uncertainties by a factor of up to $\sqrt{2}$.

All pure-QCD systematic uncertainties are taken as correlated between observable bins as well as weak bosons and their decay channels, but uncorrelated between different processes, including EW V+jets production. Following the approach in [67], the residual level of decorrelation between the decay modes is estimated from the difference between the differential higher-order K-factors for W+jets production and $Z(\to \ell\ell)$ + jets and $Z(\to \nu\nu)$ + jets production relative to their average and assigned as an additional uncertainty, denoted by $\delta^{(3)}K_{\rm (N)NLO}$. A similar uncertainty is estimated for EW Vjj production using the higher-order K-factors calculated in ref. [81]. The uncertainty band for the HEJ predictions in the VBF region is estimated from the envelope of the seven variations of the renormalisation and factorisation scales by factors of 0.5 and 2.

Pure EW uncertainties in V+jets and Vjj production arise predominantly from unknown high-$p_{\rm T}$ EW effects due to truncation of the perturbative series. This uncertainty is estimated through naive Sudakov exponentiation, denoted $\delta^{(1)}\kappa_{\rm nNLO\,EW}$, which is taken to be correlated between the weak boson decay channels. In the case of V+jets production, an additional conservative uncertainty $\delta^{(2)}\kappa_{\rm nNLO\,EW}$ is assigned, given by 5% of the absolute full NLO EW correction, which is taken to be uncorrelated between the weak boson decay channels. Moreover, an uncertainty in the Sudakov approximation at two-loop level in V+jets production is estimated by assigning an additional uncertainty $\delta^{(3)}\kappa_{\rm nNLO\,EW}$, given by the difference between the next-to-leading logarithmic Sudakov approximation and the naive exponentiation of the full NLO EW correction, which is also taken to be uncorrelated between the weak boson decay channels. All pure EW systematic uncertainties are taken to be correlated across bins in a given observable.

An uncertainty in unknown non-factorising mixed QCD and EW effects is estimated from the difference between the additive and multiplicative combination of QCD and EW higher-order corrections, denoted $\delta K_{\rm mix}$. This systematic uncertainty is taken to be correlated between bins in a given observable and between weak boson decay channels.

PDF uncertainties are estimated by using the sum in quadrature of the set of independent PDF4LHC +LUXqed Hessian eigenvectors. The $\alpha_{\rm s}$ uncertainty is estimated from ± 0.001 shifts around the nominal value of 0.118 in the PDF sets.

To evaluate systematic uncertainties, prompt single-photon production was also simulated using the Pythia 8.186 [85] generator. Events were simulated using tree-level matrix elements for γ+jet final states and LO QCD dijet events, with the inclusion of initial- and final-state parton showers.

JHEP08(2024)223

The PYTHIA simulation includes LO γ+jet events from both the direct processes (the 'hard' $qg \to q\gamma$ and $q\bar{q} \to g\gamma$ component) and the photon bremsstrahlung in LO QCD dijet events. The bremsstrahlung component was modelled by final-state QED radiation arising from calculations of all $2 \to 2$ QCD processes. The NNPDF2.3LO PDF set was used in the matrix element calculation, the parton shower, and the simulation of the multi-parton interactions. The samples include a simulation of the underlying event with parameters set according to the A14 tune [47]. The Lund string model [86, 87] was used for the description of the fragmentation into hadrons.

Finally, the uncertainty in the interference between top-quark pair production and tW production is estimated by taking the difference relative to the prediction where the nominal tW sample is replaced with a version employing an alternative diagram subtraction scheme [57].

5 Event selection and reconstruction

The data used in this analysis were collected with the ATLAS detector in pp collisions at $\sqrt{s} = 13$ TeV during the Run 2 data-taking from 2015 to 2018. After applying necessary selections to ensure good detector operation conditions, a total integrated luminosity of 140 fb^{-1} is available. The uncertainty in the combined Run 2 integrated luminosity is 0.83% [88], obtained using the LUCID-2 detector [15] for the primary luminosity measurements. The average number of inelastic pp collisions per bunch crossing is 33.7 in the data sample considered. Most of these pp collisions have an interaction vertex that is consistent with the beam-spot envelope.

5.1 Trigger selection

Events for the primary $p_{\mathrm{T}}^{\mathrm{miss}}$ measurement were selected by the two-stage trigger system [16] using the transverse momentum imbalance within the calorimeter system [89] and requiring hadronic jets in the final state. Due to increasing number of simultaneous pp interactions in different years of the Run 2 data-taking the minimum $p_{\mathrm{T}}^{\mathrm{miss}}$ threshold of the triggers used increased from 70 GeV to 120 GeV over the data-taking period to suppress the impact of the energy contributed by pile-up collisions on the rate of accepted events. The algorithm used to calculate this $p_{\mathrm{T}}^{\mathrm{miss}}$ also varied for the same reason. All $p_{\mathrm{T}}^{\mathrm{miss}}$ triggers used in the analysis were fully efficient in events for which the offline $p_{\mathrm{T}}^{\mathrm{miss}} > 200$ GeV.

Since muons deposit very little energy in the calorimeters, the calorimeter-based $p_{\mathrm{T}}^{\mathrm{miss}}$ triggers also selected events with high-p_{T} muons in the final-state. These events are used for the single-muon and double-muon auxiliary measurements. For events with $p_{\mathrm{T}}^{\mathrm{recoil}} > 200$ GeV, this trigger selection was 100% efficient for the subset of those events with a muon with $p_{\mathrm{T}} \geq 30$ GeV.

A combination of low- and high-p_{T} single-electron triggers was used to select events for the single-electron and double-electron auxiliary measurements. Two single-electron triggers, with a minimum p_{T} threshold of 24 (26) GeV in 2015–2016 (2017–2018) and `Tight` electron identification criteria [90], selected events in the low-p_{T} region. In the high-p_{T} region, where the rate of single electron triggers is low compared to that which can be accommodated by the trigger system bandwidth, several triggers with less restrictive electron identification were employed to increase the trigger efficiency. Events satisfying the low- or high-p_{T} threshold trigger were retained, with an efficiency of around 97% for electrons with $p_{\mathrm{T}} \geq 80\,\mathrm{GeV}$. The details of the electron trigger combination procedure are summarised in ref. [90]. The simulation reproduces the single-electron trigger efficiency measured in data to within 5% for electrons with $p_{\mathrm{T}} < 60\,\mathrm{GeV}$, and to better than 1% in the high-p_{T} region. The residual mismodelling is corrected for by reweighting simulated events using data-driven scale factors. Both statistical and systematic uncertainties in the derived trigger scale factors are propagated to the measured observables.

Events selected for the single photon auxiliary measurement are required to have a photon candidate with a minimum p_{T} of 120 (140) GeV at the trigger-level satisfying the `Loose` photon identification criteria [90] in 2015 (2016–2018). In the p_{T} range above 200 (300) GeV a trigger with only a p_{T} selection was used in addition (logical 'OR') to improve the efficiency of the trigger selection during 2015 (2016–2018) data-taking. The photon triggers were fully efficient in the single photon auxiliary measurement region phase space.

5.2 Reconstruction and offline selection

Events selected by the trigger system undergo a number of offline reconstruction and calibration steps before they can be used for the analysis.

Candidate interaction vertices are reconstructed by associating at least two reconstructed tracks with $p_{\mathrm{T}} > 500\,\mathrm{MeV}$ to a common origin along the pp collision axis [91]. Events with at least one such vertex are selected. In the case of multiple candidate vertices in an event, the primary vertex is defined to be one with the highest sum of squared transverse momenta of associated tracks.

Reconstructed tracks in the inner detector (ID) and clusters of energy deposits in the EM calorimeter are used as inputs to the reconstruction of electrons and photons. The electron and photon reconstruction [92] uses three-dimensional clusters of energy depositions (topo-clusters) built from topologically connected EM and hadronic calorimeter cells [93] to restore energy from bremsstrahlung photons or from electrons from photon conversions. The transition region between the barrel and endcaps of the EM calorimeter, $1.37 < |\eta| < 1.52$, is excluded. The electron candidates are reconstructed from topo-clusters matched to ID tracks. These tracks are refitted to account for energy losses due to bremsstrahlung. Topo-clusters not matched to any track or matched to conversion vertices are reconstructed as unconverted or converted photon candidates, respectively. The conversion vertices are formed from one or two tracks that are consistent with a massless particle decaying within the ID volume. Electron candidates in the e+jets (2e+jets) region are required to satisfy the `Tight` (`Medium`) identification working point (WP) [94]. The efficiency to select `Tight` (`Medium`) electron candidates reaches a plateau of 88% (93%) for $p_{\mathrm{T}} > 80\,\mathrm{GeV}$ electrons. To reject electrons from heavy-flavour decays the `HighPtCaloOnly` isolation selection [92], with 92%–98% efficiency depending on the electron p_{T}, is applied.

Photon candidates with shower shape variables corresponding to the `Tight` identification working point and satisfying `Tight` isolation criteria are accepted for the single-photon auxiliary measurement [92]. This combination of identification and isolation requirements provides a good rejection of photons from non-prompt backgrounds while maintaining high efficiency for prompt photon selection. The electron or photon candidate energy is calibrated using energy depositions in the calorimeters and track measurements in the ID [92]. The precision of the energy calibration of electrons (photons) is better than 0.2% (0.5%), verified in situ using $Z \to \ell\ell$ and $Z \to \ell\ell\gamma$ events.

The muon reconstruction uses track segments in the ID and muon spectrometer (MS), as well as calorimeter information. Muon candidates are formed by matching the MS and ID tracks and performing a combined fit that makes use of corresponding MS and ID hits, and accounts for the energy depositions in the calorimeter cells along the muon candidate trajectory. Identification requirements for muons are formed using selections on track quality and the compatibility between the ID and MS tracks. Muon candidates in single-muon and two-muon auxiliary measurements are required to satisfy the `Medium` [95] identification WP. The efficiency for identifying `Medium` muons exceeds 98% for the selection criteria applied in this analysis. To reject muons produced in semileptonic decays of hadrons, the `FixedCutLoose` [96] requirement is imposed on the activity around muon candidates in the muon auxiliary measurement. The `FixedCutLoose` efficiency for selecting a prompt muon ranges from 93% in the low-p_{T} region to 100% for muons with $p_{\mathrm{T}} > 50\,\mathrm{GeV}$. The muon momentum scale is calibrated using $J/\psi \to \mu\mu$ and $Z \to \mu\mu$ events. The precision of the muon momentum measurements changes from 0.05% for muons within $|\eta| = 1$ to 0.15% for muons in the $|\eta| \sim 2.5$ forward region.

Events with no `Loose` electrons or muons [92, 95] (regardless of their isolation conditions) are selected for the primary $p_{\mathrm{T}}^{\mathrm{miss}}$ measurement. These criteria ensure a very high purity of the signal event sample, since the `Loose` identification WPs select at least 92% of prompt fiducial electrons or photons and more than 99% of prompt fiducial muons. These requirements also reject events with electrons or muons coming from τ-lepton decays. Hadronically decaying τ-leptons are reconstructed using jets identified by the anti-k_t jet algorithm, with the radius parameter $R = 0.4$, as a seed, which is then associated to tracks consistent with τ-lepton production at the interaction vertex [97]. They are then identified as τ-leptons by a recurrent neural network (RNN) algorithm [98]. The `Loose` identification WP provides between 87% and 79% identification efficiency for τ-leptons while providing a multijet background rejection factor of 21 to 90 respectively depending on the number of associated tracks. Events with at least one hadronically decaying τ-lepton satisfying the `Loose` selection are removed.

Jets are reconstructed using the anti-k_t jet algorithm with the radius parameter $R = 0.4$ using an algorithmic combination of the calorimeter energy depositions and the charged-particle tracks. First, calorimeter cells are grouped into topo-clusters using a nearest-neighbour algorithm [93] that exploits the significance of the cell energy compared to the noise expected in the pile-up environment for each year of running. The direction of each topo-cluster receives an origin correction to account for the primary vertex position that is different in every event. The jet measurements are further improved using the particle flow (`PFlow`) algorithm [99], which replaces the charged particle calorimeter energy deposits by the momenta of the tracks measured in the ID that are associated with the topo-clusters. The `PFlow` jets have better energy and angular resolution, as well as reduced sensitivity to pile-up, compared to jets reconstructed from calorimeter information only. To suppress signals arising from calorimeter noise and other non-collision backgrounds, reconstructed jets are required to satisfy a `Loose` identification selection [100]. This selection has a better than 99.5% efficiency for keeping

JHEP08(2024)223

jets from pp collisions. Due to the large instantaneous luminosity, the jets reconstructed in one bunch crossing could originate from different pp collisions. To suppress jets arising from vertices other than the primary collision vertex a jet-vertex tagging algorithm (JVT) [101, 102], based on a combination of track-based variables, is used. Jets with $p_T < 60$ GeV in the central $|\eta| < 2.5$ region are accepted only if the `Tight` JVT selection is satisfied. In addition, a `Tight` requirement from the forward jet vertex-tagging algorithm (fJVT) is used to reject pile-up jets in the forward region $|\eta| \geq 2.5$.

The jet four-momentum measurement is calibrated using information from both simulation and data [103]. First, the jet energy is corrected for pile-up contamination. An MC-based absolute jet energy correction is used to restore the energy and direction of the jet to that at the particle-level. Next, the global sequential calibration is employed to remove the dependence of the jet response on the energy distribution inside the jet, and the fluctuations of the shower development in the calorimeter. Finally a residual in situ correction, determined from Z+jets, γ+jet and multijet events, is applied to recover the remaining differences between data and simulation. Over the rapidity range considered, the jet energy is measured with 1%–3.5% accuracy depending on transverse momentum.

The missing transverse momentum vector p_T^{miss} (p_T^{recoil} in the events with prompt leptons or photons) is calculated as the magnitude of the vector sum of the transverse momenta of all particles produced in the event [104]. Detector signals associated with identified physics objects constitute a hard term, while the signals that are not part of these objects form a soft term. The p_T^{miss} reconstruction uses energy deposits from the calorimeter, muons reconstructed in the MS, and tracks from the ID.

The p_T^{miss} is then given by $p_T^{\text{miss}} = \sqrt{(p_x^{\text{miss}})^2 + (p_y^{\text{miss}})^2}$, where $p_{x(y)}^{\text{miss}}$ are calculated as follows:

$$p_{x(y)}^{\text{miss}} = p_{x(y)}^{\text{miss},e} + p_{x(y)}^{\text{miss},\gamma} + p_{x(y)}^{\text{miss},\tau} + p_{x(y)}^{\text{miss},\mu} + p_{x(y)}^{\text{miss,jets}} + p_{x(y)}^{\text{miss,soft}} \tag{5.1}$$

where each term is calculated as the negative sum of the calibrated reconstructed objects, projected onto the x and y directions. The soft term, $p_{x(y)}^{\text{miss,soft}}$, is calculated from tracks associated with the primary vertex but not to any of the high-p_T objects.

For the calculation of p_T^{recoil} in the auxiliary measurements, the same expression is used, but the identified prompt leptons or photons are excluded.

Events involving τ-leptons can enter the signal region if the τ-lepton is not reconstructed. Conversely, in the auxiliary measurement regions, it is possible for events where a jet is misreconstructed as a τ-lepton to affect the $p_{x(y)}^{\text{miss}}$ calculation. In principle, if this effect is not accounted for it could lead to biases when correlating the regions. However, τ-lepton reconstruction is found to be well modelled across all the measured regions.

Since physics objects are reconstructed independently of each other, there is a possibility that the same detector signals are used to build multiple jets, photons or leptons. To avoid double-counting of particle level physics objects, the following procedure is employed. First, leptonically decaying τ-leptons closer than $\Delta R = 0.2$ to an electron or muon are discarded. Second, electrons that share the same ID track with a muon are rejected. Third, jets are removed if the jet momentum direction is closer than $\Delta R < 0.2$ to any electron candidate. In turn, all electrons that are within $\Delta R = 0.4$ of a jet are discarded. Similarly, jets are discarded if they are within $\Delta R = 0.2$ of a muon and have less than three associated tracks, while muons within $\Delta R = 0.4$ of a jet are rejected. Finally, jets that are within $\Delta R = 0.2$ of a hadronically decaying τ-lepton are removed. If a lepton is removed by this procedure, the event is still considered for other measurement regions with fewer or no leptons.

6 Background estimation

Two categories of background contribute to all the measurements made: non-collision backgrounds, produced by beam-gas or cosmic rays events or calorimeter noise, and reducible backgrounds, which arise when a miscalibration or a misidentification of physics objects leads to an artificially large missing transverse momentum or a spurious particle candidate. In addition, in the $Z \to \nu\nu$ measurement, contributions from other SM processes that satisfy the true event selection and therefore cannot be distinguished from $Z \to \nu\nu$ events within the fiducial region are treated as an irreducible background. In this section the background estimation methods are briefly described.

6.1 Non-collision background

Muons produced away from the proton-proton collision but in-time with it can create significant energy depositions in the calorimeter that can be reconstructed as hadronic jets, and thus lead to events with a single jet and a large $p_{\mathrm{T}}^{\mathrm{miss}}$ signature. Such muons can be created by the cosmic-ray showers, or by interactions upstream of the ATLAS detector between the beam and the LHC collimators, or residual gas in the beam pipe. The azimuthal angle distribution of the fake jets they produce has a characteristic shape, with pronounced peaks at $\phi = 0$ and $\phi = \pi$. Moreover, these muons enter the calorimeter earlier than jets from the interaction point, and so have very different timing properties. The non-collision background contribution is strongly reduced by the identification requirements applied to the leading jet in event. The residual contribution from this background source is evaluated using a data-driven approach that exploits the differences in time between the signal jets produced in the collision vertex and the non-collision background jets, and is subtracted. This amounts to a few thousand events over the course of the data-taking period. The difference between the subtracted and non-subtracted sample is taken as the uncertainty and propagated through to the final results.

6.2 Multijet background in the $p_{\mathrm{T}}^{\mathrm{miss}}$+jets selection

Jet production processes containing no prompt $p_{\mathrm{T}}^{\mathrm{miss}}$ can contribute to the event yield in the primary measurements when jets are mis-reconstructed or mis-calibrated, giving rise to fake $p_{\mathrm{T}}^{\mathrm{miss}}$. In addition, decays of heavy flavour hadrons among the jet constituents may produce neutrinos that can generate the $p_{\mathrm{T}}^{\mathrm{miss}}$. In such cases the $p_{\mathrm{T}}^{\mathrm{miss}}$ vector will typically be aligned with the direction of the jet, and the $\Delta\phi\left(\text{jet}, p_{\mathrm{T}}^{\mathrm{miss}}\right) > 0.4$ requirement removes most of this type of background. However, the $p_{\mathrm{T}}^{\mathrm{miss}}$+jets selection will contain a residual multijet background, since in such cases the $p_{\mathrm{T}}^{\mathrm{miss}}$ can receive contributions from several jets and the resulting $p_{\mathrm{T}}^{\mathrm{miss}}$ direction may not align with any one of them. The probability to reconstruct a large $p_{\mathrm{T}}^{\mathrm{miss}}$ in any given multijet event is rather low, but the jet production cross-section is large. This implies that a simulation-based approach would require a very large simulated event sample, with an extremely accurate modelling of hadron production and calorimeter performance, especially in the tails of the distributions. These considerations mandate a data-driven method.

Reference [105] contains a detailed description of the jet smearing method used to estimate the multijet background contribution in the primary measurements. A high-statistics sample of low-$p_{\mathrm{T}}^{\mathrm{miss}}$ events with well-measured hadron jets is collected using a set of inclusive jet triggers with different $p_{\mathrm{T}}^{\mathrm{jet}}$ thresholds. A set of 'pseudodata' events is created by fluctuating the jet energies in these events using a function, constrained using data, that models the detector response to jets. Each fluctuation is considered as a separate event; the altered four-momenta of the jets are stored and the $p_{\mathrm{T}}^{\mathrm{miss}}$ vector is recalculated. This approach produces pseudodata events with fake $p_{\mathrm{T}}^{\mathrm{miss}}$ populating a range up to about 2 TeV.

The distribution of the multijet background in each differential cross-section measured is taken from the pseudodata distributions after applying the ≥ 1 jet or VBF event selection as appropriate, while the normalisations are obtained from the fit to data in a dedicated multijet background-enriched control region, defined using the $p_{\mathrm{T}}^{\mathrm{miss}}$+jets event selection as given in table 2, but with the requirement on the azimuthal angle between the jet direction and $p_{\mathrm{T}}^{\mathrm{miss}}$ vectors inverted i.e., $\Delta\phi\left(\mathrm{jet}, p_{\mathrm{T}}^{\mathrm{miss}}\right) \leq 0.3$.

Events with $0.3 < \Delta\phi\left(\mathrm{jet}, p_{\mathrm{T}}^{\mathrm{miss}}\right) < 0.4$ satisfying the $p_{\mathrm{T}}^{\mathrm{miss}}$+jets requirements but with the $p_{\mathrm{T}}^{\mathrm{miss}}$ selection relaxed to 130 GeV (as low as possible considering trigger thresholds) are used to verify the multijet background estimation procedure. In this region, where the multijet background contributes approximately four times more events than the other SM processes, very good agreement is observed between the data and predictions. A similar region without the relaxed $p_{\mathrm{T}}^{\mathrm{miss}}$ requirement, which is closer to the kinematic regime probed by this analysis, is also tested. Figure 1 shows the distribution of events in this validation region as a function of $p_{\mathrm{T}}^{\mathrm{miss}}$. Although the multijet background is not the dominant contributor to the yield in this validation region, it represents a significant fraction of the first few bins, where its inclusion leads to a good agreement between prediction and data. The multijet component in these validation regions is approximately an order of magnitude more important than in the signal region. There is a very good agreement between the prediction and data.

The multijet background contribution in the $p_{\mathrm{T}}^{\mathrm{miss}}$+jets event selection in the ≥ 1 jet region is smaller than 1% for $p_{\mathrm{T}}^{\mathrm{recoil}} \leq 300$ GeV and falls steeply as $p_{\mathrm{T}}^{\mathrm{miss}}$ increases. In the VBF region the multijet background contribution is around 1%–2% in the $m_{jj} < 2$ TeV region, and is negligible in the high-m_{jj} range.

6.3 Background from misidentified photons and leptons in the auxiliary measurements

The main source of background in the electron and photon auxiliary measurements comes from jets that are misidentified as leptons or photons. This can occur due to fluctuations in jet formation, or in the development of hadronic showers in the calorimeter, leading to an apparently large amount of EM energy. In conjunction with inefficiencies in the inner tracker, this can lead to energy depositions that are reconstructed as a photon or an electron. Jets containing heavy flavour hadrons that decay into final states including a muon are the main source of the non-prompt muon background. The yields of such 'fake' photons and leptons

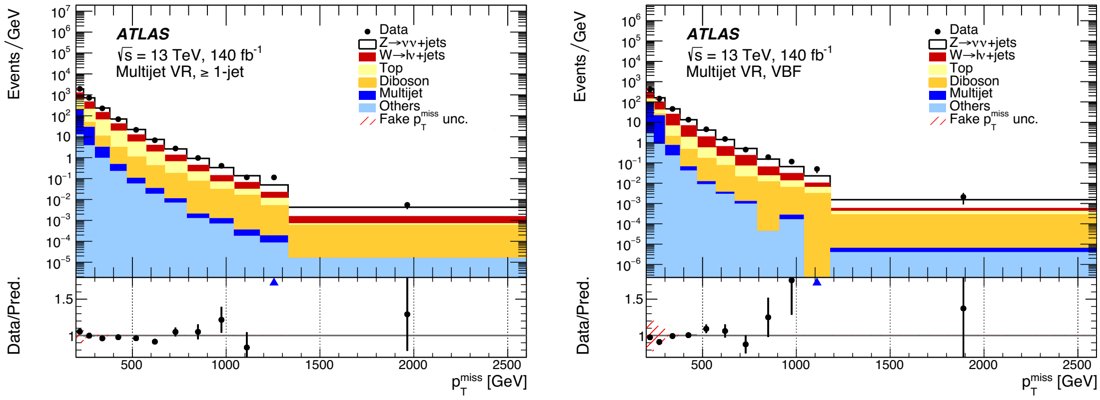

(a) (b)

Figure 1. The event yield in the multijet background validation region as a function of $p_{\mathrm{T}}^{\mathrm{miss}}$ for the (a) ≥ 1 jet selection and (b) VBF selection. Points denote the data, and different SM backgrounds are shown as histograms. The hatched band shows the full uncertainty assigned to the estimate of the fake $p_{\mathrm{T}}^{\mathrm{miss}}$ contribution from multijet events, which, since it represents a very small contribution to the final event sample and is subject to statistical variations due to the nature of the evaluation, is conservatively taken to be 100% of the estimated yield. The vertical lines represent the statistical uncertainty. The bottom panels show the ratios of the data to the predictions; the blue triangle indicate values which are out of the display range.

are heavily suppressed by the reconstruction algorithms, while the remaining contributions are removed using a set of data-driven techniques described below.

6.3.1 Jet-photon misidentification contribution to the γ+jets selection

Multijet production is the dominant source of background in the γ+jets auxiliary measurement. The `Tight` photon identification WP [92] together with the `Tight` requirement on the photon isolation energy strongly suppress the jet-photon misidentification. A data-driven two-dimensional side-band method [106, 107] is used to determine the shape and the normalisation of the residual photon misidentification background.

For this, four samples (A, B, C and D) are selected by splitting the `Tight` (A, B) and non-`Tight` (C, D) photon samples into `isolated` (A, C) and non-`isolated` (B, D) samples. Background-enriched samples of non-`Tight` photons are collected by requiring the photon to satisfy the `LoosePrime4` and to simultaneously fail to satisfy the `Tight` identification criteria. The `LoosePrime4` WP has a relaxed selection on the photon shower-shape properties that is not correlated with the photon isolation conditions, meaning the background in the four sub-regions can be treated as being uncorrelated. The yield N_{A} of background events in the γ+jets region is determined by interpolating the measured event yields in the other three control regions, $N_{\mathrm{A}} = N_{\mathrm{B}} \times \frac{N_{\mathrm{C}}}{N_{\mathrm{D}}}$. The effect of leakage of signal photons into the control regions is in the range from 1–8% for the C and D regions and from 12–20% for the B region; the contribution from other processes is negligible. These contributions are evaluated from the simulation and accounted for in the systematic uncertainties.

In most parts of the phase space the contribution of the jet-photon background is around 2%–3%. It increases to 4% in the $p_{\mathrm{T}}^{\mathrm{miss}} \leq 300\,\mathrm{GeV}$ region, while in the $m_{jj} \leq 400\,\mathrm{GeV}$ range up to 5% of events are from the photon misidentification.

JHEP08(2024)223

6.3.2 Misidentified electrons in the e+jets selection

Multijet events may satisfy the electron identification and isolation requirements because of the presence of semileptonic heavy-flavour decays, photon conversions, or hadrons inside jets being misidentified as electrons. This background is evaluated using a data-driven matrix method [108] that exploits the fact that prompt electrons (P) are better isolated in comparison to background electrons (B).

The number of electrons that satisfy the `Tight` selection, N_{T}, and which satisfy the `Loose` but fail to satisfy the `Tight` selection, $N_{!\mathrm{T}}$, can be expressed in terms of the efficiency ϵ_{P} (ϵ_{B}) with which prompt (background) electrons that satisfy the `Loose` selection also satisfy the `Tight` selection as:

$$\begin{pmatrix} N_{\mathrm{T}} \\ N_{!\mathrm{T}} \end{pmatrix} = \begin{pmatrix} \epsilon_{\mathrm{P}} & \epsilon_{\mathrm{B}} \\ 1-\epsilon_{\mathrm{P}} & 1-\epsilon_{\mathrm{B}} \end{pmatrix} \begin{pmatrix} N_{\mathrm{P}} \\ N_{\mathrm{B}} \end{pmatrix}, \tag{6.1}$$

where N_{P} (N_{B}) is the number of prompt (background) electrons. Solving this matrix equation, the number of background electrons in data that satisfy the `Tight` requirements can be obtained using event yields measured in data as:

$$\epsilon_{\mathrm{B}} N_{\mathrm{B}} = N_{\mathrm{T}}^{\mathrm{Bkg}} = \frac{\epsilon_{\mathrm{B}}}{\epsilon_{\mathrm{P}} - \epsilon_{\mathrm{B}}} \left(\left(\epsilon_{\mathrm{P}} - 1 \right) N_{\mathrm{T}} + \epsilon_{\mathrm{P}} N_{!\mathrm{T}} \right). \tag{6.2}$$

The ϵ_{P} efficiency is estimated from simulation binned in electron p_{T} and η. It changes from 85% to 95% as the electron p_{T} increases from 100 GeV to 600 GeV, where it reaches a plateau.

The ϵ_{B} efficiency is determined from data in a dedicated control region with the nominal e+jets requirements on the m_{T} and $p_{\mathrm{T}}^{\mathrm{miss}}$ inverted to enhance the background electron contribution, and the $p_{\mathrm{T}}^{\mathrm{recoil}}$ requirement removed. The events with genuine prompt electrons in this region are subtracted by using the simulation. The resulting ϵ_{B} efficiency is measured in bins of electron p_{T} and η. It decreases rapidly from 15% for electrons with p_{T} around 50 GeV to about 1% in the $p_{\mathrm{T}} \geq 500$ GeV region. Combining the measured ϵ_{P} and ϵ_{B} efficiencies, the multijet background in the e+jets auxiliary measurement is found to be less than 5% in the $p_{\mathrm{T}}^{\mathrm{recoil}} < 500$ GeV region, while it increases up to almost 20% in the $p_{\mathrm{T}}^{\mathrm{recoil}} > 1500$ GeV range.

This estimate of the background contribution from misidentified electrons is validated using the e+jets event selection but without the requirement on m_{T} or $p_{\mathrm{T}}^{\mathrm{miss}}$. Figure 2 shows the distributions of events passing this modified selection as a function of $p_{\mathrm{T}}^{\mathrm{miss}}$. The misidentified electron background contributes a significantly larger proportion of the total yield in these validation regions compared with the auxiliary measurement regions. Very good agreement between data and prediction is seen after accounting for the misindentified electron background.

6.3.3 Non-prompt lepton background in the μ+jets, 2μ+jets and 2e+jets auxiliary measurements

Heavy-flavour hadron decays with a muon in the final state are the dominant source of muon misidentification in multijet events. The relatively low branching ratio for muon-channel hadronic decays, together with a high efficiency for identifying prompt muons, leads to a very high purity in the single-muon and dimuon event samples, allowing the use of the 'fake-factor'

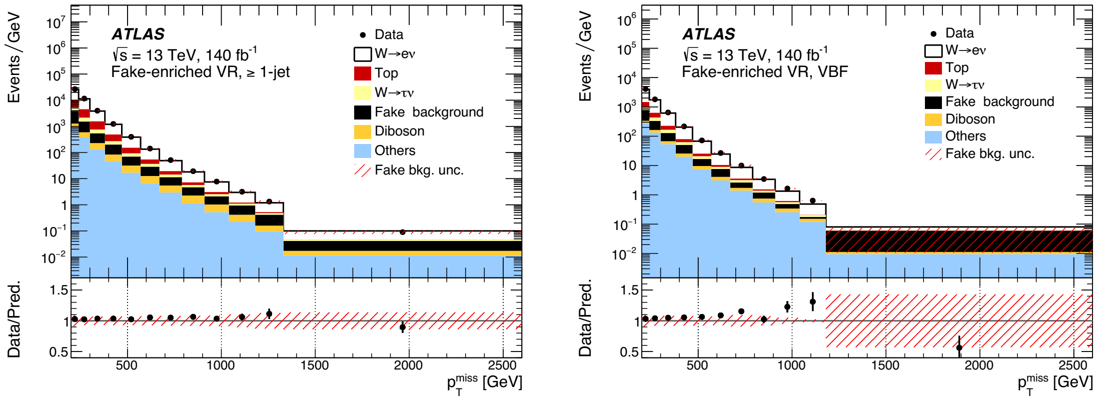

(a) (b)

Figure 2. The event yield in the e+jets background validation region as a function of p_T^{miss} for the (a) ≥ 1 jet selection and (b) VBF selection. Points denote data, and estimated backgrounds are shown as histograms. The hatched band shows the full uncertainty in the 'fake background' arising from misidentified leptons (described in section 7.2) and the vertical lines represent the statistical uncertainty. The bottom panels show the ratios of the data to the predictions.

method. A similar argument (high purity of the dielectron sample) implies that the same method can also be used in the $2e$+jets auxiliary measurement.

The fake-factor method is a simplification of eq. (6.1). It relies on the quality of the simulation in describing the detector response to a prompt lepton. Accordingly, the number of non-prompt leptons satisfying the `Tight` lepton identification, N_T^{Bkg}, can be estimated as:

$$N_T^{Bkg} = \frac{\epsilon_B}{1-\epsilon_B}\left(N_{!T} - N_{!T}^{P}\right), \tag{6.3}$$

where $N_{!T}$ is the yield of `Loose` leptons that fail to satisfy the `Tight` identification WP observed in data and $N_{!T}^{P}$ is the number of prompt leptons satisfying `Loose` but failing the `Tight` lepton identification determined in the simulation.

The fraction of fake leptons satisfying the selection ϵ_B is measured in data using a dedicated sample of events containing a pair of leptons with different flavour but the same sign charge. A small fraction of events in this sample can be attributed to true prompt lepton production in the two-boson or $t\bar{t}$ processes, while the rest are fakes. The prompt lepton contribution is accounted for using the simulation.

As a function of lepton p_T, ϵ_B for muons is flat at 5% up to around 30 GeV, after which it increases up to 55% at 1 TeV. The same ϵ_B is used in both single-muon and dimuon auxiliary measurements. The fake muon background in the μ+jets (2μ+jets) event selection is around 5% (<1%). Similarly, ϵ_B for the electron definition in the $2e$+jets region is measured as a function of electron p_T. It is found to be 14% for 7 GeV electrons and steadily increases up to 31% for 110 GeV electrons. Fake electrons are predominantly at low p_T, and due to the analysis selection these are generally accompanied by a high p_T electron, where the fake rate is low. Therefore the estimate of non-prompt electron background for $2e$+jets events is found to be relatively small, and does not exceed 1%.

JHEP08(2024)223

Production process	Final-state event selection $p_{\mathrm{T}}^{\mathrm{miss}}$+jets	2e+jets	2μ+jets	e+jets	μ+jets	γ+jets
$Z \to \nu\nu$ + jets	55%	—	—	—	—	—
$Z \to ee$ + jets	—	94%	—	—	—	—
$Z \to \mu\mu$ + jets	—	—	95%	—	2%	—
$W \to e\nu$ + jets	6%	—	—	68%	—	—
$W \to \mu\nu$ + jets	9%	—	—	—	67%	—
$W \to \tau\nu$ + jets	20%	—	—	5%	7%	—
γ + jets	—	—	—	—	—	>99%
Top	7%	3%	2%	25%	21%	—
Multi-boson	3%	3%	3%	2%	3%	<1%

Table 3. The relative contributions of SM processes to the $p_{\mathrm{T}}^{\mathrm{miss}}$+jets and auxiliary measurements event selections. The contributions are calculated using the MC simulation.

6.4 Contributions from other SM processes

SM processes with charged leptons in the final-state, involving single or double electroweak bosons as well as single top-quark and $t\bar{t}$ production, can contribute to the measured observables. This can even occur in the zero-lepton measurements, for example when one or two final-state leptons are produced outside of the analysis p_{T} or η acceptance, or are not reconstructed because of detector inefficiencies or a poor lepton isolation due to underlying event or pile-up activity around the final-state lepton.

In the inclusive $p_{\mathrm{T}}^{\mathrm{miss}}$ and $p_{\mathrm{T}}^{\mathrm{recoil}}$ measurements, events from these sources that satisfy the fiducial phase-space selection are treated as signal, and instrumental effects are corrected for later. In the $Z \to \nu\nu$ measurement, they are treated as irreducible backgrounds, and are accounted for with a semi-data-driven approach: the shapes of the distributions are taken from the SM predictions, while the normalisations are extracted from fits to data using a set of four control regions defined by adding to the $p_{\mathrm{T}}^{\mathrm{miss}}$ and other selection criteria the requirement that one or more charged leptons with $p_{\mathrm{T}} > 30$ GeV be present. A summary of the SM contributions and their relative importance in various signal regions of the analysis is given in table 3. The level of contribution varies strongly with measurement region. The photon auxiliary region contains $> 99\%$ γ+jets events, and the two-lepton auxiliary measurements are expected to consist of around 95% Z boson production events. Due to this very high purity, both the shape and normalisation of the top-quark and multi-boson contributions in these regions are taken directly from the corresponding simulation.

For the charged lepton measurements, the normalisations of the $W \to \tau\nu$ and top-quark background distributions are determined in a combined fit to the W and top-background control regions. The fit is performed separately in the electron and muon channels for each ≥ 1 jet and VBF event selection. The scale-factors for the top-quark background are found to be around 0.70–0.78, while the $W \to \tau\nu$ distributions are rescaled by factors of 1.10–1.12. The background normalisation factors in different phase-space regions and

τ-lepton decay channels agree with each other within statistical and systematic errors in the background estimation procedure.

The normalisations of the $W \to e\nu$, $W \to \mu\nu$, $W \to \tau\nu$ and top-quark contributions to the $p_{\mathrm{T}}^{\mathrm{miss}}$+jets event selection are extracted in a simultaneous fits to data in control regions for the ≥ 1 jet and VBF event selections separately. As a result, the W production contributions in the $p_{\mathrm{T}}^{\mathrm{miss}}$+jets event selection are rescaled by factors ranging from 1.04 to 1.13, depending of the phase-space region and the W boson leptonic decay channel. The top-quark background distributions scale-factors are 0.97–0.98 in both the ≥ 1 jet and VBF regions.

For the inclusive measurement, rescaled contributions are used to construct the simulated sample for unfolding. For the $Z \to \nu\nu$ measurement, they are subtracted from the data before unfolding.

7 Detector correction and systematic uncertainties

The data are corrected for detector effects so that they are presented in terms of particle-level objects, as defined in section 3.1.

7.1 Unfolding procedure

An efficiency correction and an iterative Bayesian unfolding technique are used to correct the data and obtain particle-level differential cross-sections. A prior truth distribution is used as input, and biases from the prior are accounted for by iterating the unfolding after reweighting the input distributions to the corrected data from the previous iteration. The optimal number of iterations is determined by balancing the fact that fewer iterations results in a stronger bias from the input prior (which is treated as a systematic uncertainty), whilst increasing the number of iterations increases the statistical uncertainty. Two iterations proved to be an optimal number for all measured distributions.

The inputs to the unfolding procedure are:

- **Migration matrix**. Events in a specific bin at particle level can migrate to a different bin in the reconstructed distribution, due to finite detector resolution. The migration matrix maps the true distribution onto the reconstructed distribution using events satisfying both the particle- and detector-level selections.

- **Reconstruction matching efficiency**. Due to the efficiency and acceptance of the detector, only a fraction of particle-level events are reconstructed within the target phase space. The reconstruction efficiency accounts for this and is defined as the ratio of simulated events that satisfy both the particle- and detector-level selections to all events satisfying the particle-level selection, as a function of the particle-level value of the observable being considered.

- **Fiducial fraction**. Due to the finite resolution of the detector, events that do not satisfy the particle-level selection can still satisfy the detector-level selection and be included in the detector-level distribution. The fiducial fraction accounts for this and is defined as the ratio of simulated events satisfying both the particle- and detector-level selections to those that satisfy only the detector-level selection, as a function of the detector-level value of the observable being considered.

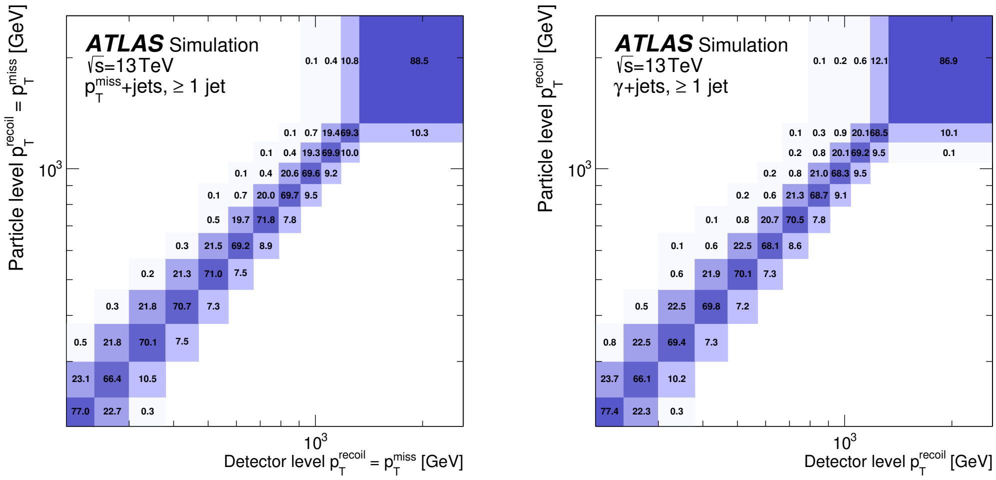

(a) (b)

Figure 3. Migration matrices for (a) the p_T^{miss} in the p_T^{miss}+jets region and (b) p_T^{recoil} in γ+jets region, the ≥ 1 jet phase space, constructed for all processes that enter the fiducial phase space.

- **Purity**. This quantity encapsulates the size of migrations between bins for events as a function of detector-level values of the observable being considered. It is defined as the fraction of the entries in a detector-level bin that are in the same bin at particle level.
- **Stability**. This quantity encapsulates the size of migrations between bins for events as a function of particle-level values of the observable being considered. It is defined as the fraction of the entries in a particle-level bin that are in the same bin at reconstruction level.

The binning of each distribution is defined so that each bin is expected to contain at least 20 reconstructed events, with a purity of at least 60%.

Figure 3 shows, as an example, the migration matrices for p_T^{miss} in the p_T^{miss}+jets and p_T^{recoil} in the γ+jets region, both for the ≥ 1 jet phases space, while figure 4 shows the matching efficiency, fiducial fraction, purity and stability for p_T^{recoil} for all auxiliary measurements in the ≥ 1 jet phase space.

The efficiency is lowest for the e+jets region, due to the requirements applied to the real p_T^{miss} and transverse mass. The highest efficiency is seen in the p_T^{miss}+jets region, which has no leptons to reconstruct. The fiducial fraction is around 0.9 in this region, due to contributions from W+jets events with a particle-level lepton that is within the fiducial acceptance. These fail to satisfy the particle-level lepton veto, but satisfy the reconstruction-level lepton veto due to inefficiencies in reconstructing the lepton. The migration matrices and purity plots are similar between all regions as the migration between p_T^{miss} bins depends primarily on the hadronic recoil. The same qualitative features are present in the p_T of the leading jet in the VBF phase space (not shown).

Several sources of systematic uncertainty in the particle-level measurements are considered:

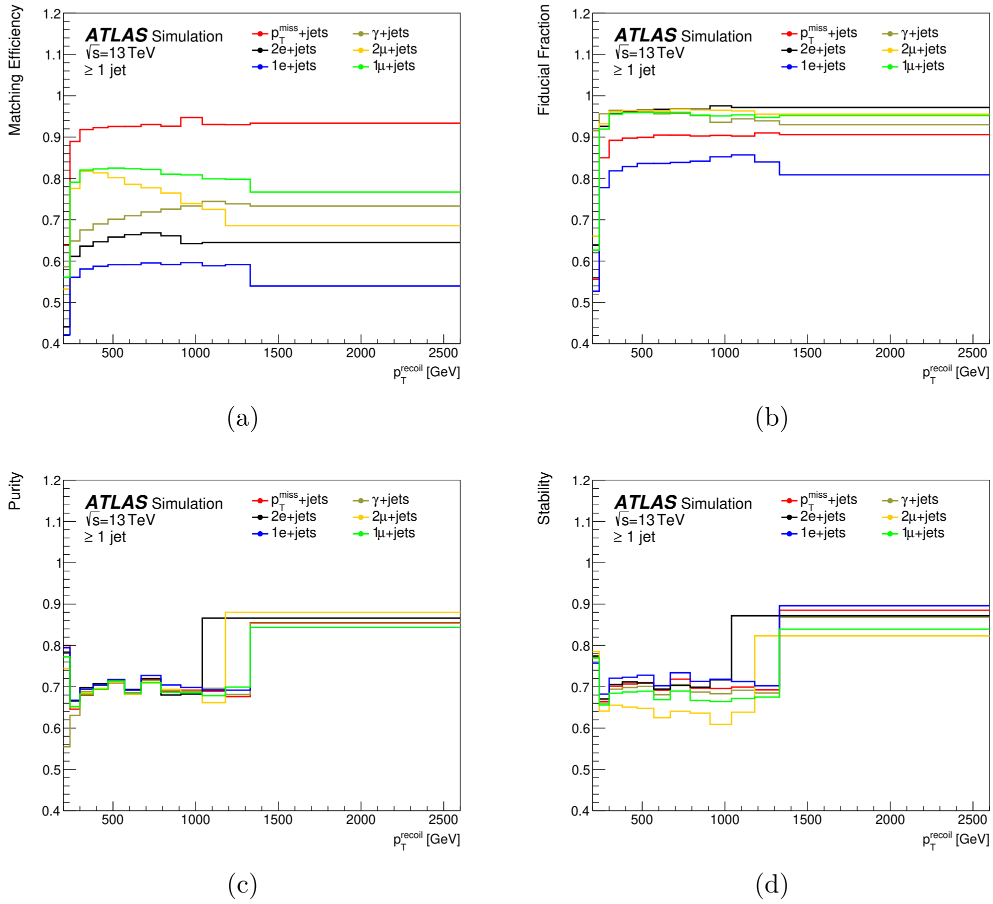

Figure 4. (a) Matching efficiency, (b) fiducial fraction, (c) purity and (d) stability for $p_{\mathrm{T}}^{\mathrm{recoil}}$, in the $p_{\mathrm{T}}^{\mathrm{miss}}$+jets, γ+jets, e+jets, μ+jets, $2e$+jets, 2μ+jets regions of the ≥ 1 jet phase space, constructed for all processes that enter the fiducial phase space. The purity and stability are high at high values of $p_{\mathrm{T}}^{\mathrm{recoil}}$ because of the large bin widths dictated by the requirement that there be at least 20 events in each bin.

- **Hidden variables:** while the iterative unfolding handles biases from the assumed prior for the distribution being unfolded, the unfolded result may still be influenced by the (mis)modelling of other 'hidden' event variables, especially if they form part of the selection. This is studied by reweighting simulated events at particle level so that the reweighted reconstructed distribution of the hidden variable matches the data. The variables considered are the leading-jet and leading-lepton kinematics, the number of jets, and the invariant mass of the dilepton system. Differences in the unfolded results with and without this additional weighting are taken as uncertainties, although they are below the percent level.

- **Migrations into the fiducial phase space:** the events that satisfy the selection criteria defining the fiducial phase space (table 2) at reconstruction-level are not identical to those that satisfy them at particle-level. If this difference, or the underlying distributions for each variable that is used in the selection, is not well modelled then

JHEP08(2024)223

the migrations in and out of the phase space will not be properly corrected for in the unfolding. For all observables in all regions, comparisons of data and simulation are made, and in each case the requirement in question is relaxed in order to study the behaviour of the observable below the selection value. Simulated events are reweighted such that the reconstructed distribution matches the data. The changes to the measurement caused by this reweighting are negligible.

- **Signal injection tests:** although the unfolding procedure and fiducial definition are designed to minimise dependence on the simulated distributions, a residual bias may be present due to the absence of BSM effects from the samples used for unfolding, while such physics may be present in the data. To test whether this is the case, various BSM processes are injected into the simulated samples, which are then treated as pseudodata and unfolded with nominal SM simulation. Three samples of Higgs boson events decaying invisibly were used, with three different Higgs boson masses (75 GeV, 125 GeV and 750 GeV), thus emulating some very extreme Higgs-to-invisible BSM scenarios. The test is repeated for $p_{\mathrm{T}}^{\mathrm{miss}}$ in the ≥ 1 jet phase space using a model with s-channel production of a DM particle (χ) via a spin-1 axial-vector mediator A, for $m_\chi = 1\,\mathrm{GeV}$ with $m_A = 50\,\mathrm{GeV}$ and 700 GeV, and $m_\chi = 355\,\mathrm{GeV}$ and $m_A = 700\,\mathrm{GeV}$, as well as spin-0 pseudoscalar mediator with $m_\chi = 1\,\mathrm{GeV}$ and $m_A = 50\,\mathrm{GeV}$. The maximum bias for any of these scenarios is 10%, seen at large $p_{\mathrm{T}}^{\mathrm{miss}}$, and all the models introducing bias are so extreme that if they were present in reality, the discrepancy would already be clearly seen in the detector-level data, before unfolding. No additional source of systematic uncertainty is therefore added from this source.

- **Sample composition variations:** for the measurement of the $p_{\mathrm{T}}^{\mathrm{miss}}$ cross-sections, the simulated samples used in the unfolding include all contributing SM processes; the mixture of these processes is constrained by applying the normalisation factors discussed in section 6.4. Uncertainties are derived by varying the composition within the uncertainties in these normalisation factors. The derived uncertainties are then propagated through the unfolding to the final measurement. SM processes involving top quarks are among those whose contribution is varied. Events originating from these processes are enriched in the presence of b-quarks. This uncertainty therefore also ensures that the resulting measurement can be used safely when comparing to predictions with increased b-quark activity.

For the measurement of $Z \to \nu\nu$ cross-sections, the contributions from non-$Z \to \nu\nu$ SM processes are subtracted before unfolding, with the amount subtracted being constrained using both the high-$p_{\mathrm{T}}^{\mathrm{miss}}$ measurement region and the control regions. The simulated sample used in the unfolding then includes only $Z \to \nu\nu$ processes. The subtraction uncertainties are propagated through the unfolding to the final measurement.

7.2 Detector calibration, resolution and identification uncertainties

The unfolding procedure relies on knowledge of the detector response, which has uncertainties associated with it. The impact of these uncertainties is determined by varying the response function in question and re-running the analysis, including the final unfolding step. The sources of uncertainty considered are given below.

- Uncertainties related to jet energy scale (JES) and jet energy resolution (JER) are derived using dijet samples following the procedures documented in ref. [103]. A subclass of JES uncertainties deals with whether the jet is likely to have been initiated by a quark or a gluon. The proportion of quark-initiated jets in the measurement regions is estimated from simulation as a function of transverse momentum and pseudorapidity.
- Uncertainties related to the electron efficiency measurement and calibration are obtained from tag-and-probe measurements of J/ψ and $Z \to e^+e^-$ events, as described in ref. [92].
- Muon uncertainties are related to muon calibration and efficiencies are obtained from J/ψ and $Z \to \mu^+\mu^-$ events, as described in ref. [95].
- τ-lepton calibration uncertainties are accounted for as documented in ref. [109].
- Measurements of $Z \to \ell\ell\gamma$ events are used to study the performance of photon reconstruction, as documented in ref. [92].
- The uncertainty in those (soft) components of $p_{\mathrm{T}}^{\mathrm{miss}}$ not accounted for already is represented by three systematic uncertainties, detailed in ref. [110].

Figure 5 shows the breakdown of the statistical and systematic uncertainties for the $p_{\mathrm{T}}^{\mathrm{miss}}$ observable in the ≥ 1 jet phase space. At high $p_{\mathrm{T}}^{\mathrm{miss}}$, the statistical uncertainty dominates, and over most of the distribution, the JES is the most significant systematic uncertainty, with the JER next in the region with no leptons or photons. Uncertainties associated with lepton and photon identification contribute in the other regions. The uncertainty due to the unfolding, and the (forward) jet vertex tagging uncertainty, are below 2%, and much smaller in most cases.

Figure 6 shows the breakdown of statistical and systematic uncertainties for the R^{miss} ratio of cross-sections, as a function of $p_{\mathrm{T}}^{\mathrm{miss}}$, in the ≥ 1 jet region. At low $p_{\mathrm{T}}^{\mathrm{miss}}$, the cancellation of JES uncertainties leads to a reduction in the combined estimate of the experimental uncertainty.

Finally, uncertainties associated with the estimation of fake backgrounds are accounted for. For the fake-lepton backgrounds, the dominant source comes from theory uncertainties, such as QCD scale variations, affecting the generator predictions in the regions used to measure the efficiencies. This uncertainty can be up to 100% of the predicted background yield. Smaller sources include statistical uncertainties relating to the limited number of events in data in those regions, and uncertainties in the method (evaluated for example by modifying the definition of the regions). Uncertainties from these sources are typically around 10% of the predicted yield. After unfolding, the fake leptons uncertainties collectively have an effect of the order of 1%–4% depending on the bin. For the fake-photon background, three sources of uncertainty are considered: the choice of WP used when selecting photons, the correlation between the A, B, C and D regions used for the estimation and the choice of generator for the prompt photon prediction. Together, these three sources result in an uncertainty of

JHEP08(2024)223

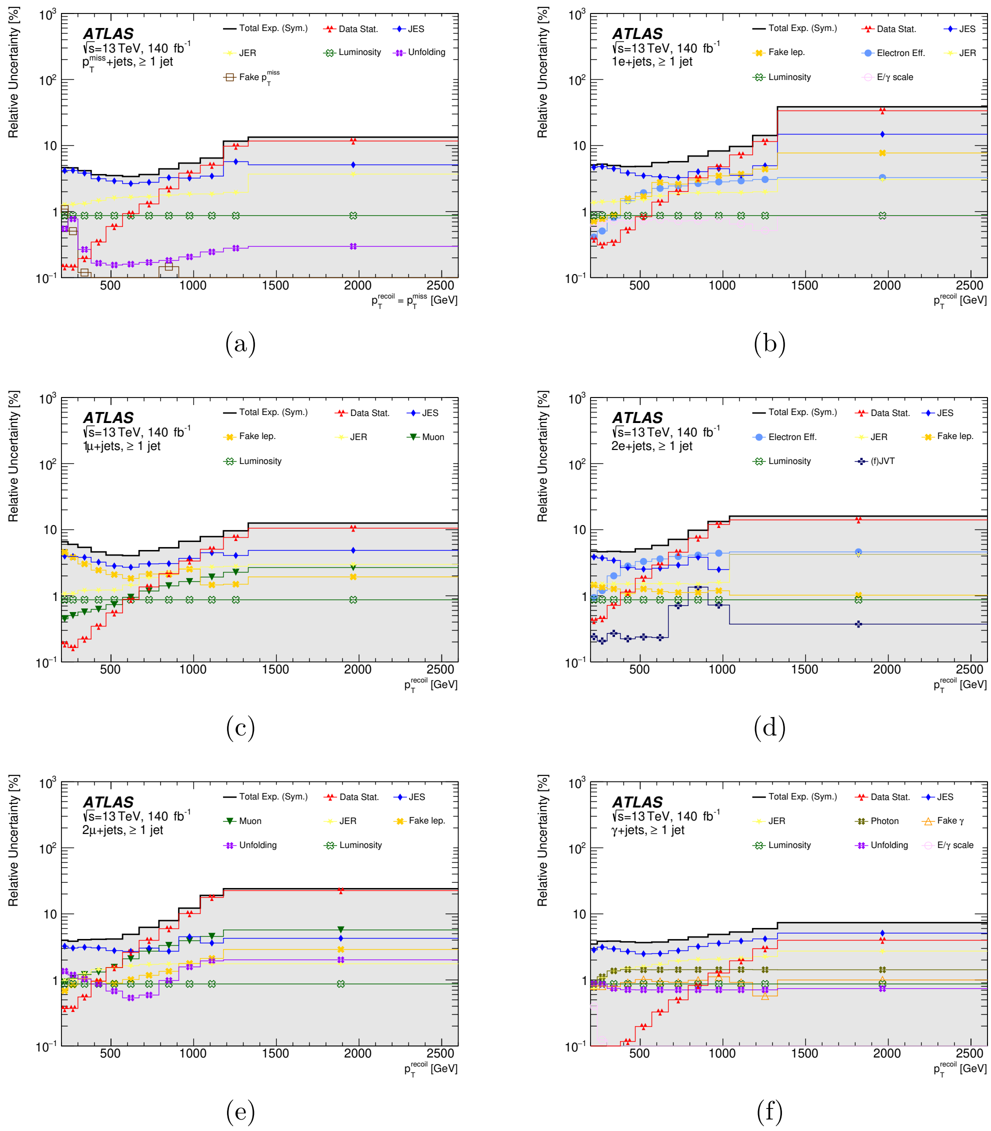

Figure 5. Uncertainty breakdown for $p_{\mathrm{T}}^{\mathrm{recoil}}$ measurements in the ≥ 1 jet phase space for the (a) $p_{\mathrm{T}}^{\mathrm{miss}}$+jets, (b) e+jets, (c) μ+jets, (d) $2e$+jets, (e) 2μ+jets, and (f) γ+jets regions, showing the statistical uncertainty and the most significant systematic uncertainties in each case. For illustrative purposes this figure shows the symmetrised uncertainties, calculated as the average of the asymmetric error in each bin. Total Exp. (Sym.) is the combination of statistical and systematic uncertainties and indicates the symmetrised total experimental uncertainty.

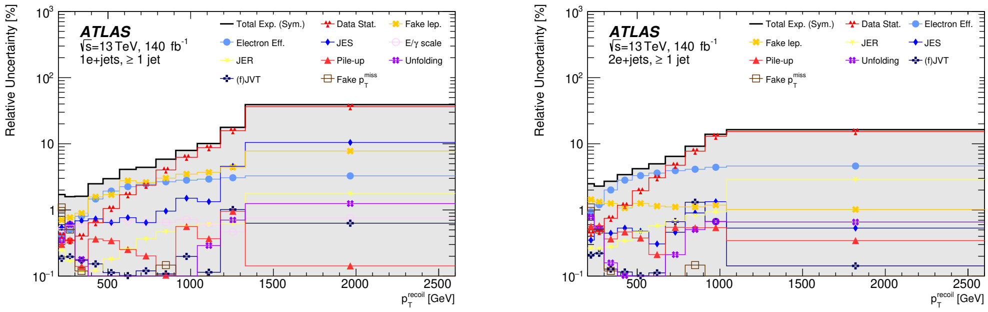

(a) (b)

Figure 6. Uncertainty breakdown of the R^{miss} ratio as a function of $p_{\text{T}}^{\text{recoil}}$. As examples, the breakdowns for the ≥ 1 jet phase space are shown for the (a) e+jets and (b) $2e$+jets region. For illustrative purposes this figure shows the symmetrised uncertainties, calculated as the average of the asymmetric error in each bin. Total Exp. (Sym.) is the combination of statistical and systematic uncertainties and indicates the symmetrised total experimental uncertainty. Compared to the individual measurements in figure 5(b) and 5(d), a cancellation of the JES and JER uncertainties is observed.

around 30% in the predicted fake photon yields. This amounts to approximately 1% in the measured cross-section after unfolding. The uncertainties in the multijet and non-collision backgrounds in the signal region represent very small contributions to the final event sample and are subject to statistical variations due to the nature of the evaluation. Therefore, they are conservatively taken to be 100% of the estimated yield, corresponding to a less than 1% uncertainty in the final measurement in the most affected bin.

8 Results and discussion

8.1 $p_{\text{T}}^{\text{miss}}$ measurements

The measured differential cross-section as a function of the magnitude of the missing transverse momentum, $p_{\text{T}}^{\text{miss}}$, is shown in figure 7 for the single jet and VBF phase spaces, in the region with no signal leptons or photons. In both cases, the cross-section falls by more than five orders of magnitude as $p_{\text{T}}^{\text{miss}}$ increases from 200 to 2500 GeV. The cross-section in the VBF phase space is lower than the single jet phase space due to the jet requirements.

Similar behaviour is seen for the transverse momentum of the hadronic system, $p_{\text{T}}^{\text{recoil}}$, after the charged lepton requirements are imposed, as shown in figure 8 for the single jet phase space. When a single muon is required, the cross-section is similar in magnitude to the zero-lepton/photon cross-section, while requiring two muons reduces it by about an order of magnitude. The cross-sections after electron requirements are somewhat smaller due to the more restrictive fiducial requirements imposed on electrons.

The SM predictions described in section 4 are also shown in figure 7 and figure 8. Apart from a difference between the normalisations, they describe the data well in all regions; a quantitative study is presented in section 8.3. Also shown are the subcomponents of the MEPS@NLO prediction. With no leptons or photons present, the dominant contribution is $Z \to \nu\nu$, with a top-quark contribution of a few per cent at low $p_{\text{T}}^{\text{miss}}$ that falls to the

JHEP08(2024)223

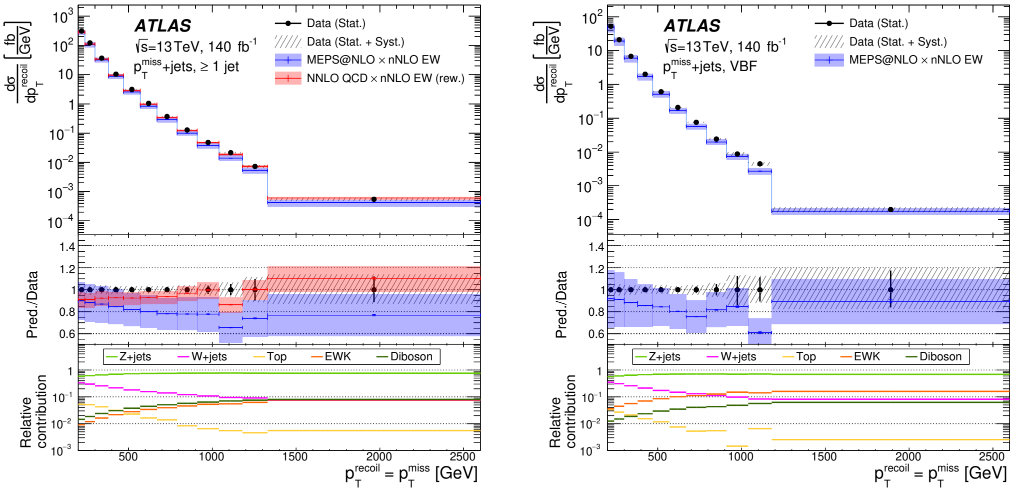

(a) (b)

Figure 7. The measured $p_{\mathrm{T}}^{\mathrm{miss}}$ differential cross-sections in the $p_{\mathrm{T}}^{\mathrm{miss}}$+jets region in (a) ≥ 1 jet and (b) VBF phase spaces, compared with the SM predictions. The middle panels show the ratios of the predictions to the data, with statistical uncertainties as solid markers and shaded bands to indicate the combined statistical and systematic uncertainties, while the lower panels show the relative contributions from different SM processes relative to the total MEPS@NLO prediction.

per-mille level at higher values. The contribution from W+jets is around 25% at low $p_{\mathrm{T}}^{\mathrm{miss}}$, but falls rapidly with $p_{\mathrm{T}}^{\mathrm{miss}}$ to form about 10% of the cross-section at higher values. The contribution from electroweak production mechanisms is around 1% at low $p_{\mathrm{T}}^{\mathrm{miss}}$, but rises rapidly with $p_{\mathrm{T}}^{\mathrm{miss}}$ to form about 10% of the cross-section at higher values.

For the one-electron and one-muon phase spaces, the top-quark contribution is around 15% at low $p_{\mathrm{T}}^{\mathrm{recoil}}$, falling to a few percent at high values. It is never more than a few percent of the two-charged-lepton cross-sections. For all the charged-lepton cross-sections, the electroweak contribution is around 1% at low $p_{\mathrm{T}}^{\mathrm{recoil}}$, rising with $p_{\mathrm{T}}^{\mathrm{recoil}}$ to be just below 10% of the cross-section.

The measured differential cross-section as a function of the m_{jj} and $\Delta\phi_{jj}$ is shown for the VBF selection in figure 9, along with the SM predictions for different sub-processes, for the $p_{\mathrm{T}}^{\mathrm{miss}}$+jets and the 2μ+jets regions. The cross-section falls rapidly with dijet mass, and the electroweak contribution rises from around 1% to 50% as m_{jj} rises from 600 GeV to 6 TeV. The overall $\Delta\phi_{jj}$ distribution peaks mildly at $\pm\pi/2$. The predicted fractional contribution from top has a peak at zero, and both the diboson and top contributions rise towards $\pm\pi$. The electroweak contribution has maxima at $\pm 0.8\pi$.

The description of the data by the SM predictions is generally good, except for the m_{jj} distribution, where the SM lies below the data at low values, but falls less steeply, to lie above the data around 2 TeV. This is discussed further in section 8.3. A resummed calculation using HEJ is also shown, which describes the m_{jj} distribution somewhat better.

Figure 10 shows some examples of the R^{miss} ratios of the results presented so far. The ratios tend to be flat or slowly falling across the measured spectra. The R^{miss} ratios benefit from a cancellation of discrepancies in modelling and some systematic uncertainties, and thus

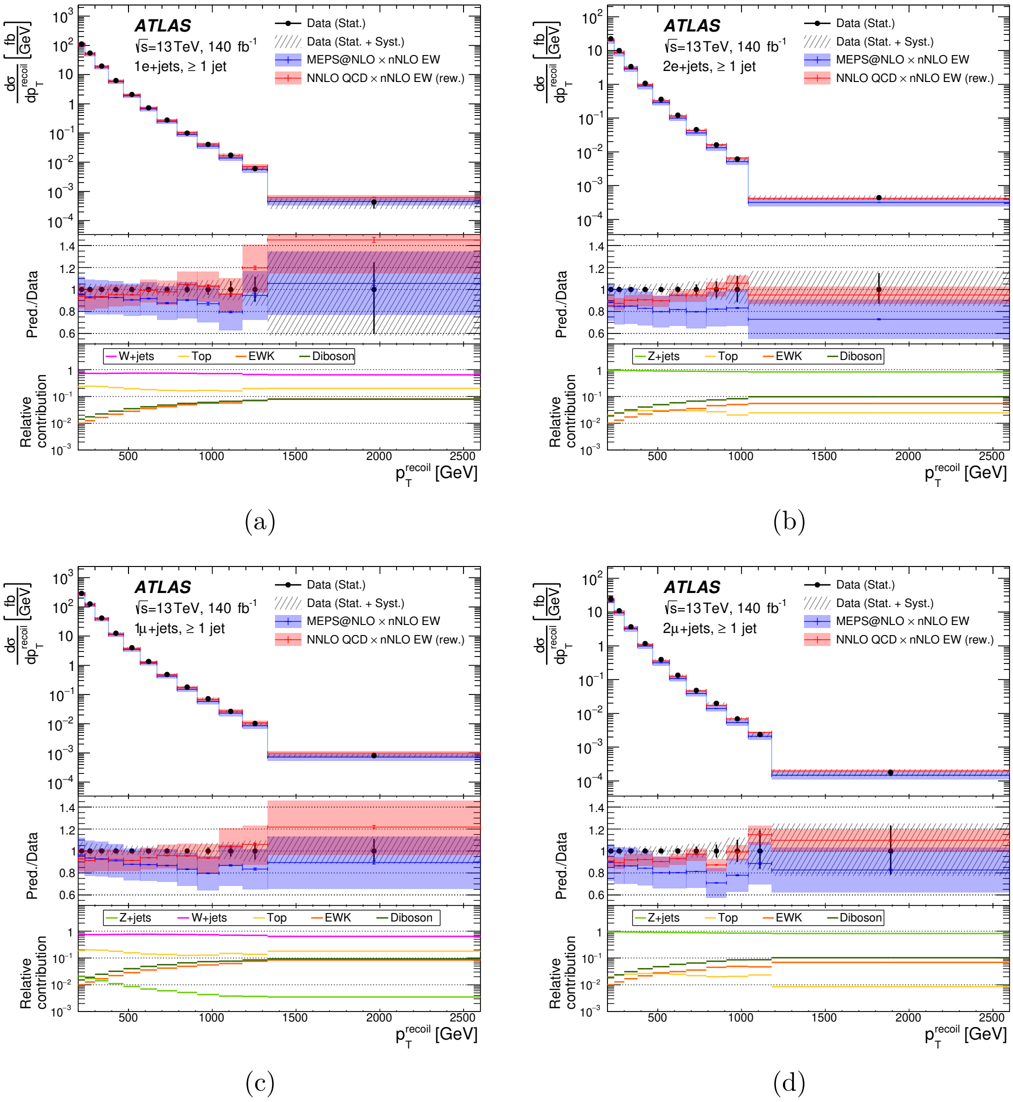

Figure 8. The measured $p_{\mathrm{T}}^{\mathrm{recoil}}$ differential cross-sections in the inclusive jet phase space compared with the SM predictions: (a) e+jets (b) $2e$+jets (c) μ+jets and (d) 2μ+jets. The middle panels show the ratios of the predictions to the data, with statistical uncertainties as solid markers and shaded bands to indicate the combined statistical and systematic uncertainties, while the lower panels show the relative contributions from different SM processes relative to the total MEPS@NLO prediction.

the agreement between data and theory is improved compared to that for the cross-sections, most notably for the m_{jj} observable.

8.2 $Z \to \nu\bar{\nu}$ measurement

The Z+jets process dominates the zero-lepton phase space. As discussed in section 7, non-Z+jets SM processes can be subtracted from the data before detector corrections to extract a measurement of Z+jets. This method gives consistent results with the inclusive measurements when the particle-level predictions for the subtracted processes are added back in after unfolding. The differential cross-section for Z+jets is shown in figure 11 as

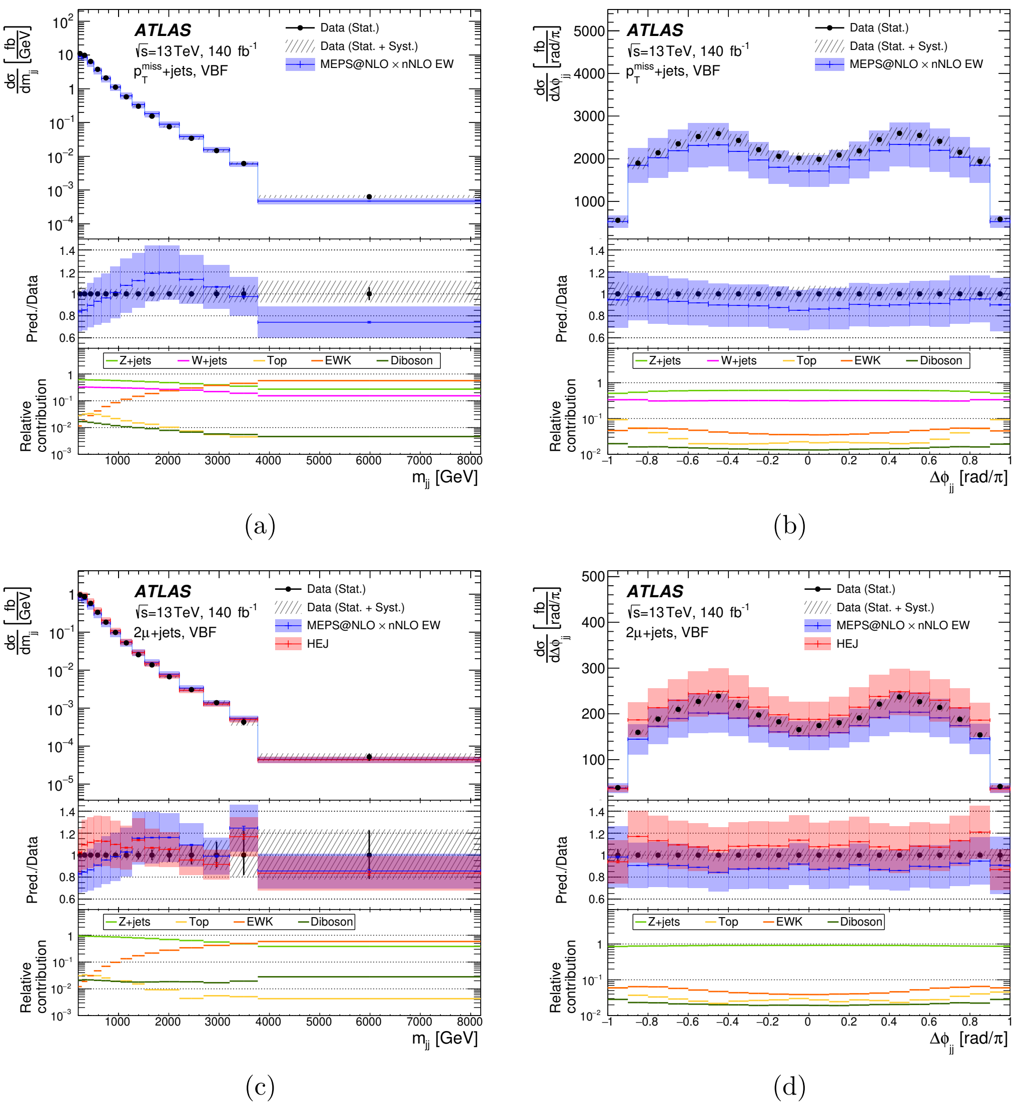

Figure 9. The measured m_{jj} and $\Delta\phi_{jj}$ distributions in the VBF phase space compared with the SM predictions, for ((a), (b)) the $p_{\mathrm{T}}^{\mathrm{miss}}$+jets and ((c), (d)) the 2μ+jets regions, for illustration. The middle panels show the ratios of the predictions to the data, with statistical uncertainties as solid markers and shaded bands to indicate the combined statistical and systematic uncertainties, while the lower panels show the relative contributions from different SM processes relative to the total MEPS@NLO prediction.

a function of p_{T}^{Z} in the ≥ 1 jet and VBF phase spaces, and as a function of m_{jj} and $\Delta\phi_{jj}$ in the VBF phase space. The level of description by the SM is similar to that for the inclusive measurement.

The production of an isolated photon in association with jets, γ+jets, in a similar kinematic region, shares several theoretical and experiment uncertainties with the Z+jets process. The measurements of this final state are shown in figure 12.

The γ+jets cross-section is generally a factor of about five above the Z+jets cross-section, with similar features. The prediction is 10%–20% above the data, although generally

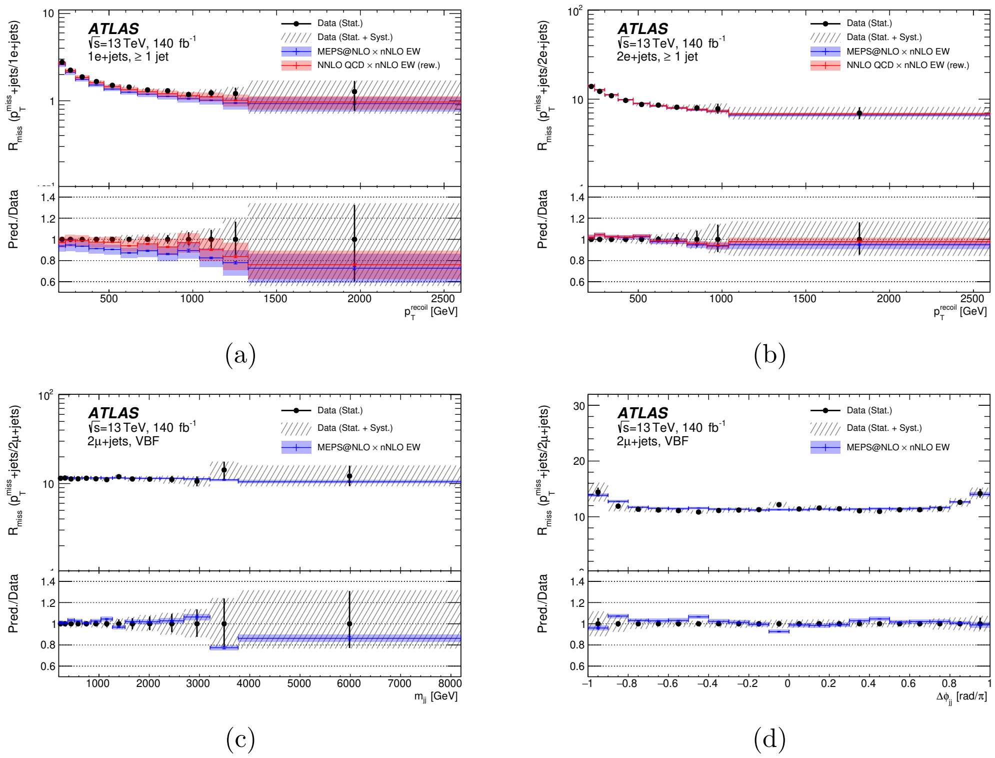

Figure 10. Comparison with SM predictions of the R^{miss} ratios of the measured differential cross-sections for (a) e+jets and (b) $2e$+jets as a function of $p_{\text{T}}^{\text{recoil}}$ in the inclusive jet phase space and for 2μ+jets as a function of (c) m_{jj} and (d) $\Delta\phi_{jj}$ in the VBF phase space. The bottom panels show the ratios of the predictions to the data with their statistical uncertainties as solid markers and shaded bands to indicate the combined statistical and systematic uncertainties.

lies within the uncertainties in the calculation for the cross-section measurements. The discrepancy remains in the R^{miss} measurements, since this normalisation issue only applies in the denominator and therefore does not cancel out. Similar shifts were observed in independent studies [111], and were found to be induced by photon isolation criteria.

8.3 Quantitative comparison to SM predictions

To quantify the level of agreement or disagreement between the measurement and the SM predictions, fits are performed by minimising the negative logarithm of the likelihood. Experimental and theoretical uncertainties are either added to a covariance matrix (if their impact is below one percent everywhere in the fitted distributions) or otherwise assigned to a nuisance parameter (NP) that is allowed to float according to the estimated uncertainty. The likelihood is evaluated for the resulting level of agreement, under the condition that the SM is the correct underlying model and taking into account the residuals, the covariance matrix and pulls on the nuisance parameters. Fits to the differential cross-sections are performed using the inclusive measurements, in all phase spaces, using the MEPS@NLO prediction. Since the γ+jets measurements show a strong normalisation offset not present in the other regions, only the $p_{\text{T}}^{\text{miss}}$+jets, e+jets, $2e$+jets, μ+jets and 2μ+jets regions (or their respective R^{miss} ratios) are used in the fits. Since the phase spaces are not orthogonal, statistical correlations

JHEP08(2024)223

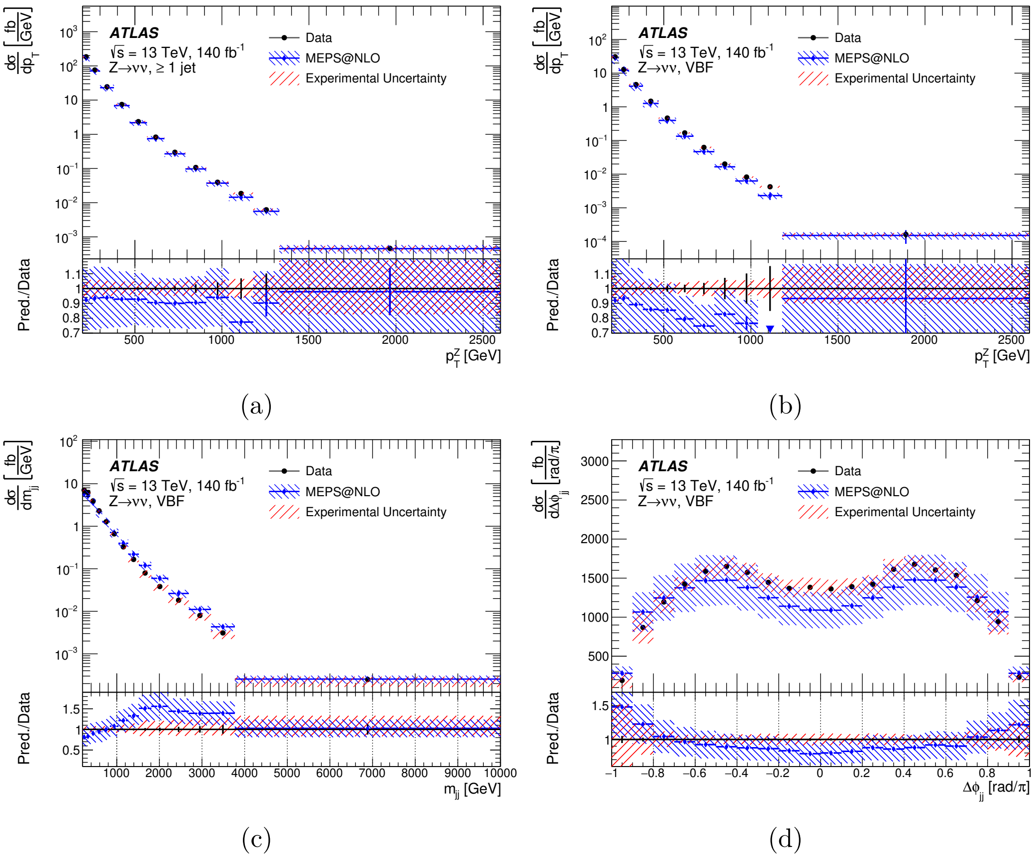

Figure 11. The measured $Z \to \nu\nu$ cross-section, differential in p_{T}^{Z} in the (a) single jet and (b) VBF phase spaces, and differential in (c) m_{jj} and (d) $\Delta\phi_{jj}$ in the VBF phase space, compared with the SM predictions. The lower panels show the ratios of the predictions to the data, along with the data statistical uncertainties (black bars) and systematic uncertainties (red hatched band).

exist between some measurements. These are evaluated using the Bootstrap method [112], and are accounted for in the correlation matrix in the fitting procedure.

The level of agreement between the fitted results and the SM for $p_{\mathrm{T}}^{\mathrm{recoil}}$ is reasonable, with a $\chi^2/\mathrm{d.o.f.} \approx 101/57$. For the differential cross-section as a function of $\Delta\phi_{jj}$, the post-fit distributions also show reasonable agreement between the measurement and the SM. For m_{jj} however, the agreement is not good, due to the poor modelling of this distribution seen in figure 9. Because of this, the combined fit using all distributions for all observables, regions and phase spaces simultaneously also shows poor agreement, with a $\chi^2/\mathrm{d.o.f.} \approx 390/70$.

Fits are also performed to ratios of the measurements, R^{miss}, defined as the fiducial cross-section differential in each kinematic variable for $p_{\mathrm{T}}^{\mathrm{miss}}$+jets events, divided by the same cross-section for events in each of the e+jets, μ+jets, $2e$+jets and 2μ+jets regions. In this case, some of the uncertainties largely or completely cancel out, and thus do not have an associated nuisance parameter. In addition, the modelling discrepancy in m_{jj} is seen in all regions and so cancels out to a large extent in R^{miss}. The ratio plots are therefore expected to give improved fit results compared to the cross-section fits. Indeed a $\chi^2/\mathrm{d.o.f.} \approx 323/220$ is obtained for the combined R^{miss} fit to all distributions in all regions, with the individual fit

JHEP08(2024)223

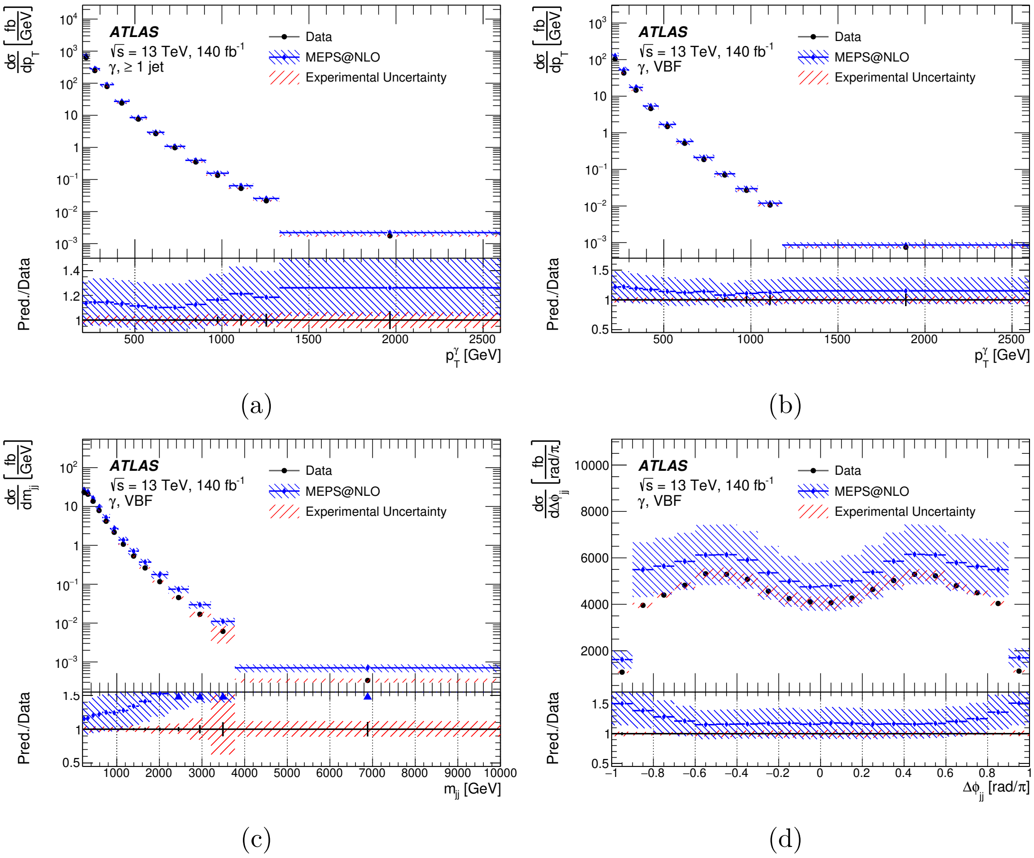

Figure 12. The measured γ+jets cross-section, differential in p_{T}^{γ} in the (a) single jet and (b) VBF phase spaces, and differential in (c) m_{jj} and (d) $\Delta\phi_{jj}$ in the VBF phase space, compared with the SM predictions. The lower panels show the ratios of the predictions to the data, along with the data statistical uncertainties (black bars) and systematic uncertainties (red hatched band).

to R^{miss} as a function of m_{jj} having $\chi^2/\mathrm{d.o.f.} \approx 62/56$, indicating that indeed the discrepancy between data and the SM predictions cancels out between the different regions.

For re-interpretation, the R^{miss} measurements are always used. Specifically, the fits use the R^{miss} distributions as a function of $p_{\mathrm{T}}^{\mathrm{miss}}$: either using just the inclusive jet phase space ($\chi^2/\mathrm{d.o.f.} \approx 48/45$) or both the inclusive jet and VBF phase spaces ($\chi^2/\mathrm{d.o.f.} \approx 110/84$). Both of these options display good agreement between the SM predictions and the measurements, and therefore can be safely used for re-interpretation and establishing constraints on new physics models.

9 Implications for physics beyond the Standard Model

Part of the motivation of these particle-level measurements is that they can easily be confronted with new SM predictions, and predictions from extensions to the SM. Since the measurements of $p_{\mathrm{T}}^{\mathrm{miss}}$ and R^{miss} are consistent with the SM, they can thus be used to set limits on BSM physics, particularly models that contain a DM candidate, the presence of which could affect the $p_{\mathrm{T}}^{\mathrm{miss}}$ distribution. This procedure was already demonstrated in the previous measurement [8] using a subset of the current data, and is extended and updated here.

JHEP08(2024)223

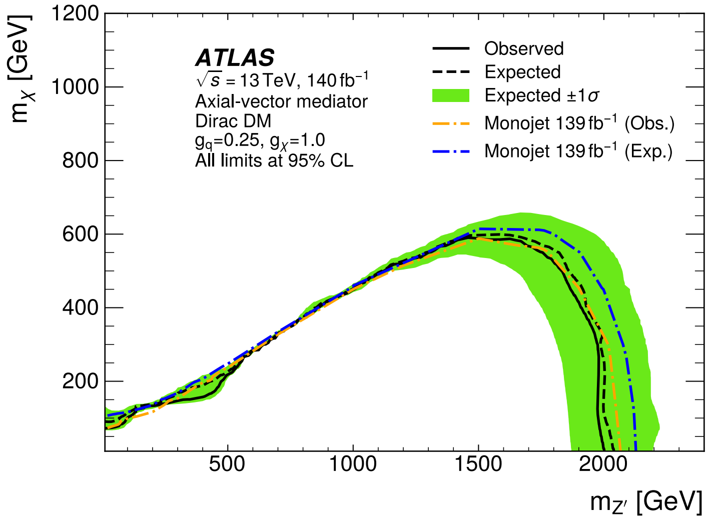

Figure 13. Exclusion limits at 95% in the plane of Dark Matter mass and mediator mass for a simplified DM model with an axial-vector coupling to the SM. The limits from this analysis, evaluated using the particle-level R^{miss} measurements, are compared with the limits from the ATLAS monojet search [4]. The region below the solid line is excluded.

A common benchmark simplified model involves extending the SM with an additional U(1) gauge symmetry, in which a DM candidate, χ, is a Dirac fermion that has charges only under this gauge group [9]. If SM quarks are also charged under this gauge group, DM particles can be produced at the LHC via the gauge boson, Z', associated with the new U(1) symmetry, which is massive assuming the U(1) symmetry is spontaneously broken. This model was searched for previously by ATLAS [4] using the same data sample as the current analysis, and by CMS [5].

The case where χ has axial-vector couplings $g_\chi = 1.0$ to the Z', and the coupling between the quarks and the Z', $g_q = 0.25$, is studied in this analysis in the $(m_\chi, m_{Z'})$ plane, to compare the sensitivity of the current measurement to that of the search results. The fitting procedure described in the previous section is used to evaluate the likelihoods associated with a fit to R^{miss} when excluding or including a BSM contribution from this model. During fitting, the predicted R^{miss} is recalculated to include the signal. The limits obtained from the likelihood ratio, shown in figure 13, are very similar to those previously published in the ATLAS search analysis [4], with mediator masses up to about 2.1 TeV excluded in the region $m_{Z'} > 2m_\chi$. The residual differences are attributed to the slightly different kinematic selections used, and the requirement for a minimum number of events in the high $p_{\text{T}}^{\text{miss}}$ bin for unfolding. This demonstrates that particle-level measurements can be used for searches and setting constraints with only a minor penalty in sensitivity, and with the advantage that it can be done in future without the need to repeat complex and time-consuming detector simulation.

A more complicated model for DM involves the introduction of an additional Higgs doublet, along with a pseudoscalar, a, which couples to DM [10, 11]. Through mixing with the pseudoscalar component of the Higgs doublet, the pseudoscalar a acts as a mediator between the SM and the dark sector. The model, referred to as 2HDM+a, has a rich phenomenology with a wide variety of possible final states produced [113–118], many of which involve $p_{\text{T}}^{\text{miss}}$

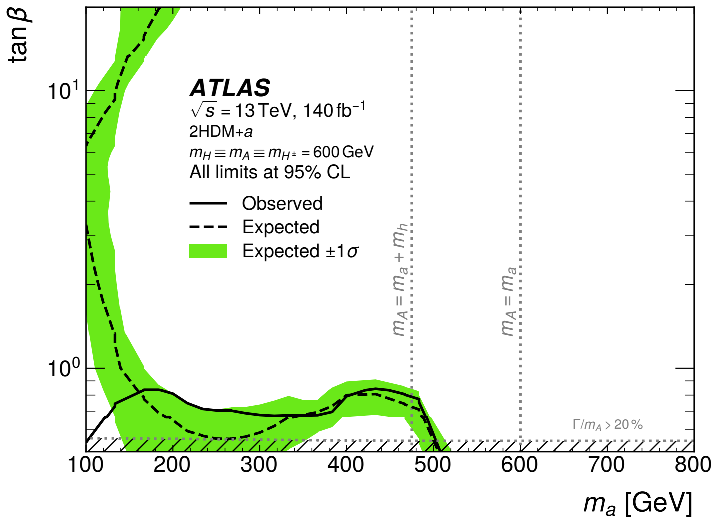

(a)

Figure 14. Exclusion limits at 95% in the (m_a, $\tan\beta$) plane for the 2HDM+a model. A region of $\tan\beta$ below 0.7 is excluded for m_a values between approximately 150 GeV and 500 GeV. The regions shaded with diagonal lines indicate the region where the width of any of the Higgs bosons exceeds 20 % of its mass; in this region the narrow-width approximation is violated and predictions become less precise. Moreover, the two vertical dashed lines represent scenarios where the mass of the neutral pseudoscalar A is either equal to the mass of the pseudoscalar a or a sum of the masses of a and Higgs boson h. The region below the solid line is excluded.

produced in association with jets or other SM objects. In this analysis, a signal scan is conducted in the (m_a, $\tan\beta$) plane where $m_A = 600$ GeV, as shown in figure 14. The scan makes use of the full set of R^{miss} measurements, in both the ≥ 1 jet and VBF phase spaces, taking into account statistical and systematic correlations.

The scan reveals two major regions of sensitivity:

- For $\tan\beta < 0.7$, masses of the pseudoscalar a up to 520 GeV are excluded because of loop-induced production of a and its subsequent decay into DM particles, $pp \to a(\to \chi\bar{\chi})$+jets. The sensitivity is larger at $m_a > 350\,\text{GeV} \approx 2m_{\text{top}}$ because here the a can be produced resonantly from top quarks. For $\tan\beta \gg 10$, there is a second island of sensitivity because of b-quark induced production of a and its subsequent decay into DM particles.

- At small m_a, the expected exclusion limits are generally stronger because of processes almost independent of $\tan\beta$, e.g., $pp \to H \to aZ$ and $pp \to H^{\pm} \to aW^{\pm}$. However, the sensitivity to these processes is not large enough to close the sensitivity gap between small and large values of $\tan\beta$.

Qualitatively the sensitivity is similar to the existing exclusion from $p_{\text{T}}^{\text{miss}}$-based searches in different final states [13]. Differences in the exclusion limits originate from differences in the SM calculations used, and from the use of the VBF phase space in addition to the ≥ 1 jet region.

JHEP08(2024)223

Overall these studies show that the inclusive, particle-level measurement provides good sensitivity to BSM physics, and is amenable to reinterpretation in terms of different models.

10 Conclusion

Inclusive measurements of $p_{\mathrm{T}}^{\mathrm{miss}}$ are made using $140\,\mathrm{fb}^{-1}$ of pp collision data at $\sqrt{s} = 13\,\mathrm{TeV}$ collected with the ATLAS detector during Run 2 of the LHC. The measurements are made in fiducial regions closely reflecting the detector acceptance, and are corrected for detector effects within these regions, yielding differential cross-sections defined in terms of final-state particles. Differential cross-sections are measured as a function of $p_{\mathrm{T}}^{\mathrm{miss}}$ in a ≥ 1 jet and a VBF phase space. The latter is defined by the presence of two jets, and the cross-section is also measured as a function of the azimuthal angular distance between the jets, $\Delta\phi_{jj}$, and the dijet invariant mass, m_{jj}. The cross-section for $Z \to \nu\nu$ production is determined, differential in the $p_{\mathrm{T}}^{\mathrm{miss}}$ and, in the VBF phase space, in $\Delta\phi_{jj}$ and m_{jj}.

Measurements of lepton+jets, dilepton+jets and γ+jets final states are also made in the same kinematic regions. Many uncertainties, both theoretical and experimental, are correlated between these measurements and the $p_{\mathrm{T}}^{\mathrm{miss}}$ measurements, and therefore cancel out in the ratio of cross-sections, R^{miss}.

Quantitative comparisons with state-of-the-art SM predictions show a reasonable description of all measured cross-sections as a function of most observables, except m_{jj}. The discrepancy in the shape of the distribution of this observable is present in the lepton+jets, dilepton+jets and γ+jets measurements as well as in the $p_{\mathrm{T}}^{\mathrm{miss}}$ region. It therefore cancels in R^{miss}, which is well described by the predictions. The resummed calculation in the HEJ prediction, available for the leptonic measurements, provides a better description of m_{jj}.

The measurements are designed to be readily reinterpreted, and the effectiveness of this is illustrated by comparisons with two DM models. Specifically, the measured R^{miss} distribution is used to reproduce limits on a simplified DM model, obtaining results consistent with a previously published search using the same data set. Limits are also set on a model involving an additional Higgs doublet and a pseudoscalar coupling to a DM particle, where again they are similar to those obtained in searches, with extended sensitivity in some regions due to the use of the VBF phase space in addition to the ≥ 1 jet region. The derived constraints are found to be only marginally weaker than for dedicated searches, while eliminating the need for complicated detector simulations. The published results can consequently be directly used for future interpretations. Information about uncertainties and correlations is provided on HEPData, along with a Rivet analysis, to facilitate the use of this LHC Run 2 measurement in future studies with other new physics models and improved SM predictions, as they become available.

Acknowledgments

We thank CERN for the very successful operation of the LHC and its injectors, as well as the support staff at CERN and at our institutions worldwide without whom ATLAS could not be operated efficiently.

JHEP08(2024)223

The crucial computing support from all WLCG partners is acknowledged gratefully, in particular from CERN, the ATLAS Tier-1 facilities at TRIUMF/SFU (Canada), NDGF (Denmark, Norway, Sweden), CC-IN2P3 (France), KIT/GridKA (Germany), INFN-CNAF (Italy), NL-T1 (The Netherlands), PIC (Spain), RAL (U.K.) and BNL (U.S.A.), the Tier-2 facilities worldwide and large non-WLCG resource providers. Major contributors of computing resources are listed in ref. [119].

We gratefully acknowledge the support of ANPCyT, Argentina; YerPhI, Armenia; ARC, Australia; BMWFW and FWF, Austria; ANAS, Azerbaijan; CNPq and FAPESP, Brazil; NSERC, NRC and CFI, Canada; CERN; ANID, Chile; CAS, MOST and NSFC, China; Minciencias, Colombia; MEYS CR, Czech Republic; DNRF and DNSRC, Denmark; IN2P3-CNRS and CEA-DRF/IRFU, France; SRNSFG, Georgia; BMBF, HGF and MPG, Germany; GSRI, Greece; RGC and Hong Kong SAR, China; ISF and Benoziyo Center, Israel; INFN, Italy; MEXT and JSPS, Japan; CNRST, Morocco; NWO, The Netherlands; RCN, Norway; FCT, Portugal; MNE/IFA, Romania; MESTD, Serbia; MSSR, Slovakia; ARRS and MIZŠ, Slovenia; DSI/NRF, South Africa; MICINN, Spain; SRC and Wallenberg Foundation, Sweden; SERI, SNSF and Cantons of Bern and Geneva, Switzerland; MOST, Taipei; TENMAK, Türkiye; STFC, United Kingdom; DOE and NSF, United States of America.

Individual groups and members have received support from BCKDF, CANARIE, CRC and DRAC, Canada; CERN-CZ, PRIMUS 21/SCI/017 and UNCE SCI/013, Czech Republic; COST, ERC, ERDF, Horizon 2020, ICSC-NextGenerationEU and Marie Skłodowska-Curie Actions, European Union; Investissements d'Avenir Labex, Investissements d'Avenir Idex and ANR, France; DFG and AvH Foundation, Germany; Herakleitos, Thales and Aristeia programmes co-financed by EU-ESF and the Greek NSRF, Greece; BSF-NSF and MINERVA, Israel; Norwegian Financial Mechanism 2014–2021, Norway; NCN and NAWA, Poland; La Caixa Banking Foundation, CERCA Programme Generalitat de Catalunya and PROMETEO and GenT Programmes Generalitat Valenciana, Spain; Göran Gustafssons Stiftelse, Sweden; The Royal Society and Leverhulme Trust, United Kingdom.

In addition, individual members wish to acknowledge support from CERN: European Organization for Nuclear Research (CERN PJAS); Chile: Agencia Nacional de Investigación y Desarrollo (FONDECYT 1190886, FONDECYT 1210400, FONDECYT 1230812, FONDECYT 1230987); China: National Natural Science Foundation of China (NSFC — 12175119, NSFC 12275265, NSFC-12075060); Czech Republic: PRIMUS Research Programme (PRIMUS/21/SCI/017); EU: H2020 European Research Council (ERC — 101002463); European Union: European Research Council (ERC — 948254, ERC 101089007), Horizon 2020 Framework Programme (MUCCA — CHIST-ERA-19-XAI-00), European Union, Future Artificial Intelligence Research (FAIR-NextGenerationEU PE00000013), Italian Center for High Performance Computing, Big Data and Quantum Computing (ICSC, NextGenerationEU); France: Agence Nationale de la Recherche (ANR-20-CE31-0013, ANR-21-CE31-0013, ANR-21-CE31-0022), Investissements d'Avenir Labex (ANR-11-LABX-0012); Germany: Baden-Württemberg Stiftung (BW Stiftung-Postdoc Eliteprogramme), Deutsche Forschungsgemeinschaft (DFG — 469666862, DFG — CR 312/5-2); Italy: Istituto Nazionale di Fisica Nucleare (ICSC, NextGenerationEU); Japan: Japan Society for the Promotion of Science (JSPS KAKENHI JP21H05085, JSPS KAKENHI JP22H01227, JSPS KAKENHI JP22H04944, JSPS KAKENHI JP22KK0227); The Netherlands: Netherlands Organisation for Scientific Research (NWO

Veni 2020 — VI.Veni.202.179); Norway: Research Council of Norway (RCN-314472); Poland: Polish National Agency for Academic Exchange (PPN/PPO/2020/1/00002/U/00001), Polish National Science Centre (NCN 2021/42/E/ST2/00350, NCN OPUS nr 2022/47/B/ST2/03059, NCN UMO-2019/34/E/ST2/00393, UMO-2020/37/B/ST2/01043, UMO-2021/40/C/ST2/00187, UMO-2022/47/O/ST2/00148); Slovenia: Slovenian Research Agency (ARIS grant J1-3010); Spain: BBVA Foundation (LEO22-1-603), Generalitat Valenciana (Artemisa, FEDER, IDIFEDER/2018/048), La Caixa Banking Foundation (LCF/BQ/PI20/11760025), Ministry of Science and Innovation (MCIN & NextGenEU PCI2022-135018-2, MICIN & FEDER PID2021-125273NB, RYC2019-028510-I, RYC2020-030254-I, RYC2021-031273-I, RYC2022-038164-I), PROMETEO and GenT Programmes Generalitat Valenciana (CIDEGENT/2019/023, CIDEGENT/2019/027); Sweden: Swedish Research Council (VR 2018-00482, VR 2022-03845, VR 2022-04683, VR grant 2021-03651), Knut and Alice Wallenberg Foundation (KAW 2017.0100, KAW 2018.0157, KAW 2018.0458, KAW 2019.0447, KAW 2022.0358); Switzerland: Swiss National Science Foundation (SNSF — PCEFP2_194658); United Kingdom: Leverhulme Trust (Leverhulme Trust RPG-2020-004); United States of America: U.S. Department of Energy (ECA DE-AC02-76SF00515), Neubauer Family Foundation.

References

[1] G. Bertone, D. Hooper and J. Silk, *Particle dark matter: Evidence, candidates and constraints*, *Phys. Rep.* **405** (2005) 279 [hep-ph/0404175] [INSPIRE].

[2] V. Trimble, *Existence and Nature of Dark Matter in the Universe*, *Ann. Rev. Astron. Astrophys.* **25** (1987) 425 [INSPIRE].

[3] J.L. Feng, *Dark Matter Candidates from Particle Physics and Methods of Detection*, *Ann. Rev. Astron. Astrophys.* **48** (2010) 495 [arXiv:1003.0904] [INSPIRE].

[4] ATLAS collaboration, *Search for new phenomena in events with an energetic jet and missing transverse momentum in pp collisions at* $\sqrt{s} = 13$ *TeV with the ATLAS detector*, *Phys. Rev. D* **103** (2021) 112006 [arXiv:2102.10874] [INSPIRE].

[5] CMS collaboration, *Search for new particles in events with energetic jets and large missing transverse momentum in proton-proton collisions at* $\sqrt{s} = 13$ *TeV*, *JHEP* **11** (2021) 153 [arXiv:2107.13021] [INSPIRE].

[6] CMS collaboration, *Measurement of the Z boson differential production cross section using its invisible decay mode* ($Z\nu\bar{\nu}$) *in proton-proton collisions at* $\sqrt{s} = 13$ *TeV*, *JHEP* **05** (2021) 205 [arXiv:2012.09254] [INSPIRE].

[7] ATLAS collaboration, *Measurement of the Z boson invisible width at* $\sqrt{s} = 13$ *TeV with the ATLAS detector*, *Phys. Lett. B* **854** (2024) 138705 [arXiv:2312.02789] [INSPIRE].

[8] ATLAS collaboration, *Measurement of detector-corrected observables sensitive to the anomalous production of events with jets and large missing transverse momentum in pp collisions at* $\sqrt{s} = 13$ *TeV using the ATLAS detector*, *Eur. Phys. J. C* **77** (2017) 765 [arXiv:1707.03263] [INSPIRE].

[9] J. Abdallah et al., *Simplified Models for Dark Matter Searches at the LHC*, *Phys. Dark Univ.* **9–10** (2015) 8 [arXiv:1506.03116] [INSPIRE].

[10] M. Bauer, U. Haisch and F. Kahlhoefer, *Simplified dark matter models with two Higgs doublets. Part I. Pseudoscalar mediators*, *JHEP* **05** (2017) 138 [arXiv:1701.07427] [INSPIRE].

[11] LHC Dark Matter Working Group, *LHC Dark Matter Working Group: Next-generation spin-0 dark matter models*, *Phys. Dark Univ.* **27** (2020) 100351 [arXiv:1810.09420] [INSPIRE].

[12] CMS collaboration, *Search for dark matter produced in association with a leptonically decaying Z boson in proton-proton collisions at* $\sqrt{s} = 13$ *TeV*, *Eur. Phys. J. C* **81** (2021) 13 [*Erratum ibid.* **81** (2021) 333] [arXiv:2008.04735] [INSPIRE].

[13] ATLAS collaboration, *Combination and summary of ATLAS dark matter searches interpreted in a 2HDM with a pseudo-scalar mediator using* $139\,fb^{-1}$ *of* $\sqrt{s} = 13$ *TeV pp collision data*, arXiv:2306.00641 [INSPIRE].

[14] ATLAS collaboration, *The ATLAS Experiment at the CERN Large Hadron Collider*, 2008 *JINST* **3** S08003 [INSPIRE].

[15] G. Avoni et al., *The new LUCID-2 detector for luminosity measurement and monitoring in ATLAS*, 2018 *JINST* **13** P07017 [INSPIRE].

[16] ATLAS collaboration, *Performance of the ATLAS Trigger System in 2015*, *Eur. Phys. J. C* **77** (2017) 317 [arXiv:1611.09661] [INSPIRE].

[17] ATLAS collaboration, *The ATLAS collaboration Software and Firmware*, ATL-SOFT-PUB-2021-001 (2021).

[18] M. Cacciari, G.P. Salam and G. Soyez, *The anti-*k_t *jet clustering algorithm*, *JHEP* **04** (2008) 063 [arXiv:0802.1189] [INSPIRE].

[19] M. Cacciari, G.P. Salam and G. Soyez, *FastJet User Manual*, *Eur. Phys. J. C* **72** (2012) 1896 [arXiv:1111.6097] [INSPIRE].

[20] F.U. Bernlochner et al., *Angles on CP-violation in Higgs boson interactions*, *Phys. Lett. B* **790** (2019) 372 [arXiv:1808.06577] [INSPIRE].

[21] E. Maguire, L. Heinrich and G. Watt, *HEPData: a repository for high energy physics data*, *J. Phys. Conf. Ser.* **898** (2017) 102006 [arXiv:1704.05473] [INSPIRE].

[22] C. Bierlich et al., *Robust Independent Validation of Experiment and Theory: Rivet version 3*, *SciPost Phys.* **8** (2020) 026 [arXiv:1912.05451] [INSPIRE].

[23] GEANT4 collaboration, *GEANT4 — a simulation toolkit*, *Nucl. Instrum. Meth. A* **506** (2003) 250 [INSPIRE].

[24] J. Allison et al., *GEANT4 developments and applications*, *IEEE Trans. Nucl. Sci.* **53** (2006) 270 [INSPIRE].

[25] ATLAS collaboration, *The ATLAS Simulation Infrastructure*, *Eur. Phys. J. C* **70** (2010) 823 [arXiv:1005.4568] [INSPIRE].

[26] T. Gleisberg et al., *Event generation with SHERPA 1.1*, *JHEP* **02** (2009) 007 [arXiv:0811.4622] [INSPIRE].

[27] F. Cascioli, P. Maierhofer and S. Pozzorini, *Scattering Amplitudes with Open Loops*, *Phys. Rev. Lett.* **108** (2012) 111601 [arXiv:1111.5206] [INSPIRE].

JHEP08(2024)223

[28] A. Denner, S. Dittmaier and L. Hofer, *Collier: a fortran-based Complex One-Loop LIbrary in Extended Regularizations*, Comput. Phys. Commun. **212** (2017) 220 [arXiv:1604.06792] [INSPIRE].

[29] T. Gleisberg and S. Höche, *Comix, a new matrix element generator*, JHEP **12** (2008) 039 [arXiv:0808.3674] [INSPIRE].

[30] S. Schumann and F. Krauss, *A Parton shower algorithm based on Catani-Seymour dipole factorisation*, JHEP **03** (2008) 038 [arXiv:0709.1027] [INSPIRE].

[31] J.-C. Winter, F. Krauss and G. Soff, *A Modified cluster hadronization model*, Eur. Phys. J. C **36** (2004) 381 [hep-ph/0311085] [INSPIRE].

[32] NNPDF collaboration, *Parton distributions for the LHC Run II*, JHEP **04** (2015) 040 [arXiv:1410.8849] [INSPIRE].

[33] S. Höche, F. Krauss, M. Schönherr and F. Siegert, *A critical appraisal of NLO + PS matching methods*, JHEP **09** (2012) 049 [arXiv:1111.1220] [INSPIRE].

[34] S. Catani, F. Krauss, B.R. Webber and R. Kühn, *QCD matrix elements + parton showers*, JHEP **11** (2001) 063 [hep-ph/0109231] [INSPIRE].

[35] S. Höche, F. Krauss, S. Schumann and F. Siegert, *QCD matrix elements and truncated showers*, JHEP **05** (2009) 053 [arXiv:0903.1219] [INSPIRE].

[36] S. Höche, F. Krauss, M. Schönherr and F. Siegert, *QCD matrix elements + parton showers: The NLO case*, JHEP **04** (2013) 027 [arXiv:1207.5030] [INSPIRE].

[37] F. Siegert, *A practical guide to event generation for prompt photon production with Sherpa*, J. Phys. G **44** (2017) 044007 [arXiv:1611.07226] [INSPIRE].

[38] S. Frixione, *Isolated photons in perturbative QCD*, Phys. Lett. B **429** (1998) 369 [hep-ph/9801442] [INSPIRE].

[39] E. Bothmann et al., *Event Generation with Sherpa 2.2*, SciPost Phys. **7** (2019) 034 [arXiv:1905.09127] [INSPIRE].

[40] ATLAS collaboration, *Multi-Boson Simulation for* 13 *TeV ATLAS Analyses*, ATL-PHYS-PUB-2017-005 (2017).

[41] S. Frixione, G. Ridolfi and P. Nason, *A Positive-weight next-to-leading-order Monte Carlo for heavy flavour hadroproduction*, JHEP **09** (2007) 126 [arXiv:0707.3088] [INSPIRE].

[42] P. Nason, *A New method for combining NLO QCD with shower Monte Carlo algorithms*, JHEP **11** (2004) 040 [hep-ph/0409146] [INSPIRE].

[43] S. Frixione, P. Nason and C. Oleari, *Matching NLO QCD computations with Parton Shower simulations: the POWHEG method*, JHEP **11** (2007) 070 [arXiv:0709.2092] [INSPIRE].

[44] S. Alioli, P. Nason, C. Oleari and E. Re, *A general framework for implementing NLO calculations in shower Monte Carlo programs: the POWHEG BOX*, JHEP **06** (2010) 043 [arXiv:1002.2581] [INSPIRE].

[45] ATLAS collaboration, *Studies on top-quark Monte Carlo modelling for Top2016*, ATL-PHYS-PUB-2016-020 (2016).

[46] T. Sjöstrand et al., *An introduction to PYTHIA 8.2*, Comput. Phys. Commun. **191** (2015) 159 [arXiv:1410.3012] [INSPIRE].

[47] ATLAS collaboration, *ATLAS Pythia 8 tunes to* 7 *TeV data*, ATL-PHYS-PUB-2014-021 (2014).

JHEP08(2024)223

[48] NNPDF collaboration, *Parton distributions with LHC data*, Nucl. Phys. B **867** (2013) 244 [arXiv:1207.1303] [INSPIRE].

[49] M. Beneke, P. Falgari, S. Klein and C. Schwinn, *Hadronic top-quark pair production with NNLL threshold resummation*, Nucl. Phys. B **855** (2012) 695 [arXiv:1109.1536] [INSPIRE].

[50] M. Cacciari, M. Czakon, M. Mangano, A. Mitov and P. Nason, *Top-pair production at hadron colliders with next-to-next-to-leading logarithmic soft-gluon resummation*, Phys. Lett. B **710** (2012) 612 [arXiv:1111.5869] [INSPIRE].

[51] P. Bärnreuther, M. Czakon and A. Mitov, *Percent Level Precision Physics at the Tevatron: First Genuine NNLO QCD Corrections to $q\bar{q} \to t\bar{t} + X$*, Phys. Rev. Lett. **109** (2012) 132001 [arXiv:1204.5201] [INSPIRE].

[52] M. Czakon and A. Mitov, *NNLO corrections to top-pair production at hadron colliders: the all-fermionic scattering channels*, JHEP **12** (2012) 054 [arXiv:1207.0236] [INSPIRE].

[53] M. Czakon and A. Mitov, *NNLO corrections to top pair production at hadron colliders: the quark-gluon reaction*, JHEP **01** (2013) 080 [arXiv:1210.6832] [INSPIRE].

[54] M. Czakon, P. Fiedler and A. Mitov, *Total Top-Quark Pair-Production Cross Section at Hadron Colliders Through $O(\alpha_S^4)$*, Phys. Rev. Lett. **110** (2013) 252004 [arXiv:1303.6254] [INSPIRE].

[55] M. Czakon and A. Mitov, *Top++: A Program for the Calculation of the Top-Pair Cross-Section at Hadron Colliders*, Comput. Phys. Commun. **185** (2014) 2930 [arXiv:1112.5675] [INSPIRE].

[56] E. Re, *Single-top Wt-channel production matched with parton showers using the POWHEG method*, Eur. Phys. J. C **71** (2011) 1547 [arXiv:1009.2450] [INSPIRE].

[57] S. Frixione, E. Laenen, P. Motylinski, C. White and B.R. Webber, *Single-top hadroproduction in association with a W boson*, JHEP **07** (2008) 029 [arXiv:0805.3067] [INSPIRE].

[58] R. Frederix, E. Re and P. Torrielli, *Single-top t-channel hadroproduction in the four-flavour scheme with POWHEG and aMC@NLO*, JHEP **09** (2012) 130 [arXiv:1207.5391] [INSPIRE].

[59] S. Alioli, P. Nason, C. Oleari and E. Re, *NLO single-top production matched with shower in POWHEG: s- and t-channel contributions*, JHEP **09** (2009) 111 [*Erratum ibid.* **02** (2010) 011] [arXiv:0907.4076] [INSPIRE].

[60] M. Aliev, H. Lacker, U. Langenfeld, S. Moch, P. Uwer and M. Wiedermann, *HATHOR: HAdronic Top and Heavy quarks crOss section calculatoR*, Comput. Phys. Commun. **182** (2011) 1034 [arXiv:1007.1327] [INSPIRE].

[61] P. Kant et al., *HatHor for single top-quark production: Updated predictions and uncertainty estimates for single top-quark production in hadronic collisions*, Comput. Phys. Commun. **191** (2015) 74 [arXiv:1406.4403] [INSPIRE].

[62] ATLAS collaboration, *The Pythia 8 A3 tune description of ATLAS minimum bias and inelastic measurements incorporating the Donnachie-Landshoff diffractive model*, ATL-PHYS-PUB-2016-017 (2016).

[63] F. Buccioni et al., *OpenLoops 2*, Eur. Phys. J. C **79** (2019) 866 [arXiv:1907.13071] [INSPIRE].

[64] F. Buccioni, S. Pozzorini and M. Zoller, *On-the-fly reduction of open loops*, Eur. Phys. J. C **78** (2018) 70 [arXiv:1710.11452] [INSPIRE].

[65] J. Butterworth et al., *PDF4LHC recommendations for LHC Run II*, J. Phys. G **43** (2016) 023001 [arXiv:1510.03865] [INSPIRE].

[66] NNPDF collaboration, *Illuminating the photon content of the proton within a global PDF analysis*, SciPost Phys. **5** (2018) 008 [arXiv:1712.07053] [INSPIRE].

JHEP08(2024)223

[67] J.M. Lindert et al., *Precise predictions for V + jets dark matter backgrounds*, *Eur. Phys. J. C* **77** (2017) 829 [arXiv:1705.04664] [INSPIRE].

[68] A. Denner, S. Dittmaier, T. Kasprzik and A. Mück, *Electroweak corrections to dilepton + jet production at hadron colliders*, *JHEP* **06** (2011) 069 [arXiv:1103.0914] [INSPIRE].

[69] A. Denner, S. Dittmaier, T. Kasprzik and A. Mück, *Electroweak corrections to monojet production at the LHC*, *Eur. Phys. J. C* **73** (2013) 2297 [arXiv:1211.5078] [INSPIRE].

[70] S. Kallweit, J.M. Lindert, P. Maierhöfer, S. Pozzorini and M. Schönherr, *NLO QCD + EW predictions for V + jets including off-shell vector-boson decays and multijet merging*, *JHEP* **04** (2016) 021 [arXiv:1511.08692] [INSPIRE].

[71] A. Denner, S. Dittmaier, T. Kasprzik and A. Mück, *Electroweak corrections to W + jet hadroproduction including leptonic W-boson decays*, *JHEP* **08** (2009) 075 [arXiv:0906.1656] [INSPIRE].

[72] J.H. Kühn, A. Kulesza, S. Pozzorini and M. Schulze, *Logarithmic electroweak corrections to hadronic $Z+1$ jet production at large transverse momentum*, *Phys. Lett. B* **609** (2005) 277 [hep-ph/0408308] [INSPIRE].

[73] J.H. Kühn, A. Kulesza, S. Pozzorini and M. Schulze, *Electroweak corrections to large transverse momentum production of W bosons at the LHC*, *Phys. Lett. B* **651** (2007) 160 [hep-ph/0703283] [INSPIRE].

[74] J.H. Kühn, A. Kulesza, S. Pozzorini and M. Schulze, *One-loop weak corrections to hadronic production of Z bosons at large transverse momenta*, *Nucl. Phys. B* **727** (2005) 368 [hep-ph/0507178] [INSPIRE].

[75] J.H. Kühn, A. Kulesza, S. Pozzorini and M. Schulze, *Electroweak corrections to hadronic production of W bosons at large transverse momenta*, *Nucl. Phys. B* **797** (2008) 27 [arXiv:0708.0476] [INSPIRE].

[76] A. Gehrmann-De Ridder, T. Gehrmann, E.W.N. Glover, A. Huss and T.A. Morgan, *Precise QCD predictions for the production of a Z boson in association with a hadronic jet*, *Phys. Rev. Lett.* **117** (2016) 022001 [arXiv:1507.02850] [INSPIRE].

[77] A. Gehrmann-De Ridder, T. Gehrmann, E.W.N. Glover, A. Huss and T.A. Morgan, *The NNLO QCD corrections to Z boson production at large transverse momentum*, *JHEP* **07** (2016) 133 [arXiv:1605.04295] [INSPIRE].

[78] R. Boughezal, X. Liu and F. Petriello, *Phenomenology of the Z-boson plus jet process at NNLO*, *Phys. Rev. D* **94** (2016) 074015 [arXiv:1602.08140] [INSPIRE].

[79] R. Boughezal, X. Liu and F. Petriello, *W-boson plus jet differential distributions at NNLO in QCD*, *Phys. Rev. D* **94** (2016) 113009 [arXiv:1602.06965] [INSPIRE].

[80] ATLAS collaboration, *Measurements of the production cross section of a Z boson in association with jets in pp collisions at $\sqrt{s} = 13$ TeV with the ATLAS detector*, *Eur. Phys. J. C* **77** (2017) 361 [arXiv:1702.05725] [INSPIRE].

[81] J.M. Lindert, S. Pozzorini and M. Schönherr, *Precise predictions for $V + 2$ jet backgrounds in searches for invisible Higgs decays*, *JHEP* **01** (2023) 070 [arXiv:2204.07652] [INSPIRE].

[82] J.R. Andersen and J.M. Smillie, *Constructing All-Order Corrections to Multi-Jet Rates*, *JHEP* **01** (2010) 039 [arXiv:0908.2786] [INSPIRE].

[83] J.R. Andersen and J.M. Smillie, *Multiple Jets at the LHC with High Energy Jets*, *JHEP* **06** (2011) 010 [arXiv:1101.5394] [INSPIRE].

[84] J.R. Andersen et al., *HEJ 2.2: W boson pairs and Higgs boson plus jet production at high energies*, arXiv:2303.15778 [DOI:10.21468/SciPostPhysCodeb.21] [INSPIRE].

[85] T. Sjöstrand, S. Mrenna and P.Z. Skands, *A Brief Introduction to PYTHIA 8.1*, *Comput. Phys. Commun.* **178** (2008) 852 [arXiv:0710.3820] [INSPIRE].

[86] B. Andersson, G. Gustafson, G. Ingelman and T. Sjöstrand, *Parton Fragmentation and String Dynamics*, *Phys. Rep.* **97** (1983) 31 [INSPIRE].

[87] T. Sjöstrand, *Jet Fragmentation of Nearby Partons*, *Nucl. Phys. B* **248** (1984) 469 [INSPIRE].

[88] ATLAS collaboration, *Luminosity determination in pp collisions at* $\sqrt{s} = 13$ *TeV using the ATLAS detector at the LHC*, *Eur. Phys. J. C* **83** (2023) 982 [arXiv:2212.09379] [INSPIRE].

[89] ATLAS collaboration, *Performance of the missing transverse momentum triggers for the ATLAS detector during Run-2 data taking*, *JHEP* **08** (2020) 080 [arXiv:2005.09554] [INSPIRE].

[90] ATLAS collaboration, *Performance of electron and photon triggers in ATLAS during LHC Run 2*, *Eur. Phys. J. C* **80** (2020) 47 [arXiv:1909.00761] [INSPIRE].

[91] ATLAS collaboration, *Vertex Reconstruction Performance of the ATLAS Detector at* $\sqrt{s} = 13$ *TeV*, ATL-PHYS-PUB-2015-026 (2015).

[92] ATLAS collaboration, *Electron and photon performance measurements with the ATLAS detector using the 2015–2017 LHC proton-proton collision data*, 2019 *JINST* **14** P12006 [arXiv:1908.00005] [INSPIRE].

[93] ATLAS collaboration, *Topological cell clustering in the ATLAS calorimeters and its performance in LHC Run 1*, *Eur. Phys. J. C* **77** (2017) 490 [arXiv:1603.02934] [INSPIRE].

[94] ATLAS collaboration, *Electron and photon energy calibration with the ATLAS detector using 2015–2016 LHC proton-proton collision data*, 2019 *JINST* **14** P03017 [arXiv:1812.03848] [INSPIRE].

[95] ATLAS collaboration, *Muon reconstruction and identification efficiency in ATLAS using the full Run 2 pp collision data set at* $\sqrt{s} = 13$ *TeV*, *Eur. Phys. J. C* **81** (2021) 578 [arXiv:2012.00578] [INSPIRE].

[96] ATLAS collaboration, *Muon reconstruction performance of the ATLAS detector in proton-proton collision data at* $\sqrt{s} = 13$ *TeV*, *Eur. Phys. J. C* **76** (2016) 292 [arXiv:1603.05598] [INSPIRE].

[97] ATLAS collaboration, *Reconstruction, Energy Calibration, and Identification of Hadronically Decaying Tau Leptons in the ATLAS Experiment for Run-2 of the LHC*, ATL-PHYS-PUB-2015-045 (2015).

[98] ATLAS collaboration, *Identification of hadronic tau lepton decays using neural networks in the ATLAS experiment*, ATL-PHYS-PUB-2019-033 (2019).

[99] ATLAS collaboration, *Jet reconstruction and performance using particle flow with the ATLAS Detector*, *Eur. Phys. J. C* **77** (2017) 466 [arXiv:1703.10485] [INSPIRE].

[100] ATLAS collaboration, *Selection of jets produced in* 13 *TeV proton-proton collisions with the ATLAS detector*, ATLAS-CONF-2015-029 (2015).

[101] ATLAS collaboration, *Performance of pile-up mitigation techniques for jets in pp collisions at* $\sqrt{s} = 8$ *TeV using the ATLAS detector*, *Eur. Phys. J. C* **76** (2016) 581 [arXiv:1510.03823] [INSPIRE].

[102] ATLAS collaboration, *Forward Jet Vertex Tagging: A new technique for the identification and rejection of forward pileup jets*, ATL-PHYS-PUB-2015-034 (2015).

JHEP08(2024)223

[103] ATLAS collaboration, *Jet energy scale and resolution measured in proton-proton collisions at $\sqrt{s} = 13$ TeV with the ATLAS detector*, *Eur. Phys. J. C* **81** (2021) 689 [arXiv:2007.02645] [INSPIRE].

[104] ATLAS collaboration, *Performance of algorithms that reconstruct missing transverse momentum in $\sqrt{s} = 8$ TeV proton-proton collisions in the ATLAS detector*, *Eur. Phys. J. C* **77** (2017) 241 [arXiv:1609.09324] [INSPIRE].

[105] ATLAS collaboration, *Search for squarks and gluinos with the ATLAS detector in final states with jets and missing transverse momentum using 4.7 fb^{-1} of $\sqrt{s} = 7$ TeV proton-proton collision data*, *Phys. Rev. D* **87** (2013) 012008 [arXiv:1208.0949] [INSPIRE].

[106] ATLAS collaboration, *Measurement of the inclusive isolated prompt photon cross section in pp collisions at $\sqrt{s} = 8$ TeV with the ATLAS detector*, *JHEP* **08** (2016) 005 [arXiv:1605.03495] [INSPIRE].

[107] ATLAS collaboration, *Measurement of the cross section for isolated-photon plus jet production in pp collisions at $\sqrt{s} = 13$ TeV using the ATLAS detector*, *Phys. Lett. B* **780** (2018) 578 [arXiv:1801.00112] [INSPIRE].

[108] ATLAS collaboration, *Tools for estimating fake/non-prompt lepton backgrounds with the ATLAS detector at the LHC*, 2023 *JINST* **18** T11004 [arXiv:2211.16178] [INSPIRE].

[109] ATLAS collaboration, *Measurement of the tau lepton reconstruction and identification performance in the ATLAS experiment using pp collisions at $\sqrt{s} = 13$ TeV*, ATLAS-CONF-2017-029 (2017).

[110] ATLAS collaboration, *Performance of missing transverse momentum reconstruction with the ATLAS detector using proton-proton collisions at $\sqrt{s} = 13$ TeV*, *Eur. Phys. J. C* **78** (2018) 903 [arXiv:1802.08168] [INSPIRE].

[111] X. Chen, T. Gehrmann, N. Glover, M. Höfer and A. Huss, *Isolated photon and photon + jet production at NNLO QCD accuracy*, *JHEP* **04** (2020) 166 [arXiv:1904.01044] [INSPIRE].

[112] ATLAS collaboration, *Evaluating statistical uncertainties and correlations using the bootstrap method*, ATL-PHYS-PUB-2021-011 (2021).

[113] P. Pani and G. Polesello, *Dark matter production in association with a single top-quark at the LHC in a two-Higgs-doublet model with a pseudoscalar mediator*, *Phys. Dark Univ.* **21** (2018) 8 [arXiv:1712.03874] [INSPIRE].

[114] X. Cid Vidal et al., *Report from Working Group 3: Beyond the Standard Model physics at the HL-LHC and HE-LHC*, in *CERN Yellow Reports: Monographs* **7**, CERN (2019), pp. 585–865 [DOI:10.23731/CYRM-2019-007.585] [arXiv:1812.07831] [INSPIRE].

[115] ATLAS collaboration, *ATLAS sensitivity to Two-Higgs-Doublet models with an additional pseudoscalar exploiting four top quark signatures with 3 ab^{-1} of $\sqrt{s} = 14$ TeV proton-proton collisions*, ATL-PHYS-PUB-2018-027 (2018).

[116] U. Haisch and G. Polesello, *Searching for heavy Higgs bosons in the $t\bar{t}Z$ and tbW final states*, *JHEP* **09** (2018) 151 [arXiv:1807.07734] [INSPIRE].

[117] J.M. Butterworth, M. Habedank, P. Pani and A. Vaitkus, *A study of collider signatures for two Higgs doublet models with a Pseudoscalar mediator to Dark Matter*, *SciPost Phys. Core* **4** (2021) 003 [arXiv:2009.02220] [INSPIRE].

[118] T. Robens, *The THDMa Revisited*, *Symmetry* **13** (2021) 2341 [arXiv:2106.02962] [INSPIRE].

[119] ATLAS collaboration, *ATLAS Computing Acknowledgements*, ATL-SOFT-PUB-2023-001 (2023).

The ATLAS collaboration

G. Aad[103], E. Aakvaag[16], B. Abbott[121], K. Abeling[55], N.J. Abicht[49], S.H. Abidi[29], M. Aboelela[44], A. Aboulhorma[35e], H. Abramowicz[152], H. Abreu[151], Y. Abulaiti[118], B.S. Acharya[69a,69b,l], A. Ackermann[63a], C. Adam Bourdarios[4], L. Adamczyk[86a], S.V. Addepalli[26], M.J. Addison[102], J. Adelman[116], A. Adiguzel[21c], T. Adye[135], A.A. Affolder[137], Y. Afik[39], M.N. Agaras[13], J. Agarwala[73a,73b], A. Aggarwal[101], C. Agheorghiesei[27c], A. Ahmad[36], F. Ahmadov[38,y], W.S. Ahmed[105], S. Ahuja[96], X. Ai[62e], G. Aielli[76a,76b], A. Aikot[164], M. Ait Tamlihat[35e], B. Aitbenchikh[35a], I. Aizenberg[170], M. Akbiyik[101], T.P.A. Åkesson[99], A.V. Akimov[37], D. Akiyama[169], N.N. Akolkar[24], S. Aktas[21a], K. Al Khoury[41], G.L. Alberghi[23b], J. Albert[166], P. Albicocco[53], G.L. Albouy[60], S. Alderweireldt[52], Z.L. Alegria[122], M. Aleksa[36], I.N. Aleksandrov[38], C. Alexa[27b], T. Alexopoulos[10], F. Alfonsi[23b], M. Algren[56], M. Alhroob[142], B. Ali[133], H.M.J. Ali[92], S. Ali[149], S.W. Alibocus[93], M. Aliev[33c], G. Alimonti[71a], W. Alkakhi[55], C. Allaire[66], B.M.M. Allbrooke[147], J.F. Allen[52], C.A. Allendes Flores[138f], P.P. Allport[20], A. Aloisio[72a,72b], F. Alonso[91], C. Alpigiani[139], M. Alvarez Estevez[100], A. Alvarez Fernandez[101], M. Alves Cardoso[56], M.G. Alviggi[72a,72b], M. Aly[102], Y. Amaral Coutinho[83b], A. Ambler[105], C. Amelung[36], M. Amerl[102], C.G. Ames[110], D. Amidei[107], K.J. Amirie[156], S.P. Amor Dos Santos[131a], K.R. Amos[164], S. An[84], V. Ananiev[126], C. Anastopoulos[140], T. Andeen[11], J.K. Anders[36], S.Y. Andrean[47a,47b], A. Andreazza[71a,71b], S. Angelidakis[9], A. Angerami[41,aa], A.V. Anisenkov[37], A. Annovi[74a], C. Antel[56], M.T. Anthony[140], E. Antipov[146], M. Antonelli[53], F. Anulli[75a], M. Aoki[84], T. Aoki[154], J.A. Aparisi Pozo[164], M.A. Aparo[147], L. Aperio Bella[48], C. Appelt[18], A. Apyan[26], S.J. Arbiol Val[87], C. Arcangeletti[53], A.T.H. Arce[51], E. Arena[93], J-F. Arguin[109], S. Argyropoulos[54], J.-H. Arling[48], O. Arnaez[4], H. Arnold[115], G. Artoni[75a,75b], H. Asada[112], K. Asai[119], S. Asai[154], N.A. Asbah[36], K. Assamagan[29], R. Astalos[28a], K.S.V. Astrand[99], S. Atashi[160], R.J. Atkin[33a], M. Atkinson[163], H. Atmani[35f], P.A. Atmasiddha[129], K. Augsten[133], S. Auricchio[72a,72b], A.D. Auriol[20], V.A. Austrup[102], G. Avolio[36], K. Axiotis[56], G. Azuelos[109,ae], D. Babal[28b], H. Bachacou[136], K. Bachas[153,p], A. Bachiu[34], F. Backman[47a,47b], A. Badea[39], T.M. Baer[107], P. Bagnaia[75a,75b], M. Bahmani[18], D. Bahner[54], K. Bai[124], A.J. Bailey[164], J.T. Baines[135], L. Baines[95], O.K. Baker[173], E. Bakos[15], D. Bakshi Gupta[8], V. Balakrishnan[121], R. Balasubramanian[115], E.M. Baldin[37], P. Balek[86a], E. Ballabene[23b,23a], F. Balli[136], L.M. Baltes[63a], W.K. Balunas[32], J. Balz[101], E. Banas[87], M. Bandieramonte[130], A. Bandyopadhyay[24], S. Bansal[24], L. Barak[152], M. Barakat[48], E.L. Barberio[106], D. Barberis[57b,57a], M. Barbero[103], M.Z. Barel[115], K.N. Barends[33a], T. Barillari[111], M-S. Barisits[36], T. Barklow[144], P. Baron[123], D.A. Baron Moreno[102], A. Baroncelli[62a], G. Barone[29], A.J. Barr[127], J.D. Barr[97], F. Barreiro[100], J. Barreiro Guimarães da Costa[14a], U. Barron[152], M.G. Barros Teixeira[131a], S. Barsov[37], F. Bartels[63a], R. Bartoldus[144], A.E. Barton[92], P. Bartos[28a], A. Basan[101], M. Baselga[49], A. Bassalat[66,b], M.J. Basso[157a], R.L. Bates[59], S. Batlamous[35e], B. Batool[142], M. Battaglia[137], D. Battulga[18], M. Bauce[75a,75b], M. Bauer[36], P. Bauer[24], L.T. Bazzano Hurrell[30], J.B. Beacham[51], T. Beau[128], J.Y. Beaucamp[91], P.H. Beauchemin[159], P. Bechtle[24], H.P. Beck[19,o],

JHEP08(2024)223

K. Becker[168], A.J. Beddall[82], V.A. Bednyakov[38], C.P. Bee[146], L.J. Beemster[15], T.A. Beermann[36], M. Begalli[83d], M. Begel[29], A. Behera[146], J.K. Behr[48], J.F. Beirer[36], F. Beisiegel[24], M. Belfkir[117b], G. Bella[152], L. Bellagamba[23b], A. Bellerive[34], P. Bellos[20], K. Beloborodov[37], D. Benchekroun[35a], F. Bendebba[35a], Y. Benhammou[152], K.C. Benkendorfer[61], L. Beresford[48], M. Beretta[53], E. Bergeaas Kuutmann[162], N. Berger[4], B. Bergmann[133], J. Beringer[17a], G. Bernardi[5], C. Bernius[144], F.U. Bernlochner[24], F. Bernon[36,103], A. Berrocal Guardia[13], T. Berry[96], P. Berta[134], A. Berthold[50], S. Bethke[111], A. Betti[75a,75b], A.J. Bevan[95], N.K. Bhalla[54], M. Bhamjee[33c], S. Bhatta[146], D.S. Bhattacharya[167], P. Bhattarai[144], K.D. Bhide[54], V.S. Bhopatkar[122], R.M. Bianchi[130], G. Bianco[23b,23a], O. Biebel[110], R. Bielski[124], M. Biglietti[77a], C.S. Billingsley[44], M. Bindi[55], A. Bingul[21b], C. Bini[75a,75b], A. Biondini[93], C.J. Birch-sykes[102], G.A. Bird[32], M. Birman[170], M. Biros[134], S. Biryukov[147], T. Bisanz[49], E. Bisceglie[43b,43a], J.P. Biswal[135], D. Biswas[142], K. Bjørke[126], I. Bloch[48], A. Blue[59], U. Blumenschein[95], J. Blumenthal[101], V.S. Bobrovnikov[37], M. Boehler[54], B. Boehm[167], D. Bogavac[36], A.G. Bogdanchikov[37], C. Bohm[47a], V. Boisvert[96], P. Bokan[36], T. Bold[86a], M. Bomben[5], M. Bona[95], M. Boonekamp[136], C.D. Booth[96], A.G. Borbély[59], I.S. Bordulev[37], H.M. Borecka-Bielska[109], G. Borissov[92], D. Bortoletto[127], D. Boscherini[23b], M. Bosman[13], J.D. Bossio Sola[36], K. Bouaouda[35a], N. Bouchhar[164], J. Boudreau[130], E.V. Bouhova-Thacker[92], D. Boumediene[40], R. Bouquet[57b,57a], A. Boveia[120], J. Boyd[36], D. Boye[29], I.R. Boyko[38], J. Bracinik[20], N. Brahimi[4], G. Brandt[172], O. Brandt[32], F. Braren[48], B. Brau[104], J.E. Brau[124], R. Brener[170], L. Brenner[115], R. Brenner[162], S. Bressler[170], D. Britton[59], D. Britzger[111], I. Brock[24], G. Brooijmans[41], E. Brost[29], L.M. Brown[166], L.E. Bruce[61], T.L. Bruckler[127], P.A. Bruckman de Renstrom[87], B. Brüers[48], A. Bruni[23b], G. Bruni[23b], M. Bruschi[23b], N. Bruscino[75a,75b], T. Buanes[16], Q. Buat[139], D. Buchin[111], A.G. Buckley[59], O. Bulekov[37], B.A. Bullard[144], S. Burdin[93], C.D. Burgard[49], A.M. Burger[36], B. Burghgrave[8], O. Burlayenko[54], J.T.P. Burr[32], C.D. Burton[11], J.C. Burzynski[143], E.L. Busch[41], V. Büscher[101], P.J. Bussey[59], J.M. Butler[25], C.M. Buttar[59], J.M. Butterworth[97], W. Buttinger[135], C.J. Buxo Vazquez[108], A.R. Buzykaev[37], S. Cabrera Urbán[164], L. Cadamuro[66], D. Caforio[58], H. Cai[130], Y. Cai[14a,14e], Y. Cai[14c], V.M.M. Cairo[36], O. Cakir[3a], N. Calace[36], P. Calafiura[17a], G. Calderini[128], P. Calfayan[68], G. Callea[59], L.P. Caloba[83b], D. Calvet[40], S. Calvet[40], M. Calvetti[74a,74b], R. Camacho Toro[128], S. Camarda[36], D. Camarero Munoz[26], P. Camarri[76a,76b], M.T. Camerlingo[72a,72b], D. Cameron[36], C. Camincher[166], M. Campanelli[97], A. Camplani[42], V. Canale[72a,72b], A.C. Canbay[3a], E. Canonero[96], J. Cantero[164], Y. Cao[163], F. Capocasa[26], M. Capua[43b,43a], A. Carbone[71a,71b], R. Cardarelli[76a], J.C.J. Cardenas[8], F. Cardillo[164], G. Carducci[43b,43a], T. Carli[36], G. Carlino[72a], J.I. Carlotto[13], B.T. Carlson[130,q], E.M. Carlson[166,157a], L. Carminati[71a,71b], A. Carnelli[136], M. Carnesale[75a,75b], S. Caron[114], E. Carquin[138f], S. Carrá[71a], G. Carratta[23b,23a], A.M. Carroll[124], T.M. Carter[52], M.P. Casado[13,i], M. Caspar[48], F.L. Castillo[4], L. Castillo Garcia[13], V. Castillo Gimenez[164], N.F. Castro[131a,131e], A. Catinaccio[36], J.R. Catmore[126], T. Cavaliere[4], V. Cavaliere[29], N. Cavalli[23b,23a], Y.C. Cekmecelioglu[48], E. Celebi[21a], S. Cella[36], F. Celli[127], M.S. Centonze[70a,70b], V. Cepaitis[56], K. Cerny[123], A.S. Cerqueira[83a], A. Cerri[147], L. Cerrito[76a,76b], F. Cerutti[17a], B. Cervato[142], A. Cervelli[23b], G. Cesarini[53],

JHEP08(2024)223

S.A. Cetin[82], D. Chakraborty[116], J. Chan[17a], W.Y. Chan[154], J.D. Chapman[32], E. Chapon[136], B. Chargeishvili[150b], D.G. Charlton[20], M. Chatterjee[19], C. Chauhan[134], Y. Che[14c], S. Chekanov[6], S.V. Chekulaev[157a], G.A. Chelkov[38,a], A. Chen[107], B. Chen[152], B. Chen[166], H. Chen[14c], H. Chen[29], J. Chen[62c], J. Chen[143], M. Chen[127], S. Chen[154], S.J. Chen[14c], X. Chen[62c,136], X. Chen[14b,ad], Y. Chen[62a], C.L. Cheng[171], H.C. Cheng[64a], S. Cheong[144], A. Cheplakov[38], E. Cheremushkina[48], E. Cherepanova[115], R. Cherkaoui El Moursli[35e], E. Cheu[7], K. Cheung[65], L. Chevalier[136], V. Chiarella[53], G. Chiarelli[74a], N. Chiedde[103], G. Chiodini[70a], A.S. Chisholm[20], A. Chitan[27b], M. Chitishvili[164], M.V. Chizhov[38], K. Choi[11], Y. Chou[139], E.Y.S. Chow[114], K.L. Chu[170], M.C. Chu[64a], X. Chu[14a,14e], J. Chudoba[132], J.J. Chwastowski[87], D. Cieri[111], K.M. Ciesla[86a], V. Cindro[94], A. Ciocio[17a], F. Cirotto[72a,72b], Z.H. Citron[170], M. Citterio[71a], D.A. Ciubotaru[27b], A. Clark[56], P.J. Clark[52], C. Clarry[156], J.M. Clavijo Columbie[48], S.E. Clawson[48], C. Clement[47a,47b], J. Clercx[48], Y. Coadou[103], M. Cobal[69a,69c], A. Coccaro[57b], R.F. Coelho Barrue[131a], R. Coelho Lopes De Sa[104], S. Coelli[71a], B. Cole[41], J. Collot[60], P. Conde Muiño[131a,131g], M.P. Connell[33c], S.H. Connell[33c], E.I. Conroy[127], F. Conventi[72a,af], H.G. Cooke[20], A.M. Cooper-Sarkar[127], A. Cordeiro Oudot Choi[128], L.D. Corpe[40], M. Corradi[75a,75b], F. Corriveau[105,w], A. Cortes-Gonzalez[18], M.J. Costa[164], F. Costanza[4], D. Costanzo[140], B.M. Cote[120], G. Cowan[96], K. Cranmer[171], D. Cremonini[23b,23a], S. Crépé-Renaudin[60], F. Crescioli[128], M. Cristinziani[142], M. Cristoforetti[78a,78b], V. Croft[115], J.E. Crosby[122], G. Crosetti[43b,43a], A. Cueto[100], H. Cui[14a,14e], Z. Cui[7], W.R. Cunningham[59], F. Curcio[164], J.R. Curran[52], P. Czodrowski[36], M.M. Czurylo[36], M.J. Da Cunha Sargedas De Sousa[57b,57a], J.V. Da Fonseca Pinto[83b], C. Da Via[102], W. Dabrowski[86a], T. Dado[49], S. Dahbi[149], T. Dai[107], D. Dal Santo[19], C. Dallapiccola[104], M. Dam[42], G. D'amen[29], V. D'Amico[110], J. Damp[101], J.R. Dandoy[34], M. Danninger[143], V. Dao[36], G. Darbo[57b], S.J. Das[29,ag], F. Dattola[48], S. D'Auria[71a,71b], A. D'avanzo[72a,72b], C. David[33a], T. Davidek[134], B. Davis-Purcell[34], I. Dawson[95], H.A. Day-hall[133], K. De[8], R. De Asmundis[72a], N. De Biase[48], S. De Castro[23b,23a], N. De Groot[114], P. de Jong[115], H. De la Torre[116], A. De Maria[14c], A. De Salvo[75a], U. De Sanctis[76a,76b], F. De Santis[70a,70b], A. De Santo[147], J.B. De Vivie De Regie[60], D.V. Dedovich[38], J. Degens[93], A.M. Deiana[44], F. Del Corso[23b,23a], J. Del Peso[100], F. Del Rio[63a], L. Delagrange[128], F. Deliot[136], C.M. Delitzsch[49], M. Della Pietra[72a,72b], D. Della Volpe[56], A. Dell'Acqua[36], L. Dell'Asta[71a,71b], M. Delmastro[4], P.A. Delsart[60], S. Demers[173], M. Demichev[38], S.P. Denisov[37], L. D'Eramo[40], D. Derendarz[87], F. Derue[128], P. Dervan[93], K. Desch[24], C. Deutsch[24], F.A. Di Bello[57b,57a], A. Di Ciaccio[76a,76b], L. Di Ciaccio[4], A. Di Domenico[75a,75b], C. Di Donato[72a,72b], A. Di Girolamo[36], G. Di Gregorio[36], A. Di Luca[78a,78b], B. Di Micco[77a,77b], R. Di Nardo[77a,77b], M. Diamantopoulou[34], F.A. Dias[115], T. Dias Do Vale[143], M.A. Diaz[138a,138b], F.G. Diaz Capriles[24], M. Didenko[164], E.B. Diehl[107], S. Díez Cornell[48], C. Diez Pardos[142], C. Dimitriadi[162,24], A. Dimitrievska[17a], J. Dingfelder[24], I-M. Dinu[27b], S.J. Dittmeier[63b], F. Dittus[36], M. Divisek[134], F. Djama[103], T. Djobava[150b], C. Doglioni[102,99], A. Dohnalova[28a], J. Dolejsi[134], Z. Dolezal[134], K.M. Dona[39], M. Donadelli[83c], B. Dong[108], J. Donini[40], A. D'Onofrio[72a,72b], M. D'Onofrio[93], J. Dopke[135], A. Doria[72a], N. Dos Santos Fernandes[131a], P. Dougan[102], M.T. Dova[91], A.T. Doyle[59], M.A. Draguet[127],

E. Dreyer[170], I. Drivas-koulouris[10], M. Drnevich[118], M. Drozdova[56], D. Du[62a], T.A. du Pree[115], F. Dubinin[37], M. Dubovsky[28a], E. Duchovni[170], G. Duckeck[110], O.A. Ducu[27b], D. Duda[52], A. Dudarev[36], E.R. Duden[26], M. D'uffizi[102], L. Duflot[66], M. Dührssen[36], I. Duminica[27g], A.E. Dumitriu[27b], M. Dunford[63a], S. Dungs[49], K. Dunne[47a,47b], A. Duperrin[103], H. Duran Yildiz[3a], M. Düren[58], A. Durglishvili[150b], B.L. Dwyer[116], G.I. Dyckes[17a], M. Dyndal[86a], B.S. Dziedzic[87], Z.O. Earnshaw[147], G.H. Eberwein[127], B. Eckerova[28a], S. Eggebrecht[55], E. Egidio Purcino De Souza[128], L.F. Ehrke[56], G. Eigen[16], K. Einsweiler[17a], T. Ekelof[162], P.A. Ekman[99], S. El Farkh[35b], Y. El Ghazali[35b], H. El Jarrari[36], A. El Moussaouy[109], V. Ellajosyula[162], M. Ellert[162], F. Ellinghaus[172], N. Ellis[36], J. Elmsheuser[29], M. Elsawy[117a], M. Elsing[36], D. Emeliyanov[135], Y. Enari[154], I. Ene[17a], S. Epari[13], P.A. Erland[87], M. Errenst[172], M. Escalier[66], C. Escobar[164], E. Etzion[152], G. Evans[131a], H. Evans[68], L.S. Evans[96], A. Ezhilov[37], S. Ezzarqtouni[35a], F. Fabbri[23b,23a], L. Fabbri[23b,23a], G. Facini[97], V. Fadeyev[137], R.M. Fakhrutdinov[37], D. Fakoudis[101], S. Falciano[75a], L.F. Falda Ulhoa Coelho[36], P.J. Falke[24], F. Fallavollita[111], J. Faltova[134], C. Fan[163], Y. Fan[14a], Y. Fang[14a,14e], M. Fanti[71a,71b], M. Faraj[69a,69b], Z. Farazpay[98], A. Farbin[8], A. Farilla[77a], T. Farooque[108], S.M. Farrington[52], F. Fassi[35e], D. Fassouliotis[9], M. Faucci Giannelli[76a,76b], W.J. Fawcett[32], L. Fayard[66], P. Federic[134], P. Federicova[132], O.L. Fedin[37,a], M. Feickert[171], L. Feligioni[103], D.E. Fellers[124], C. Feng[62b], M. Feng[14b], Z. Feng[115], M.J. Fenton[160], L. Ferencz[48], R.A.M. Ferguson[92], S.I. Fernandez Luengo[138f], P. Fernandez Martinez[13], M.J.V. Fernoux[103], J. Ferrando[92], A. Ferrari[162], P. Ferrari[115,114], R. Ferrari[73a], D. Ferrere[56], C. Ferretti[107], F. Fiedler[101], P. Fiedler[133], A. Filipčič[94], E.K. Filmer[1], F. Filthaut[114], M.C.N. Fiolhais[131a,131c,c], L. Fiorini[164], W.C. Fisher[108], T. Fitschen[102], P.M. Fitzhugh[136], I. Fleck[142], P. Fleischmann[107], T. Flick[172], M. Flores[33d,ab], L.R. Flores Castillo[64a], L. Flores Sanz De Acedo[36], F.M. Follega[78a,78b], N. Fomin[16], J.H. Foo[156], A. Formica[136], A.C. Forti[102], E. Fortin[36], A.W. Fortman[17a], M.G. Foti[17a], L. Fountas[9,j], D. Fournier[66], H. Fox[92], P. Francavilla[74a,74b], S. Francescato[61], S. Franchellucci[56], M. Franchini[23b,23a], S. Franchino[63a], D. Francis[36], L. Franco[114], V. Franco Lima[36], L. Franconi[48], M. Franklin[61], G. Frattari[26], W.S. Freund[83b], Y.Y. Frid[152], J. Friend[59], N. Fritzsche[50], A. Froch[54], D. Froidevaux[36], J.A. Frost[127], Y. Fu[62a], S. Fuenzalida Garrido[138f], M. Fujimoto[103], K.Y. Fung[64a], E. Furtado De Simas Filho[83e], M. Furukawa[154], J. Fuster[164], A. Gabrielli[23b,23a], A. Gabrielli[156], P. Gadow[36], G. Gagliardi[57b,57a], L.G. Gagnon[17a], S. Galantzan[152], E.J. Gallas[127], B.J. Gallop[135], K.K. Gan[120], S. Ganguly[154], Y. Gao[52], F.M. Garay Walls[138a,138b], B. Garcia[29], C. García[164], A. Garcia Alonso[115], A.G. Garcia Caffaro[173], J.E. García Navarro[164], M. Garcia-Sciveres[17a], G.L. Gardner[129], R.W. Gardner[39], N. Garelli[159], D. Garg[80], R.B. Garg[144,m], J.M. Gargan[52], C.A. Garner[156], C.M. Garvey[33a], P. Gaspar[83b], V.K. Gassmann[159], G. Gaudio[73a], V. Gautam[13], P. Gauzzi[75a,75b], I.L. Gavrilenko[37], A. Gavrilyuk[37], C. Gay[165], G. Gaycken[48], E.N. Gazis[10], A.A. Geanta[27b], C.M. Gee[137], A. Gekow[120], C. Gemme[57b], M.H. Genest[60], A.D. Gentry[113], S. George[96], W.F. George[20], T. Geralis[46], P. Gessinger-Befurt[36], M.E. Geyik[172], M. Ghani[168], K. Ghorbanian[95], A. Ghosal[142], A. Ghosh[160], A. Ghosh[7], B. Giacobbe[23b], S. Giagu[75a,75b], T. Giani[115], P. Giannetti[74a], A. Giannini[62a], S.M. Gibson[96], M. Gignac[137], D.T. Gil[86b], A.K. Gilbert[86a], B.J. Gilbert[41],

D. Gillberg[34], G. Gilles[115], L. Ginabat[128], D.M. Gingrich[2,ae], M.P. Giordani[69a,69c], P.F. Giraud[136], G. Giugliarelli[69a,69c], D. Giugni[71a], F. Giuli[36], I. Gkialas[9,j], L.K. Gladilin[37], C. Glasman[100], G.R. Gledhill[124], G. Glemža[48], M. Glisic[124], I. Gnesi[43b,f], Y. Go[29], M. Goblirsch-Kolb[36], B. Gocke[49], D. Godin[109], B. Gokturk[21a], S. Goldfarb[106], T. Golling[56], M.G.D. Gololo[33g], D. Golubkov[37], J.P. Gombas[108], A. Gomes[131a,131b], G. Gomes Da Silva[142], A.J. Gomez Delegido[164], R. Gonçalo[131a,131c], L. Gonella[20], A. Gongadze[150c], F. Gonnella[20], J.L. Gonski[144], R.Y. González Andana[52], S. González de la Hoz[164], R. Gonzalez Lopez[93], C. Gonzalez Renteria[17a], M.V. Gonzalez Rodrigues[48], R. Gonzalez Suarez[162], S. Gonzalez-Sevilla[56], L. Goossens[36], B. Gorini[36], E. Gorini[70a,70b], A. Gorišek[94], T.C. Gosart[129], A.T. Goshaw[51], M.I. Gostkin[38], S. Goswami[122], C.A. Gottardo[36], S.A. Gotz[110], M. Gouighri[35b], V. Goumarre[48], A.G. Goussiou[139], N. Govender[33c], I. Grabowska-Bold[86a], K. Graham[34], E. Gramstad[126], S. Grancagnolo[70a,70b], C.M. Grant[1,136], P.M. Gravila[27f], F.G. Gravili[70a,70b], H.M. Gray[17a], M. Greco[70a,70b], C. Grefe[24], I.M. Gregor[48], K.T. Greif[160], P. Grenier[144], S.G. Grewe[111], A.A. Grillo[137], K. Grimm[31], S. Grinstein[13,s], J.-F. Grivaz[66], E. Gross[170], J. Grosse-Knetter[55], J.C. Grundy[127], L. Guan[107], C. Gubbels[165], J.G.R. Guerrero Rojas[164], G. Guerrieri[69a,69c], F. Guescini[111], R. Gugel[101], J.A.M. Guhit[107], A. Guida[18], E. Guilloton[168], S. Guindon[36], F. Guo[14a,14e], J. Guo[62c], L. Guo[48], Y. Guo[107], R. Gupta[48], R. Gupta[130], S. Gurbuz[24], S.S. Gurdasani[54], G. Gustavino[36], M. Guth[56], P. Gutierrez[121], L.F. Gutierrez Zagazeta[129], M. Gutsche[50], C. Gutschow[97], C. Gwenlan[127], C.B. Gwilliam[93], E.S. Haaland[126], A. Haas[118], M. Habedank[48], C. Haber[17a], H.K. Hadavand[8], A. Hadef[50], S. Hadzic[111], A.I. Hagan[92], J.J. Hahn[142], E.H. Haines[97], M. Haleem[167], J. Haley[122], J.J. Hall[140], G.D. Hallewell[103], L. Halser[19], K. Hamano[166], M. Hamer[24], G.N. Hamity[52], E.J. Hampshire[96], J. Han[62b], K. Han[62a], L. Han[14c], L. Han[62a], S. Han[17a], Y.F. Han[156], K. Hanagaki[84], M. Hance[137], D.A. Hangal[41], H. Hanif[143], M.D. Hank[129], J.B. Hansen[42], P.H. Hansen[42], K. Hara[158], D. Harada[56], T. Harenberg[172], S. Harkusha[37], M.L. Harris[104], Y.T. Harris[127], J. Harrison[13], N.M. Harrison[120], P.F. Harrison[168], N.M. Hartman[111], N.M. Hartmann[110], Y. Hasegawa[141], S. Hassan[16], R. Hauser[108], C.M. Hawkes[20], R.J. Hawkings[36], Y. Hayashi[154], S. Hayashida[112], D. Hayden[108], C. Hayes[107], R.L. Hayes[115], C.P. Hays[127], J.M. Hays[95], H.S. Hayward[93], F. He[62a], M. He[14a,14e], Y. He[155], Y. He[48], Y. He[97], N.B. Heatley[95], V. Hedberg[99], A.L. Heggelund[126], N.D. Hehir[95,*], C. Heidegger[54], K.K. Heidegger[54], W.D. Heidorn[81], J. Heilman[34], S. Heim[48], T. Heim[17a], J.G. Heinlein[129], J.J. Heinrich[124], L. Heinrich[111,ac], J. Hejbal[132], A. Held[171], S. Hellesund[16], C.M. Helling[165], S. Hellman[47a,47b], R.C.W. Henderson[92], L. Henkelmann[32], A.M. Henriques Correia[36], H. Herde[99], Y. Hernández Jiménez[146], L.M. Herrmann[24], T. Herrmann[50], G. Herten[54], R. Hertenberger[110], L. Hervas[36], M.E. Hesping[101], N.P. Hessey[157a], E. Hill[156], S.J. Hillier[20], J.R. Hinds[108], F. Hinterkeuser[24], M. Hirose[125], S. Hirose[158], D. Hirschbuehl[172], T.G. Hitchings[102], B. Hiti[94], J. Hobbs[146], R. Hobincu[27e], N. Hod[170], M.C. Hodgkinson[140], B.H. Hodkinson[127], A. Hoecker[36], D.D. Hofer[107], J. Hofer[48], T. Holm[24], M. Holzbock[111], L.B.A.H. Hommels[32], B.P. Honan[102], J. Hong[62c], T.M. Hong[130], B.H. Hooberman[163], W.H. Hopkins[6], Y. Horii[112], S. Hou[149], A.S. Howard[94], J. Howarth[59], J. Hoya[6], M. Hrabovsky[123], A. Hrynevich[48], T. Hryn'ova[4], P.J. Hsu[65], S.-C. Hsu[139], M. Hu[17a],

Q. Hu[62a], S. Huang[64b], X. Huang[14a,14e], Y. Huang[140], Y. Huang[14a], Z. Huang[102], Z. Hubacek[133], M. Huebner[24], F. Huegging[24], T.B. Huffman[127], C.A. Hugli[48], M. Huhtinen[36], S.K. Huiberts[16], R. Hulsken[105], N. Huseynov[12], J. Huston[108], J. Huth[61], R. Hyneman[144], G. Iacobucci[56], G. Iakovidis[29], I. Ibragimov[142], L. Iconomidou-Fayard[66], J.P. Iddon[36], P. Iengo[72a,72b], R. Iguchi[154], T. Iizawa[127], Y. Ikegami[84], N. Ilic[156], H. Imam[35a], M. Ince Lezki[56], T. Ingebretsen Carlson[47a,47b], G. Introzzi[73a,73b], M. Iodice[77a], V. Ippolito[75a,75b], R.K. Irwin[93], M. Ishino[154], W. Islam[171], C. Issever[18,48], S. Istin[21a,ai], H. Ito[169], R. Iuppa[78a,78b], A. Ivina[170], J.M. Izen[45], V. Izzo[72a], P. Jacka[132,133], P. Jackson[1], B.P. Jaeger[143], C.S. Jagfeld[110], G. Jain[157a], P. Jain[54], K. Jakobs[54], T. Jakoubek[170], J. Jamieson[59], K.W. Janas[86a], M. Javurkova[104], L. Jeanty[124], J. Jejelava[150a,z], P. Jenni[54,g], C.E. Jessiman[34], C. Jia[62b], J. Jia[146], X. Jia[61], X. Jia[14a,14e], Z. Jia[14c], C. Jiang[52], S. Jiggins[48], J. Jimenez Pena[13], S. Jin[14c], A. Jinaru[27b], O. Jinnouchi[155], P. Johansson[140], K.A. Johns[7], J.W. Johnson[137], D.M. Jones[147], E. Jones[48], P. Jones[32], R.W.L. Jones[92], T.J. Jones[93], H.L. Joos[55,36], R. Joshi[120], J. Jovicevic[15], X. Ju[17a], J.J. Junggeburth[104], T. Junkermann[63a], A. Juste Rozas[13,s], M.K. Juzek[87], S. Kabana[138e], A. Kaczmarska[87], M. Kado[111], H. Kagan[120], M. Kagan[144], A. Kahn[41], A. Kahn[129], C. Kahra[101], T. Kaji[154], E. Kajomovitz[151], N. Kakati[170], I. Kalaitzidou[54], C.W. Kalderon[29], N.J. Kang[137], D. Kar[33g], K. Karava[127], M.J. Kareem[157b], E. Karentzos[54], I. Karkanias[153], O. Karkout[115], S.N. Karpov[38], Z.M. Karpova[38], V. Kartvelishvili[92], A.N. Karyukhin[37], E. Kasimi[153], J. Katzy[48], S. Kaur[34], K. Kawade[141], M.P. Kawale[121], C. Kawamoto[88], T. Kawamoto[62a], E.F. Kay[36], F.I. Kaya[159], S. Kazakos[108], V.F. Kazanin[37], Y. Ke[146], J.M. Keaveney[33a], R. Keeler[166], G.V. Kehris[61], J.S. Keller[34], A.S. Kelly[97], J.J. Kempster[147], P.D. Kennedy[101], O. Kepka[132], B.P. Kerridge[135], S. Kersten[172], B.P. Kerševan[94], L. Keszeghova[28a], S. Ketabchi Haghighat[156], R.A. Khan[130], A. Khanov[122], A.G. Kharlamov[37], T. Kharlamova[37], E.E. Khoda[139], M. Kholodenko[37], T.J. Khoo[18], G. Khoriauli[167], J. Khubua[150b,*], Y.A.R. Khwaira[66], B. Kibirige[33g], A. Kilgallon[124], D.W. Kim[47a,47b], Y.K. Kim[39], N. Kimura[97], M.K. Kingston[55], A. Kirchhoff[55], C. Kirfel[24], F. Kirfel[24], J. Kirk[135], A.E. Kiryunin[111], C. Kitsaki[10], O. Kivernyk[24], M. Klassen[63a], C. Klein[34], L. Klein[167], M.H. Klein[44], S.B. Klein[56], U. Klein[93], P. Klimek[36], A. Klimentov[29], T. Klioutchnikova[36], P. Kluit[115], S. Kluth[111], E. Kneringer[79], T.M. Knight[156], A. Knue[49], R. Kobayashi[88], D. Kobylianskii[170], S.F. Koch[127], M. Kocian[144], P. Kodyš[134], D.M. Koeck[124], P.T. Koenig[24], T. Koffas[34], O. Kolay[50], I. Koletsou[4], T. Komarek[123], K. Köneke[54], A.X.Y. Kong[1], T. Kono[119], V. Konstantinides[97], N. Konstantinidis[97], P. Kontaxakis[56], B. Konya[99], R. Kopeliansky[41], S. Koperny[86a], K. Korcyl[87], K. Kordas[153,e], A. Korn[97], S. Korn[55], I. Korolkov[13], N. Korotkova[37], B. Kortman[115], O. Kortner[111], S. Kortner[111], W.H. Kostecka[116], V.V. Kostyukhin[142], A. Kotsokechagia[136], A. Kotwal[51], A. Koulouris[36], A. Kourkoumeli-Charalampidi[73a,73b], C. Kourkoumelis[9], E. Kourlitis[111,ac], O. Kovanda[124], R. Kowalewski[166], W. Kozanecki[136], A.S. Kozhin[37], V.A. Kramarenko[37], G. Kramberger[94], P. Kramer[101], M.W. Krasny[128], A. Krasznahorkay[36], J.W. Kraus[172], J.A. Kremer[48], T. Kresse[50], J. Kretzschmar[93], K. Kreul[18], P. Krieger[156], S. Krishnamurthy[104], M. Krivos[134], K. Krizka[20], K. Kroeninger[49], H. Kroha[111], J. Kroll[132], J. Kroll[129], K.S. Krowpman[108], U. Kruchonak[38], H. Krüger[24], N. Krumnack[81], M.C. Kruse[51],

JHEP08(2024)223

O. Kuchinskaia[37], S. Kuday[3a], S. Kuehn[36], R. Kuesters[54], T. Kuhl[48], V. Kukhtin[38], Y. Kulchitsky[37,a], S. Kuleshov[138d,138b], M. Kumar[33g], N. Kumari[48], P. Kumari[157b], A. Kupco[132], T. Kupfer[49], A. Kupich[37], O. Kuprash[54], H. Kurashige[85], L.L. Kurchaninov[157a], O. Kurdysh[66], Y.A. Kurochkin[37], A. Kurova[37], M. Kuze[155], A.K. Kvam[104], J. Kvita[123], T. Kwan[105], N.G. Kyriacou[107], L.A.O. Laatu[103], C. Lacasta[164], F. Lacava[75a,75b], H. Lacker[18], D. Lacour[128], N.N. Lad[97], E. Ladygin[38], A. Lafarge[40], B. Laforge[128], T. Lagouri[173], F.Z. Lahbabi[35a], S. Lai[55], I.K. Lakomiec[86a], N. Lalloue[60], J.E. Lambert[166], S. Lammers[68], W. Lampl[7], C. Lampoudis[153,e], G. Lamprinoudis[101], A.N. Lancaster[116], E. Lançon[29], U. Landgraf[54], M.P.J. Landon[95], V.S. Lang[54], O.K.B. Langrekken[126], A.J. Lankford[160], F. Lanni[36], K. Lantzsch[24], A. Lanza[73a], A. Lapertosa[57b,57a], J.F. Laporte[136], T. Lari[71a], F. Lasagni Manghi[23b], M. Lassnig[36], V. Latonova[132], A. Laudrain[101], A. Laurier[151], S.D. Lawlor[140], Z. Lawrence[102], R. Lazaridou[168], M. Lazzaroni[71a,71b], B. Le[102], E.M. Le Boulicaut[51], L.T. Le Pottier[17a], B. Leban[23b,23a], A. Lebedev[81], M. LeBlanc[102], F. Ledroit-Guillon[60], A.C.A. Lee[97], S.C. Lee[149], S. Lee[47a,47b], T.F. Lee[93], L.L. Leeuw[33c], H.P. Lefebvre[96], M. Lefebvre[166], C. Leggett[17a], G. Lehmann Miotto[36], M. Leigh[56], W.A. Leight[104], W. Leinonen[114], A. Leisos[153,r], M.A.L. Leite[83c], C.E. Leitgeb[18], R. Leitner[134], K.J.C. Leney[44], T. Lenz[24], S. Leone[74a], C. Leonidopoulos[52], A. Leopold[145], C. Leroy[109], R. Les[108], C.G. Lester[32], M. Levchenko[37], J. Levêque[4], L.J. Levinson[170], G. Levrini[23b,23a], M.P. Lewicki[87], D.J. Lewis[4], A. Li[5], B. Li[62b], C. Li[62a], C-Q. Li[111], H. Li[62a], H. Li[62b], H. Li[14c], H. Li[14b], H. Li[62b], J. Li[62c], K. Li[139], L. Li[62c], M. Li[14a,14e], Q.Y. Li[62a], S. Li[14a,14e], S. Li[62d,62c,d], T. Li[5], X. Li[105], Z. Li[127], Z. Li[154], Z. Li[14a,14e], S. Liang[14a,14e], Z. Liang[14a], M. Liberatore[136], B. Liberti[76a], K. Lie[64c], J. Lieber Marin[83e], H. Lien[68], K. Lin[108], R.E. Lindley[7], J.H. Lindon[2], E. Lipeles[129], A. Lipniacka[16], A. Lister[165], J.D. Little[4], B. Liu[14a], B.X. Liu[143], D. Liu[62d,62c], E.H.L. Liu[20], J.B. Liu[62a], J.K.K. Liu[32], K. Liu[62d], K. Liu[62d,62c], M. Liu[62a], M.Y. Liu[62a], P. Liu[14a], Q. Liu[62d,139,62c], X. Liu[62a], X. Liu[62b], Y. Liu[14d,14e], Y.L. Liu[62b], Y.W. Liu[62a], J. Llorente Merino[143], S.L. Lloyd[95], E.M. Lobodzinska[48], P. Loch[7], T. Lohse[18], K. Lohwasser[140], E. Loiacono[48], M. Lokajicek[132,*], J.D. Lomas[20], J.D. Long[163], I. Longarini[160], L. Longo[70a,70b], R. Longo[163], I. Lopez Paz[67], A. Lopez Solis[48], N. Lorenzo Martinez[4], A.M. Lory[110], G. Löschcke Centeno[147], O. Loseva[37], X. Lou[47a,47b], X. Lou[14a,14e], A. Lounis[66], P.A. Love[92], G. Lu[14a,14e], M. Lu[66], S. Lu[129], Y.J. Lu[65], H.J. Lubatti[139], C. Luci[75a,75b], F.L. Lucio Alves[14c], F. Luehring[68], I. Luise[146], O. Lukianchuk[66], O. Lundberg[145], B. Lund-Jensen[145,*], N.A. Luongo[6], M.S. Lutz[36], A.B. Lux[25], D. Lynn[29], R. Lysak[132], E. Lytken[99], V. Lyubushkin[38], T. Lyubushkina[38], M.M. Lyukova[146], M.Firdaus M. Soberi[52], H. Ma[29], K. Ma[62a], L.L. Ma[62b], W. Ma[62a], Y. Ma[122], D.M. Mac Donell[166], G. Maccarrone[53], J.C. MacDonald[101], P.C. Machado De Abreu Farias[83e], R. Madar[40], T. Madula[97], J. Maeda[85], T. Maeno[29], H. Maguire[140], V. Maiboroda[136], A. Maio[131a,131b,131d], K. Maj[86a], O. Majersky[48], S. Majewski[124], N. Makovec[66], V. Maksimovic[15], B. Malaescu[128], Pa. Malecki[87], V.P. Maleev[37], F. Malek[60,n], M. Mali[94], D. Malito[96], U. Mallik[80], S. Maltezos[10], S. Malyukov[38], J. Mamuzic[13], G. Mancini[53], M.N. Mancini[26], G. Manco[73a,73b], J.P. Mandalia[95], I. Mandić[94], L. Manhaes de Andrade Filho[83a], I.M. Maniatis[170], J. Manjarres Ramos[90], D.C. Mankad[170], A. Mann[110], S. Manzoni[36],

JHEP08(2024)223

L. Mao[62c], X. Mapekula[33c], A. Marantis[153,r], G. Marchiori[5], M. Marcisovsky[132], C. Marcon[71a], M. Marinescu[20], S. Marium[48], M. Marjanovic[121], M. Markovitch[66], E.J. Marshall[92], Z. Marshall[17a], S. Marti-Garcia[164], T.A. Martin[168], V.J. Martin[52], B. Martin dit Latour[16], L. Martinelli[75a,75b], M. Martinez[13,s], P. Martinez Agullo[164], V.I. Martinez Outschoorn[104], P. Martinez Suarez[13], S. Martin-Haugh[135], G. Martinovicova[134], V.S. Martoiu[27b], A.C. Martyniuk[97], A. Marzin[36], D. Mascione[78a,78b], L. Masetti[101], T. Mashimo[154], J. Masik[102], A.L. Maslennikov[37], P. Massarotti[72a,72b], P. Mastrandrea[74a,74b], A. Mastroberardino[43b,43a], T. Masubuchi[154], T. Mathisen[162], J. Matousek[134], N. Matsuzawa[154], J. Maurer[27b], A.J. Maury[66], B. Maček[94], D.A. Maximov[37], A.E. May[102], R. Mazini[149], I. Maznas[116], M. Mazza[108], S.M. Mazza[137], E. Mazzeo[71a,71b], C. Mc Ginn[29], J.P. Mc Gowan[166], S.P. Mc Kee[107], C.C. McCracken[165], E.F. McDonald[106], A.E. McDougall[115], J.A. Mcfayden[147], R.P. McGovern[129], G. Mchedlidze[150b], R.P. Mckenzie[33g], T.C. Mclachlan[48], D.J. Mclaughlin[97], S.J. McMahon[135], C.M. Mcpartland[93], R.A. McPherson[166,w], S. Mehlhase[110], A. Mehta[93], D. Melini[164], B.R. Mellado Garcia[33g], A.H. Melo[55], F. Meloni[48], S.B. Menary[102], A.M. Mendes Jacques Da Costa[102], H.Y. Meng[156], L. Meng[92], S. Menke[111], M. Mentink[36], E. Meoni[43b,43a], G. Mercado[116], C. Merlassino[69a,69c], L. Merola[72a,72b], C. Meroni[71a,71b], J. Metcalfe[6], A.S. Mete[6], C. Meyer[68], J-P. Meyer[136], R.P. Middleton[135], L. Mijović[52], G. Mikenberg[170], M. Mikestikova[132], M. Mikuž[94], H. Mildner[101], A. Milic[36], D.W. Miller[39], E.H. Miller[144], L.S. Miller[34], A. Milov[170], D.A. Milstead[47a,47b], T. Min[14c], A.A. Minaenko[37], I.A. Minashvili[150b], L. Mince[59], A.I. Mincer[118], B. Mindur[86a], M. Mineev[38], Y. Mino[88], L.M. Mir[13], M. Miralles Lopez[59], M. Mironova[17a], A. Mishima[154], M.C. Missio[114], A. Mitra[168], V.A. Mitsou[164], Y. Mitsumori[112], O. Miu[156], P.S. Miyagawa[95], T. Mkrtchyan[63a], M. Mlinarevic[97], T. Mlinarevic[97], M. Mlynarikova[36], S. Mobius[19], P. Mogg[110], M.H. Mohamed Farook[113], A.F. Mohammed[14a,14e], S. Mohapatra[41], G. Mokgatitswane[33g], L. Moleri[170], B. Mondal[142], S. Mondal[133], K. Mönig[48], E. Monnier[103], L. Monsonis Romero[164], J. Montejo Berlingen[13], M. Montella[120], F. Montereali[77a,77b], F. Monticelli[91], S. Monzani[69a,69c], N. Morange[66], A.L. Moreira De Carvalho[131a], M. Moreno Llácer[164], C. Moreno Martinez[56], P. Morettini[57b], S. Morgenstern[36], M. Morii[61], M. Morinaga[154], F. Morodei[75a,75b], L. Morvaj[36], P. Moschovakos[36], B. Moser[36], M. Mosidze[150b], T. Moskalets[54], P. Moskvitina[114], J. Moss[31,k], A. Moussa[35d], E.J.W. Moyse[104], O. Mtintsilana[33g], S. Muanza[103], J. Mueller[130], D. Muenstermann[92], R. Müller[19], G.A. Mullier[162], A.J. Mullin[32], J.J. Mullin[129], D.P. Mungo[156], D. Munoz Perez[164], F.J. Munoz Sanchez[102], M. Murin[102], W.J. Murray[168,135], M. Muškinja[94], C. Mwewa[29], A.G. Myagkov[37,a], A.J. Myers[8], G. Myers[107], M. Myska[133], B.P. Nachman[17a], O. Nackenhorst[49], K. Nagai[127], K. Nagano[84], J.L. Nagle[29,ag], E. Nagy[103], A.M. Nairz[36], Y. Nakahama[84], K. Nakamura[84], K. Nakkalil[5], H. Nanjo[125], R. Narayan[44], E.A. Narayanan[113], I. Naryshkin[37], M. Naseri[34], S. Nasri[117b], C. Nass[24], G. Navarro[22a], J. Navarro-Gonzalez[164], R. Nayak[152], A. Nayaz[18], P.Y. Nechaeva[37], F. Nechansky[48], L. Nedic[127], T.J. Neep[20], A. Negri[73a,73b], M. Negrini[23b], C. Nellist[115], C. Nelson[105], K. Nelson[107], S. Nemecek[132], M. Nessi[36,h], M.S. Neubauer[163], F. Neuhaus[101], J. Neundorf[48], R. Newhouse[165], P.R. Newman[20], C.W. Ng[130], Y.W.Y. Ng[48], B. Ngair[117a], H.D.N. Nguyen[109], R.B. Nickerson[127], R. Nicolaidou[136], J. Nielsen[137],

M. Niemeyer[55], J. Niermann[55], N. Nikiforou[36], V. Nikolaenko[37,a], I. Nikolic-Audit[128], K. Nikolopoulos[20], P. Nilsson[29], I. Ninca[48], H.R. Nindhito[56], G. Ninio[152], A. Nisati[75a], N. Nishu[2], R. Nisius[111], J-E. Nitschke[50], E.K. Nkadimeng[33g], T. Nobe[154], D.L. Noel[32], T. Nommensen[148], M.B. Norfolk[140], R.R.B. Norisam[97], B.J. Norman[34], M. Noury[35a], J. Novak[94], T. Novak[48], L. Novotny[133], R. Novotny[113], L. Nozka[123], K. Ntekas[160], N.M.J. Nunes De Moura Junior[83b], E. Nurse[97], J. Ocariz[128], A. Ochi[85], I. Ochoa[131a], S. Oerdek[48,t], J.T. Offermann[39], A. Ogrodnik[134], A. Oh[102], C.C. Ohm[145], H. Oide[84], R. Oishi[154], M.L. Ojeda[48], Y. Okumura[154], L.F. Oleiro Seabra[131a], S.A. Olivares Pino[138d], G. Oliveira Correa[13], D. Oliveira Damazio[29], D. Oliveira Goncalves[83a], J.L. Oliver[160], Ö.O. Öncel[54], A.P. O'Neill[19], A. Onofre[131a,131e], P.U.E. Onyisi[11], M.J. Oreglia[39], G.E. Orellana[91], D. Orestano[77a,77b], N. Orlando[13], R.S. Orr[156], V. O'Shea[59], L.M. Osojnak[129], R. Ospanov[62a], G. Otero y Garzon[30], H. Otono[89], P.S. Ott[63a], G.J. Ottino[17a], M. Ouchrif[35d], F. Ould-Saada[126], T. Ovsiannikova[139], M. Owen[59], R.E. Owen[135], K.Y. Oyulmaz[21a], V.E. Ozcan[21a], F. Ozturk[87], N. Ozturk[8], S. Ozturk[82], H.A. Pacey[127], A. Pacheco Pages[13], C. Padilla Aranda[13], G. Padovano[75a,75b], S. Pagan Griso[17a], G. Palacino[68], A. Palazzo[70a,70b], J. Pampel[24], J. Pan[173], T. Pan[64a], D.K. Panchal[11], C.E. Pandini[115], J.G. Panduro Vazquez[96], H.D. Pandya[1], H. Pang[14b], P. Pani[48], G. Panizzo[69a,69c], L. Panwar[128], L. Paolozzi[56], S. Parajuli[163], A. Paramonov[6], C. Paraskevopoulos[53], D. Paredes Hernandez[64b], A. Pareti[73a,73b], K.R. Park[41], T.H. Park[156], M.A. Parker[32], F. Parodi[57b,57a], E.W. Parrish[116], V.A. Parrish[52], J.A. Parsons[41], U. Parzefall[54], B. Pascual Dias[109], L. Pascual Dominguez[152], E. Pasqualucci[75a], S. Passaggio[57b], F. Pastore[96], P. Patel[87], U.M. Patel[51], J.R. Pater[102], T. Pauly[36], C.I. Pazos[159], J. Pearkes[144], M. Pedersen[126], R. Pedro[131a], S.V. Peleganchuk[37], O. Penc[36], E.A. Pender[52], G.D. Penn[173], K.E. Penski[110], M. Penzin[37], B.S. Peralva[83d], A.P. Pereira Peixoto[139], L. Pereira Sanchez[144], D.V. Perepelitsa[29,ag], E. Perez Codina[157a], M. Perganti[10], H. Pernegger[36], O. Perrin[40], K. Peters[48], R.F.Y. Peters[102], B.A. Petersen[36], T.C. Petersen[42], E. Petit[103], V. Petousis[133], C. Petridou[153,e], T. Petru[134], A. Petrukhin[142], M. Pettee[17a], N.E. Pettersson[36], A. Petukhov[37], K. Petukhova[134], R. Pezoa[138f], L. Pezzotti[36], G. Pezzullo[173], T.M. Pham[171], T. Pham[106], P.W. Phillips[135], G. Piacquadio[146], E. Pianori[17a], F. Piazza[124], R. Piegaia[30], D. Pietreanu[27b], A.D. Pilkington[102], M. Pinamonti[69a,69c], J.L. Pinfold[2], B.C. Pinheiro Pereira[131a], A.E. Pinto Pinoargote[101,136], L. Pintucci[69a,69c], K.M. Piper[147], A. Pirttikoski[56], D.A. Pizzi[34], L. Pizzimento[64b], A. Pizzini[115], M.-A. Pleier[29], V. Plesanovs[54], V. Pleskot[134], E. Plotnikova[38], G. Poddar[95], R. Poettgen[99], L. Poggioli[128], I. Pokharel[55], S. Polacek[134], G. Polesello[73a], A. Poley[143,157a], A. Polini[23b], C.S. Pollard[168], Z.B. Pollock[120], E. Pompa Pacchi[75a,75b], D. Ponomarenko[114], L. Pontecorvo[36], S. Popa[27a], G.A. Popeneciu[27d], A. Poreba[36], D.M. Portillo Quintero[157a], S. Pospisil[133], M.A. Postill[140], P. Postolache[27c], K. Potamianos[168], P.A. Potepa[86a], I.N. Potrap[38], C.J. Potter[32], H. Potti[1], J. Poveda[164], M.E. Pozo Astigarraga[36], A. Prades Ibanez[164], J. Pretel[54], D. Price[102], M. Primavera[70a], M.A. Principe Martin[100], R. Privara[123], T. Procter[59], M.L. Proffitt[139], N. Proklova[129], K. Prokofiev[64c], G. Proto[111], J. Proudfoot[6], M. Przybycien[86a], W.W. Przygoda[86b], A. Psallidas[46], J.E. Puddefoot[140], D. Pudzha[37], D. Pyatiizbyantseva[37], J. Qian[107], D. Qichen[102], Y. Qin[13], T. Qiu[52], A. Quadt[55], M. Queitsch-Maitland[102], G. Quetant[56], R.P. Quinn[165], G. Rabanal Bolanos[61], D. Rafanoharana[54], F. Ragusa[71a,71b], J.L. Rainbolt[39], J.A. Raine[56], S. Rajagopalan[29], E. Ramakoti[37], I.A. Ramirez-Berend[34], K. Ran[48,14e], N.P. Rapheeha[33g], H. Rasheed[27b], V. Raskina[128], D.F. Rassloff[63a], A. Rastogi[17a], S. Rave[101], B. Ravina[55], I. Ravinovich[170], M. Raymond[36], A.L. Read[126], N.P. Readioff[140], D.M. Rebuzzi[73a,73b], G. Redlinger[29], A.S. Reed[111], K. Reeves[26], J.A. Reidelsturz[172], D. Reikher[152], A. Rej[49], C. Rembser[36], M. Renda[27b], M.B. Rendel[111], F. Renner[48], A.G. Rennie[160], A.L. Rescia[48], S. Resconi[71a], M. Ressegotti[57b,57a], S. Rettie[36], J.G. Reyes Rivera[108], E. Reynolds[17a], O.L. Rezanova[37], P. Reznicek[134], H. Riani[35d], N. Ribaric[92], E. Ricci[78a,78b], R. Richter[111], S. Richter[47a,47b], E. Richter-Was[86b], M. Ridel[128], S. Ridouani[35d], P. Rieck[118], P. Riedler[36], E.M. Riefel[47a,47b], J.O. Rieger[115], M. Rijssenbeek[146], M. Rimoldi[36], L. Rinaldi[23b,23a], T.T. Rinn[29], M.P. Rinnagel[110], G. Ripellino[162], I. Riu[13], J.C. Rivera Vergara[166], F. Rizatdinova[122], E. Rizvi[95], B.R. Roberts[17a], S.H. Robertson[105,w], D. Robinson[32], C.M. Robles Gajardo[138f], M. Robles Manzano[101], A. Robson[59], A. Rocchi[76a,76b], C. Roda[74a,74b], S. Rodriguez Bosca[36], Y. Rodriguez Garcia[22a], A. Rodriguez Rodriguez[54], A.M. Rodríguez Vera[116], S. Roe[36], J.T. Roemer[160], A.R. Roepe-Gier[137], J. Roggel[172], O. Røhne[126], R.A. Rojas[104], C.P.A. Roland[128], J. Roloff[29], A. Romaniouk[37], E. Romano[73a,73b], M. Romano[23b], A.C. Romero Hernandez[163], N. Rompotis[93], L. Roos[128], S. Rosati[75a], B.J. Rosser[39], E. Rossi[127], E. Rossi[72a,72b], L.P. Rossi[61], L. Rossini[54], R. Rosten[120], M. Rotaru[27b], B. Rottler[54], C. Rougier[90], D. Rousseau[66], D. Rousso[32], A. Roy[163], S. Roy-Garand[156], A. Rozanov[103], Z.M.A. Rozario[59], Y. Rozen[151], A. Rubio Jimenez[164], A.J. Ruby[93], V.H. Ruelas Rivera[18], T.A. Ruggeri[1], A. Ruggiero[127], A. Ruiz-Martinez[164], A. Rummler[36], Z. Rurikova[54], N.A. Rusakovich[38], H.L. Russell[166], G. Russo[75a,75b], J.P. Rutherfoord[7], S. Rutherford Colmenares[32], K. Rybacki[92], M. Rybar[134], E.B. Rye[126], A. Ryzhov[44], J.A. Sabater Iglesias[56], P. Sabatini[164], H.F-W. Sadrozinski[137], F. Safai Tehrani[75a], B. Safarzadeh Samani[135], S. Saha[1], M. Sahinsoy[111], A. Saibel[164], M. Saimpert[136], M. Saito[154], T. Saito[154], A. Sala[71a,71b], D. Salamani[36], A. Salnikov[144], J. Salt[164], A. Salvador Salas[152], D. Salvatore[43b,43a], F. Salvatore[147], A. Salzburger[36], D. Sammel[54], E. Sampson[92], D. Sampsonidis[153,e], D. Sampsonidou[124], J. Sánchez[164], V. Sanchez Sebastian[164], H. Sandaker[126], C.O. Sander[48], J.A. Sandesara[104], M. Sandhoff[172], C. Sandoval[22b], D.P.C. Sankey[135], T. Sano[88], A. Sansoni[53], L. Santi[75a,75b], C. Santoni[40], H. Santos[131a,131b], A. Santra[170], K.A. Saoucha[161], J.G. Saraiva[131a,131d], J. Sardain[7], O. Sasaki[84], K. Sato[158], C. Sauer[63b], F. Sauerburger[54], E. Sauvan[4], P. Savard[156,ae], R. Sawada[154], C. Sawyer[135], L. Sawyer[98], I. Sayago Galvan[164], C. Sbarra[23b], A. Sbrizzi[23b,23a], T. Scanlon[97], J. Schaarschmidt[139], U. Schäfer[101], A.C. Schaffer[66,44], D. Schaile[110], R.D. Schamberger[146], C. Scharf[18], M.M. Schefer[19], V.A. Schegelsky[37], D. Scheirich[134], F. Schenck[18], M. Schernau[160], C. Scheulen[55], C. Schiavi[57b,57a], M. Schioppa[43b,43a], B. Schlag[144,m], K.E. Schleicher[54], S. Schlenker[36], J. Schmeing[172], M.A. Schmidt[172], K. Schmieden[101], C. Schmitt[101], N. Schmitt[101], S. Schmitt[48], L. Schoeffel[136], A. Schoening[63b], P.G. Scholer[34], E. Schopf[127], M. Schott[101], J. Schovancova[36], S. Schramm[56], T. Schroer[56], H-C. Schultz-Coulon[63a], M. Schumacher[54], B.A. Schumm[137], Ph. Schune[136], A.J. Schuy[139], H.R. Schwartz[137], A. Schwartzman[144], T.A. Schwarz[107], Ph. Schwemling[136], R. Schwienhorst[108], A. Sciandra[137], G. Sciolla[26], F. Scuri[74a], C.D. Sebastiani[93],

JHEP08(2024)223

K. Sedlaczek[116], P. Seema[18], S.C. Seidel[113], A. Seiden[137], B.D. Seidlitz[41], C. Seitz[48], J.M. Seixas[83b], G. Sekhniaidze[72a], L. Selem[60], N. Semprini-Cesari[23b,23a], D. Sengupta[56], V. Senthilkumar[164], L. Serin[66], L. Serkin[69a,69b], M. Sessa[76a,76b], H. Severini[121], F. Sforza[57b,57a], A. Sfyrla[56], Q. Sha[14a], E. Shabalina[55], A.H. Shah[32], R. Shaheen[145], J.D. Shahinian[129], D. Shaked Renous[170], L.Y. Shan[14a], M. Shapiro[17a], A. Sharma[36], A.S. Sharma[165], P. Sharma[80], P.B. Shatalov[37], K. Shaw[147], S.M. Shaw[102], A. Shcherbakova[37], Q. Shen[62c,5], D.J. Sheppard[143], P. Sherwood[97], L. Shi[97], X. Shi[14a], C.O. Shimmin[173], J.D. Shinner[96], I.P.J. Shipsey[127], S. Shirabe[89], M. Shiyakova[38,u], J. Shlomi[170], M.J. Shochet[39], J. Shojaii[106], D.R. Shope[126], B. Shrestha[121], S. Shrestha[120,ah], E.M. Shrif[33g], M.J. Shroff[166], P. Sicho[132], A.M. Sickles[163], E. Sideras Haddad[33g], A.C. Sidley[115], A. Sidoti[23b], F. Siegert[50], Dj. Sijacki[15], F. Sili[91], J.M. Silva[52], M.V. Silva Oliveira[29], S.B. Silverstein[47a], S. Simion[66], R. Simoniello[36], E.L. Simpson[59], H. Simpson[147], L.R. Simpson[107], N.D. Simpson[99], S. Simsek[82], S. Sindhu[55], P. Sinervo[156], S. Singh[156], S. Sinha[48], S. Sinha[102], M. Sioli[23b,23a], I. Siral[36], E. Sitnikova[48], J. Sjölin[47a,47b], A. Skaf[55], E. Skorda[20], P. Skubic[121], M. Slawinska[87], V. Smakhtin[170], B.H. Smart[135], S.Yu. Smirnov[37], Y. Smirnov[37], L.N. Smirnova[37,a], O. Smirnova[99], A.C. Smith[41], E.A. Smith[39], H.A. Smith[127], J.L. Smith[102], R. Smith[144], M. Smizanska[92], K. Smolek[133], A.A. Snesarev[37], S.R. Snider[156], H.L. Snoek[115], S. Snyder[29], R. Sobie[166,w], A. Soffer[152], C.A. Solans Sanchez[36], E.Yu. Soldatov[37], U. Soldevila[164], A.A. Solodkov[37], S. Solomon[26], A. Soloshenko[38], K. Solovieva[54], O.V. Solovyanov[40], V. Solovyev[37], P. Sommer[36], A. Sonay[13], W.Y. Song[157b], A. Sopczak[133], A.L. Sopio[97], F. Sopkova[28b], J.D. Sorenson[113], I.R. Sotarriva Alvarez[155], V. Sothilingam[63a], O.J. Soto Sandoval[138c,138b], S. Sottocornola[68], R. Soualah[161], Z. Soumaimi[35e], D. South[48], N. Soybelman[170], S. Spagnolo[70a,70b], M. Spalla[111], D. Sperlich[54], T.M. Spieker[63a], G. Spigo[36], S. Spinali[92], D.P. Spiteri[59], M. Spousta[134], E.J. Staats[34], R. Stamen[63a], A. Stampekis[20], M. Standke[24], E. Stanecka[87], W. Stanek-Maslouska[48], M.V. Stange[50], B. Stanislaus[17a], M.M. Stanitzki[48], B. Stapf[48], E.A. Starchenko[37], G.H. Stark[137], J. Stark[90], P. Staroba[132], P. Starovoitov[63a], S. Stärz[105], R. Staszewski[87], G. Stavropoulos[46], J. Steentoft[162], P. Steinberg[29], B. Stelzer[143,157a], H.J. Stelzer[130], O. Stelzer-Chilton[157a], H. Stenzel[58], T.J. Stevenson[147], G.A. Stewart[36], J.R. Stewart[122], M.C. Stockton[36], G. Stoicea[27b], M. Stolarski[131a], S. Stonjek[111], A. Straessner[50], J. Strandberg[145], S. Strandberg[47a,47b], M. Stratmann[172], M. Strauss[121], T. Strebler[103], P. Strizenec[28b], R. Ströhmer[167], D.M. Strom[124], R. Stroynowski[44], A. Strubig[47a,47b], S.A. Stucci[29], B. Stugu[16], J. Stupak[121], N.A. Styles[48], D. Su[144], S. Su[62a], W. Su[62d], X. Su[62a], D. Suchy[28a], K. Sugizaki[154], V.V. Sulin[37], M.J. Sullivan[93], D.M.S. Sultan[127], L. Sultanaliyeva[37], S. Sultansoy[3b], T. Sumida[88], S. Sun[107], S. Sun[171], O. Sunneborn Gudnadottir[162], N. Sur[103], M.R. Sutton[147], H. Suzuki[158], M. Svatos[132], M. Swiatlowski[157a], T. Swirski[167], I. Sykora[28a], M. Sykora[134], T. Sykora[134], D. Ta[101], K. Tackmann[48,t], A. Taffard[160], R. Tafirout[157a], J.S. Tafoya Vargas[66], Y. Takubo[84], M. Talby[103], A.A. Talyshev[37], K.C. Tam[64b], N.M. Tamir[152], A. Tanaka[154], J. Tanaka[154], R. Tanaka[66], M. Tanasini[57b,57a], Z. Tao[165], S. Tapia Araya[138f], S. Tapprogge[101], A. Tarek Abouelfadl Mohamed[108], S. Tarem[151], K. Tariq[14a], G. Tarna[103,27b], G.F. Tartarelli[71a], P. Tas[134], M. Tasevsky[132], E. Tassi[43b,43a], A.C. Tate[163], G. Tateno[154],

Y. Tayalati[35e,v], G.N. Taylor[106], W. Taylor[157b], A.S. Tee[171], R. Teixeira De Lima[144], P. Teixeira-Dias[96], J.J. Teoh[156], K. Terashi[154], J. Terron[100], S. Terzo[13], M. Testa[53], R.J. Teuscher[156,w], A. Thaler[79], O. Theiner[56], N. Themistokleous[52], T. Theveneaux-Pelzer[103], O. Thielmann[172], D.W. Thomas[96], J.P. Thomas[20], E.A. Thompson[17a], P.D. Thompson[20], E. Thomson[129], R.E. Thornberry[44], Y. Tian[55], V. Tikhomirov[37,a], Yu.A. Tikhonov[37], S. Timoshenko[37], D. Timoshyn[134], E.X.L. Ting[1], P. Tipton[173], S.H. Tlou[33g], K. Todome[155], S. Todorova-Nova[134], S. Todt[50], M. Togawa[84], J. Tojo[89], S. Tokár[28a], K. Tokushuku[84], O. Toldaiev[68], R. Tombs[32], M. Tomoto[84,112], L. Tompkins[144,m], K.W. Topolnicki[86b], E. Torrence[124], H. Torres[90], E. Torró Pastor[164], M. Toscani[30], C. Tosciri[39], M. Tost[11], D.R. Tovey[140], A. Traeet[16], I.S. Trandafir[27b], T. Trefzger[167], A. Tricoli[29], I.M. Trigger[157a], S. Trincaz-Duvoid[128], D.A. Trischuk[26], B. Trocmé[60], L. Truong[33c], M. Trzebinski[87], A. Trzupek[87], F. Tsai[146], M. Tsai[107], A. Tsiamis[153,e], P.V. Tsiareshka[37], S. Tsigaridas[157a], A. Tsirigotis[153,r], V. Tsiskaridze[156], E.G. Tskhadadze[150a], M. Tsopoulou[153], Y. Tsujikawa[88], I.I. Tsukerman[37], V. Tsulaia[17a], S. Tsuno[84], K. Tsuri[119], D. Tsybychev[146], Y. Tu[64b], A. Tudorache[27b], V. Tudorache[27b], A.N. Tuna[61], S. Turchikhin[57b,57a], I. Turk Cakir[3a], R. Turra[71a], T. Turtuvshin[38,x], P.M. Tuts[41], S. Tzamarias[153,e], E. Tzovara[101], F. Ukegawa[158], P.A. Ulloa Poblete[138c,138b], E.N. Umaka[29], G. Unal[36], A. Undrus[29], G. Unel[160], J. Urban[28b], P. Urquijo[106], P. Urrejola[138a], G. Usai[8], R. Ushioda[155], M. Usman[109], Z. Uysal[82], V. Vacek[133], B. Vachon[105], K.O.H. Vadla[126], T. Vafeiadis[36], A. Vaitkus[97], C. Valderanis[110], E. Valdes Santurio[47a,47b], M. Valente[157a], S. Valentinetti[23b,23a], A. Valero[164], E. Valiente Moreno[164], A. Vallier[90], J.A. Valls Ferrer[164], D.R. Van Arneman[115], T.R. Van Daalen[139], A. Van Der Graaf[49], P. Van Gemmeren[6], M. Van Rijnbach[126], S. Van Stroud[97], I. Van Vulpen[115], P. Vana[134], M. Vanadia[76a,76b], W. Vandelli[36], E.R. Vandewall[122], D. Vannicola[152], L. Vannoli[53], R. Vari[75a], E.W. Varnes[7], C. Varni[17b], T. Varol[149], D. Varouchas[66], L. Varriale[164], K.E. Varvell[148], M.E. Vasile[27b], L. Vaslin[84], G.A. Vasquez[166], A. Vasyukov[38], R. Vavricka[101], F. Vazeille[40], T. Vazquez Schroeder[36], J. Veatch[31], V. Vecchio[102], M.J. Veen[104], I. Veliscek[29], L.M. Veloce[156], F. Veloso[131a,131c], S. Veneziano[75a], A. Ventura[70a,70b], S. Ventura Gonzalez[136], A. Verbytskyi[111], M. Verducci[74a,74b], C. Vergis[95], M. Verissimo De Araujo[83b], W. Verkerke[115], J.C. Vermeulen[115], C. Vernieri[144], M. Vessella[104], M.C. Vetterli[143,ae], A. Vgenopoulos[153,e], N. Viaux Maira[138f], T. Vickey[140], O.E. Vickey Boeriu[140], G.H.A. Viehhauser[127], L. Vigani[63b], M. Villa[23b,23a], M. Villaplana Perez[164], E.M. Villhauer[52], E. Vilucchi[53], M.G. Vincter[34], G.S. Virdee[20], A. Vishwakarma[52], A. Visibile[115], C. Vittori[36], I. Vivarelli[23b,23a], E. Voevodina[111], F. Vogel[110], J.C. Voigt[50], P. Vokac[133], Yu. Volkotrub[86b], J. Von Ahnen[48], E. Von Toerne[24], B. Vormwald[36], V. Vorobel[134], K. Vorobev[37], M. Vos[164], K. Voss[142], M. Vozak[115], L. Vozdecky[121], N. Vranjes[15], M. Vranjes Milosavljevic[15], M. Vreeswijk[115], N.K. Vu[62d,62c], R. Vuillermet[36], O. Vujinovic[101], I. Vukotic[39], S. Wada[158], C. Wagner[104], J.M. Wagner[17a], W. Wagner[172], S. Wahdan[172], H. Wahlberg[91], M. Wakida[112], J. Walder[135], R. Walker[110], W. Walkowiak[142], A. Wall[129], E.J. Wallin[99], T. Wamorkar[6], A.Z. Wang[137], C. Wang[101], C. Wang[11], H. Wang[17a], J. Wang[64c], R.-J. Wang[101], R. Wang[61], R. Wang[6], S.M. Wang[149], S. Wang[62b], T. Wang[62a], W.T. Wang[80], W. Wang[14a], X. Wang[14c], X. Wang[163], X. Wang[62c], Y. Wang[62d], Y. Wang[14c], Z. Wang[107], Z. Wang[62d,51,62c],

JHEP08(2024)223

Z. Wang[107], A. Warburton[105], R.J. Ward[20], N. Warrack[59], S. Waterhouse[96], A.T. Watson[20], H. Watson[59], M.F. Watson[20], E. Watton[59,135], G. Watts[139], B.M. Waugh[97], J.M. Webb[54], C. Weber[29], H.A. Weber[18], M.S. Weber[19], S.M. Weber[63a], C. Wei[62a], Y. Wei[127], A.R. Weidberg[127], E.J. Weik[118], J. Weingarten[49], M. Weirich[101], C. Weiser[54], C.J. Wells[48], T. Wenaus[29], B. Wendland[49], T. Wengler[36], N.S. Wenke[111], N. Wermes[24], M. Wessels[63a], A.M. Wharton[92], A.S. White[61], A. White[8], M.J. White[1], D. Whiteson[160], L. Wickremasinghe[125], W. Wiedenmann[171], M. Wielers[135], C. Wiglesworth[42], D.J. Wilbern[121], H.G. Wilkens[36], J.J.H. Wilkinson[32], D.M. Williams[41], H.H. Williams[129], S. Williams[32], S. Willocq[104], B.J. Wilson[102], P.J. Windischhofer[39], F.I. Winkel[30], F. Winklmeier[124], B.T. Winter[54], J.K. Winter[102], M. Wittgen[144], M. Wobisch[98], Z. Wolffs[115], J. Wollrath[160], M.W. Wolter[87], H. Wolters[131a,131c], M.C. Wong[137], E.L. Woodward[41], S.D. Worm[48], B.K. Wosiek[87], K.W. Woźniak[87], S. Wozniewski[55], K. Wraight[59], C. Wu[20], M. Wu[14d], M. Wu[114], S.L. Wu[171], X. Wu[56], Y. Wu[62a], Z. Wu[4], J. Wuerzinger[111,ac], T.R. Wyatt[102], B.M. Wynne[52], S. Xella[42], L. Xia[14c], M. Xia[14b], J. Xiang[64c], M. Xie[62a], X. Xie[62a], S. Xin[14a,14e], A. Xiong[124], J. Xiong[17a], D. Xu[14a], H. Xu[62a], L. Xu[62a], R. Xu[129], T. Xu[107], Y. Xu[14b], Z. Xu[52], Z. Xu[14c], B. Yabsley[148], S. Yacoob[33a], Y. Yamaguchi[155], E. Yamashita[154], H. Yamauchi[158], T. Yamazaki[17a], Y. Yamazaki[85], J. Yan[62c], S. Yan[59], Z. Yan[104], H.J. Yang[62c,62d], H.T. Yang[62a], S. Yang[62a], T. Yang[64c], X. Yang[36], X. Yang[14a], Y. Yang[44], Y. Yang[62a], Z. Yang[62a], W-M. Yao[17a], H. Ye[14c], H. Ye[55], J. Ye[14a], S. Ye[29], X. Ye[62a], Y. Yeh[97], I. Yeletskikh[38], B.K. Yeo[17b], M.R. Yexley[97], P. Yin[41], K. Yorita[169], S. Younas[27b], C.J.S. Young[36], C. Young[144], C. Yu[14a,14e], Y. Yu[62a], M. Yuan[107], R. Yuan[62d], L. Yue[97], M. Zaazoua[62a], B. Zabinski[87], E. Zaid[52], Z.K. Zak[87], T. Zakareishvili[164], N. Zakharchuk[34], S. Zambito[56], J.A. Zamora Saa[138d,138b], J. Zang[154], D. Zanzi[54], O. Zaplatilek[133], C. Zeitnitz[172], H. Zeng[14a], J.C. Zeng[163], D.T. Zenger Jr[26], O. Zenin[37], T. Ženiš[28a], S. Zenz[95], S. Zerradi[35a], D. Zerwas[66], M. Zhai[14a,14e], D.F. Zhang[140], J. Zhang[62b], J. Zhang[6], K. Zhang[14a,14e], L. Zhang[14c], P. Zhang[14a,14e], R. Zhang[171], S. Zhang[107], S. Zhang[44], T. Zhang[154], X. Zhang[62c], X. Zhang[62b], Y. Zhang[62c,5], Y. Zhang[97], Y. Zhang[14c], Z. Zhang[17a], Z. Zhang[66], H. Zhao[139], T. Zhao[62b], Y. Zhao[137], Z. Zhao[62a], Z. Zhao[62a], A. Zhemchugov[38], J. Zheng[14c], K. Zheng[163], X. Zheng[62a], Z. Zheng[144], D. Zhong[163], B. Zhou[107], H. Zhou[7], N. Zhou[62c], Y. Zhou[14c], Y. Zhou[7], C.G. Zhu[62b], J. Zhu[107], Y. Zhu[62c], Y. Zhu[62a], X. Zhuang[14a], K. Zhukov[37], N.I. Zimine[38], J. Zinsser[63b], M. Ziolkowski[142], L. Živković[15], A. Zoccoli[23b,23a], K. Zoch[61], T.G. Zorbas[140], O. Zormpa[46], W. Zou[41], L. Zwalinski[36]

[1] *Department of Physics, University of Adelaide, Adelaide, Australia*
[2] *Department of Physics, University of Alberta, Edmonton AB, Canada*
[3] [(a)] *Department of Physics, Ankara University, Ankara;* [(b)] *Division of Physics, TOBB University of Economics and Technology, Ankara, Türkiye*
[4] *LAPP, Université Savoie Mont Blanc, CNRS/IN2P3, Annecy, France*
[5] *APC, Université Paris Cité, CNRS/IN2P3, Paris, France*
[6] *High Energy Physics Division, Argonne National Laboratory, Argonne IL, United States of America*
[7] *Department of Physics, University of Arizona, Tucson AZ, United States of America*
[8] *Department of Physics, University of Texas at Arlington, Arlington TX, United States of America*
[9] *Physics Department, National and Kapodistrian University of Athens, Athens, Greece*
[10] *Physics Department, National Technical University of Athens, Zografou, Greece*

JHEP08(2024)223

[11] Department of Physics, University of Texas at Austin, Austin TX, United States of America
[12] Institute of Physics, Azerbaijan Academy of Sciences, Baku, Azerbaijan
[13] Institut de Física d'Altes Energies (IFAE), Barcelona Institute of Science and Technology, Barcelona, Spain
[14] [(a)] Institute of High Energy Physics, Chinese Academy of Sciences, Beijing; [(b)] Physics Department, Tsinghua University, Beijing; [(c)] Department of Physics, Nanjing University, Nanjing; [(d)] School of Science, Shenzhen Campus of Sun Yat-sen University; [(e)] University of Chinese Academy of Science (UCAS), Beijing, China
[15] Institute of Physics, University of Belgrade, Belgrade, Serbia
[16] Department for Physics and Technology, University of Bergen, Bergen, Norway
[17] [(a)] Physics Division, Lawrence Berkeley National Laboratory, Berkeley CA; [(b)] University of California, Berkeley CA, United States of America
[18] Institut für Physik, Humboldt Universität zu Berlin, Berlin, Germany
[19] Albert Einstein Center for Fundamental Physics and Laboratory for High Energy Physics, University of Bern, Bern, Switzerland
[20] School of Physics and Astronomy, University of Birmingham, Birmingham, United Kingdom
[21] [(a)] Department of Physics, Bogazici University, Istanbul; [(b)] Department of Physics Engineering, Gaziantep University, Gaziantep; [(c)] Department of Physics, Istanbul University, Istanbul, Türkiye
[22] [(a)] Facultad de Ciencias y Centro de Investigaciónes, Universidad Antonio Nariño, Bogotá; [(b)] Departamento de Física, Universidad Nacional de Colombia, Bogotá, Colombia
[23] [(a)] Dipartimento di Fisica e Astronomia A. Righi, Università di Bologna, Bologna; [(b)] INFN Sezione di Bologna, Italy
[24] Physikalisches Institut, Universität Bonn, Bonn, Germany
[25] Department of Physics, Boston University, Boston MA, United States of America
[26] Department of Physics, Brandeis University, Waltham MA, United States of America
[27] [(a)] Transilvania University of Brasov, Brasov; [(b)] Horia Hulubei National Institute of Physics and Nuclear Engineering, Bucharest; [(c)] Department of Physics, Alexandru Ioan Cuza University of Iasi, Iasi; [(d)] National Institute for Research and Development of Isotopic and Molecular Technologies, Physics Department, Cluj-Napoca; [(e)] National University of Science and Technology Politechnica, Bucharest; [(f)] West University in Timisoara, Timisoara; [(g)] Faculty of Physics, University of Bucharest, Bucharest, Romania
[28] [(a)] Faculty of Mathematics, Physics and Informatics, Comenius University, Bratislava; [(b)] Department of Subnuclear Physics, Institute of Experimental Physics of the Slovak Academy of Sciences, Kosice, Slovak Republic
[29] Physics Department, Brookhaven National Laboratory, Upton NY, United States of America
[30] Universidad de Buenos Aires, Facultad de Ciencias Exactas y Naturales, Departamento de Física, y CONICET, Instituto de Física de Buenos Aires (IFIBA), Buenos Aires, Argentina
[31] California State University, CA, United States of America
[32] Cavendish Laboratory, University of Cambridge, Cambridge, United Kingdom
[33] [(a)] Department of Physics, University of Cape Town, Cape Town; [(b)] iThemba Labs, Western Cape; [(c)] Department of Mechanical Engineering Science, University of Johannesburg, Johannesburg; [(d)] National Institute of Physics, University of the Philippines Diliman (Philippines); [(e)] University of South Africa, Department of Physics, Pretoria; [(f)] University of Zululand, KwaDlangezwa; [(g)] School of Physics, University of the Witwatersrand, Johannesburg, South Africa
[34] Department of Physics, Carleton University, Ottawa ON, Canada
[35] [(a)] Faculté des Sciences Ain Chock, Réseau Universitaire de Physique des Hautes Energies - Université Hassan II, Casablanca; [(b)] Faculté des Sciences, Université Ibn-Tofail, Kénitra; [(c)] Faculté des Sciences Semlalia, Université Cadi Ayyad, LPHEA-Marrakech; [(d)] LPMR, Faculté des Sciences, Université Mohamed Premier, Oujda; [(e)] Faculté des sciences, Université Mohammed V, Rabat; [(f)] Institute of Applied Physics, Mohammed VI Polytechnic University, Ben Guerir, Morocco
[36] CERN, Geneva, Switzerland
[37] Affiliated with an institute covered by a cooperation agreement with CERN
[38] Affiliated with an international laboratory covered by a cooperation agreement with CERN
[39] Enrico Fermi Institute, University of Chicago, Chicago IL, United States of America

JHEP08(2024)223

[40] *LPC, Université Clermont Auvergne, CNRS/IN2P3, Clermont-Ferrand, France*
[41] *Nevis Laboratory, Columbia University, Irvington NY, United States of America*
[42] *Niels Bohr Institute, University of Copenhagen, Copenhagen, Denmark*
[43] [(a)] *Dipartimento di Fisica, Università della Calabria, Rende;* [(b)] *INFN Gruppo Collegato di Cosenza, Laboratori Nazionali di Frascati, Italy*
[44] *Physics Department, Southern Methodist University, Dallas TX, United States of America*
[45] *Physics Department, University of Texas at Dallas, Richardson TX, United States of America*
[46] *National Centre for Scientific Research "Demokritos", Agia Paraskevi, Greece*
[47] [(a)] *Department of Physics, Stockholm University;* [(b)] *Oskar Klein Centre, Stockholm, Sweden*
[48] *Deutsches Elektronen-Synchrotron DESY, Hamburg and Zeuthen, Germany*
[49] *Fakultät Physik, Technische Universität Dortmund, Dortmund, Germany*
[50] *Institut für Kern- und Teilchenphysik, Technische Universität Dresden, Dresden, Germany*
[51] *Department of Physics, Duke University, Durham NC, United States of America*
[52] *SUPA - School of Physics and Astronomy, University of Edinburgh, Edinburgh, United Kingdom*
[53] *INFN e Laboratori Nazionali di Frascati, Frascati, Italy*
[54] *Physikalisches Institut, Albert-Ludwigs-Universität Freiburg, Freiburg, Germany*
[55] *II. Physikalisches Institut, Georg-August-Universität Göttingen, Göttingen, Germany*
[56] *Département de Physique Nucléaire et Corpusculaire, Université de Genève, Genève, Switzerland*
[57] [(a)] *Dipartimento di Fisica, Università di Genova, Genova;* [(b)] *INFN Sezione di Genova, Italy*
[58] *II. Physikalisches Institut, Justus-Liebig-Universität Giessen, Giessen, Germany*
[59] *SUPA - School of Physics and Astronomy, University of Glasgow, Glasgow, United Kingdom*
[60] *LPSC, Université Grenoble Alpes, CNRS/IN2P3, Grenoble INP, Grenoble, France*
[61] *Laboratory for Particle Physics and Cosmology, Harvard University, Cambridge MA, United States of America*
[62] [(a)] *Department of Modern Physics and State Key Laboratory of Particle Detection and Electronics, University of Science and Technology of China, Hefei;* [(b)] *Institute of Frontier and Interdisciplinary Science and Key Laboratory of Particle Physics and Particle Irradiation (MOE), Shandong University, Qingdao;* [(c)] *School of Physics and Astronomy, Shanghai Jiao Tong University, Key Laboratory for Particle Astrophysics and Cosmology (MOE), SKLPPC, Shanghai;* [(d)] *Tsung-Dao Lee Institute, Shanghai;* [(e)] *School of Physics and Microelectronics, Zhengzhou University, China*
[63] [(a)] *Kirchhoff-Institut für Physik, Ruprecht-Karls-Universität Heidelberg, Heidelberg;* [(b)] *Physikalisches Institut, Ruprecht-Karls-Universität Heidelberg, Heidelberg, Germany*
[64] [(a)] *Department of Physics, Chinese University of Hong Kong, Shatin, N.T., Hong Kong;* [(b)] *Department of Physics, University of Hong Kong, Hong Kong;* [(c)] *Department of Physics and Institute for Advanced Study, Hong Kong University of Science and Technology, Clear Water Bay, Kowloon, Hong Kong, China*
[65] *Department of Physics, National Tsing Hua University, Hsinchu, Taiwan*
[66] *IJCLab, Université Paris-Saclay, CNRS/IN2P3, 91405, Orsay, France*
[67] *Centro Nacional de Microelectrónica (IMB-CNM-CSIC), Barcelona, Spain*
[68] *Department of Physics, Indiana University, Bloomington IN, United States of America*
[69] [(a)] *INFN Gruppo Collegato di Udine, Sezione di Trieste, Udine;* [(b)] *ICTP, Trieste;* [(c)] *Dipartimento Politecnico di Ingegneria e Architettura, Università di Udine, Udine, Italy*
[70] [(a)] *INFN Sezione di Lecce;* [(b)] *Dipartimento di Matematica e Fisica, Università del Salento, Lecce, Italy*
[71] [(a)] *INFN Sezione di Milano;* [(b)] *Dipartimento di Fisica, Università di Milano, Milano, Italy*
[72] [(a)] *INFN Sezione di Napoli;* [(b)] *Dipartimento di Fisica, Università di Napoli, Napoli, Italy*
[73] [(a)] *INFN Sezione di Pavia;* [(b)] *Dipartimento di Fisica, Università di Pavia, Pavia, Italy*
[74] [(a)] *INFN Sezione di Pisa;* [(b)] *Dipartimento di Fisica E. Fermi, Università di Pisa, Pisa, Italy*
[75] [(a)] *INFN Sezione di Roma;* [(b)] *Dipartimento di Fisica, Sapienza Università di Roma, Roma, Italy*
[76] [(a)] *INFN Sezione di Roma Tor Vergata;* [(b)] *Dipartimento di Fisica, Università di Roma Tor Vergata, Roma, Italy*
[77] [(a)] *INFN Sezione di Roma Tre;* [(b)] *Dipartimento di Matematica e Fisica, Università Roma Tre, Roma, Italy*
[78] [(a)] *INFN-TIFPA;* [(b)] *Università degli Studi di Trento, Trento, Italy*
[79] *Universität Innsbruck, Department of Astro and Particle Physics, Innsbruck, Austria*
[80] *University of Iowa, Iowa City IA, United States of America*
[81] *Department of Physics and Astronomy, Iowa State University, Ames IA, United States of America*

JHEP08(2024)223

[82] Istinye University, Sariyer, Istanbul, Türkiye
[83] [(a)] Departamento de Engenharia Elétrica, Universidade Federal de Juiz de Fora (UFJF), Juiz de Fora; [(b)] Universidade Federal do Rio De Janeiro COPPE/EE/IF, Rio de Janeiro; [(c)] Instituto de Física, Universidade de São Paulo, São Paulo; [(d)] Rio de Janeiro State University, Rio de Janeiro; [(e)] Federal University of Bahia, Bahia, Brazil
[84] KEK, High Energy Accelerator Research Organization, Tsukuba, Japan
[85] Graduate School of Science, Kobe University, Kobe, Japan
[86] [(a)] AGH University of Krakow, Faculty of Physics and Applied Computer Science, Krakow; [(b)] Marian Smoluchowski Institute of Physics, Jagiellonian University, Krakow, Poland
[87] Institute of Nuclear Physics Polish Academy of Sciences, Krakow, Poland
[88] Faculty of Science, Kyoto University, Kyoto, Japan
[89] Research Center for Advanced Particle Physics and Department of Physics, Kyushu University, Fukuoka, Japan
[90] L2IT, Université de Toulouse, CNRS/IN2P3, UPS, Toulouse, France
[91] Instituto de Física La Plata, Universidad Nacional de La Plata and CONICET, La Plata, Argentina
[92] Physics Department, Lancaster University, Lancaster, United Kingdom
[93] Oliver Lodge Laboratory, University of Liverpool, Liverpool, United Kingdom
[94] Department of Experimental Particle Physics, Jožef Stefan Institute and Department of Physics, University of Ljubljana, Ljubljana, Slovenia
[95] School of Physics and Astronomy, Queen Mary University of London, London, United Kingdom
[96] Department of Physics, Royal Holloway University of London, Egham, United Kingdom
[97] Department of Physics and Astronomy, University College London, London, United Kingdom
[98] Louisiana Tech University, Ruston LA, United States of America
[99] Fysiska institutionen, Lunds universitet, Lund, Sweden
[100] Departamento de Física Teorica C-15 and CIAFF, Universidad Autónoma de Madrid, Madrid, Spain
[101] Institut für Physik, Universität Mainz, Mainz, Germany
[102] School of Physics and Astronomy, University of Manchester, Manchester, United Kingdom
[103] CPPM, Aix-Marseille Université, CNRS/IN2P3, Marseille, France
[104] Department of Physics, University of Massachusetts, Amherst MA, United States of America
[105] Department of Physics, McGill University, Montreal QC, Canada
[106] School of Physics, University of Melbourne, Victoria, Australia
[107] Department of Physics, University of Michigan, Ann Arbor MI, United States of America
[108] Department of Physics and Astronomy, Michigan State University, East Lansing MI, United States of America
[109] Group of Particle Physics, University of Montreal, Montreal QC, Canada
[110] Fakultät für Physik, Ludwig-Maximilians-Universität München, München, Germany
[111] Max-Planck-Institut für Physik (Werner-Heisenberg-Institut), München, Germany
[112] Graduate School of Science and Kobayashi-Maskawa Institute, Nagoya University, Nagoya, Japan
[113] Department of Physics and Astronomy, University of New Mexico, Albuquerque NM, United States of America
[114] Institute for Mathematics, Astrophysics and Particle Physics, Radboud University/Nikhef, Nijmegen, The Netherlands
[115] Nikhef National Institute for Subatomic Physics and University of Amsterdam, Amsterdam, The Netherlands
[116] Department of Physics, Northern Illinois University, DeKalb IL, United States of America
[117] [(a)] New York University Abu Dhabi, Abu Dhabi; [(b)] United Arab Emirates University, Al Ain, United Arab Emirates
[118] Department of Physics, New York University, New York NY, United States of America
[119] Ochanomizu University, Otsuka, Bunkyo-ku, Tokyo, Japan
[120] Ohio State University, Columbus OH, United States of America
[121] Homer L. Dodge Department of Physics and Astronomy, University of Oklahoma, Norman OK, United States of America
[122] Department of Physics, Oklahoma State University, Stillwater OK, United States of America
[123] Palacký University, Joint Laboratory of Optics, Olomouc, Czech Republic

JHEP08(2024)223

[124] *Institute for Fundamental Science, University of Oregon, Eugene, OR, United States of America*
[125] *Graduate School of Science, Osaka University, Osaka, Japan*
[126] *Department of Physics, University of Oslo, Oslo, Norway*
[127] *Department of Physics, Oxford University, Oxford, United Kingdom*
[128] *LPNHE, Sorbonne Université, Université Paris Cité, CNRS/IN2P3, Paris, France*
[129] *Department of Physics, University of Pennsylvania, Philadelphia PA, United States of America*
[130] *Department of Physics and Astronomy, University of Pittsburgh, Pittsburgh PA, United States of America*
[131] [(a)] *Laboratório de Instrumentação e Física Experimental de Partículas - LIP, Lisboa;* [(b)] *Departamento de Física, Faculdade de Ciências, Universidade de Lisboa, Lisboa;* [(c)] *Departamento de Física, Universidade de Coimbra, Coimbra;* [(d)] *Centro de Física Nuclear da Universidade de Lisboa, Lisboa;* [(e)] *Departamento de Física, Universidade do Minho, Braga;* [(f)] *Departamento de Física Teórica y del Cosmos, Universidad de Granada, Granada (Spain);* [(g)] *Departamento de Física, Instituto Superior Técnico, Universidade de Lisboa, Lisboa, Portugal*
[132] *Institute of Physics of the Czech Academy of Sciences, Prague, Czech Republic*
[133] *Czech Technical University in Prague, Prague, Czech Republic*
[134] *Charles University, Faculty of Mathematics and Physics, Prague, Czech Republic*
[135] *Particle Physics Department, Rutherford Appleton Laboratory, Didcot, United Kingdom*
[136] *IRFU, CEA, Université Paris-Saclay, Gif-sur-Yvette, France*
[137] *Santa Cruz Institute for Particle Physics, University of California Santa Cruz, Santa Cruz CA, United States of America*
[138] [(a)] *Departamento de Física, Pontificia Universidad Católica de Chile, Santiago;* [(b)] *Millennium Institute for Subatomic physics at high energy frontier (SAPHIR), Santiago;* [(c)] *Instituto de Investigación Multidisciplinario en Ciencia y Tecnología, y Departamento de Física, Universidad de La Serena;* [(d)] *Universidad Andres Bello, Department of Physics, Santiago;* [(e)] *Instituto de Alta Investigación, Universidad de Tarapacá, Arica;* [(f)] *Departamento de Física, Universidad Técnica Federico Santa María, Valparaíso, Chile*
[139] *Department of Physics, University of Washington, Seattle WA, United States of America*
[140] *Department of Physics and Astronomy, University of Sheffield, Sheffield, United Kingdom*
[141] *Department of Physics, Shinshu University, Nagano, Japan*
[142] *Department Physik, Universität Siegen, Siegen, Germany*
[143] *Department of Physics, Simon Fraser University, Burnaby BC, Canada*
[144] *SLAC National Accelerator Laboratory, Stanford CA, United States of America*
[145] *Department of Physics, Royal Institute of Technology, Stockholm, Sweden*
[146] *Departments of Physics and Astronomy, Stony Brook University, Stony Brook NY, United States of America*
[147] *Department of Physics and Astronomy, University of Sussex, Brighton, United Kingdom*
[148] *School of Physics, University of Sydney, Sydney, Australia*
[149] *Institute of Physics, Academia Sinica, Taipei, Taiwan*
[150] [(a)] *E. Andronikashvili Institute of Physics, Iv. Javakhishvili Tbilisi State University, Tbilisi;* [(b)] *High Energy Physics Institute, Tbilisi State University, Tbilisi;* [(c)] *University of Georgia, Tbilisi, Georgia*
[151] *Department of Physics, Technion, Israel Institute of Technology, Haifa, Israel*
[152] *Raymond and Beverly Sackler School of Physics and Astronomy, Tel Aviv University, Tel Aviv, Israel*
[153] *Department of Physics, Aristotle University of Thessaloniki, Thessaloniki, Greece*
[154] *International Center for Elementary Particle Physics and Department of Physics, University of Tokyo, Tokyo, Japan*
[155] *Department of Physics, Tokyo Institute of Technology, Tokyo, Japan*
[156] *Department of Physics, University of Toronto, Toronto ON, Canada*
[157] [(a)] *TRIUMF, Vancouver BC;* [(b)] *Department of Physics and Astronomy, York University, Toronto ON, Canada*
[158] *Division of Physics and Tomonaga Center for the History of the Universe, Faculty of Pure and Applied Sciences, University of Tsukuba, Tsukuba, Japan*
[159] *Department of Physics and Astronomy, Tufts University, Medford MA, United States of America*
[160] *Department of Physics and Astronomy, University of California Irvine, Irvine CA, United States of America*

JHEP08(2024)223

[161] University of Sharjah, Sharjah, United Arab Emirates
[162] Department of Physics and Astronomy, University of Uppsala, Uppsala, Sweden
[163] Department of Physics, University of Illinois, Urbana IL, United States of America
[164] Instituto de Física Corpuscular (IFIC), Centro Mixto Universidad de Valencia - CSIC, Valencia, Spain
[165] Department of Physics, University of British Columbia, Vancouver BC, Canada
[166] Department of Physics and Astronomy, University of Victoria, Victoria BC, Canada
[167] Fakultät für Physik und Astronomie, Julius-Maximilians-Universität Würzburg, Würzburg, Germany
[168] Department of Physics, University of Warwick, Coventry, United Kingdom
[169] Waseda University, Tokyo, Japan
[170] Department of Particle Physics and Astrophysics, Weizmann Institute of Science, Rehovot, Israel
[171] Department of Physics, University of Wisconsin, Madison WI, United States of America
[172] Fakultät für Mathematik und Naturwissenschaften, Fachgruppe Physik, Bergische Universität Wuppertal, Wuppertal, Germany
[173] Department of Physics, Yale University, New Haven CT, United States of America

[a] Also Affiliated with an institute covered by a cooperation agreement with CERN
[b] Also at An-Najah National University, Nablus, Palestine
[c] Also at Borough of Manhattan Community College, City University of New York, New York NY, United States of America
[d] Also at Center for High Energy Physics, Peking University, China
[e] Also at Center for Interdisciplinary Research and Innovation (CIRI-AUTH), Thessaloniki, Greece
[f] Also at Centro Studi e Ricerche Enrico Fermi, Italy
[g] Also at CERN, Geneva, Switzerland
[h] Also at Département de Physique Nucléaire et Corpusculaire, Université de Genève, Genève, Switzerland
[i] Also at Departament de Fisica de la Universitat Autonoma de Barcelona, Barcelona, Spain
[j] Also at Department of Financial and Management Engineering, University of the Aegean, Chios, Greece
[k] Also at Department of Physics, California State University, Sacramento, United States of America
[l] Also at Department of Physics, King's College London, London, United Kingdom
[m] Also at Department of Physics, Stanford University, Stanford CA, United States of America
[n] Also at Department of Physics, Stellenbosch University, South Africa
[o] Also at Department of Physics, University of Fribourg, Fribourg, Switzerland
[p] Also at Department of Physics, University of Thessaly, Greece
[q] Also at Department of Physics, Westmont College, Santa Barbara, United States of America
[r] Also at Hellenic Open University, Patras, Greece
[s] Also at Institucio Catalana de Recerca i Estudis Avancats, ICREA, Barcelona, Spain
[t] Also at Institut für Experimentalphysik, Universität Hamburg, Hamburg, Germany
[u] Also at Institute for Nuclear Research and Nuclear Energy (INRNE) of the Bulgarian Academy of Sciences, Sofia, Bulgaria
[v] Also at Institute of Applied Physics, Mohammed VI Polytechnic University, Ben Guerir, Morocco
[w] Also at Institute of Particle Physics (IPP), Canada
[x] Also at Institute of Physics and Technology, Mongolian Academy of Sciences, Ulaanbaatar, Mongolia
[y] Also at Institute of Physics, Azerbaijan Academy of Sciences, Baku, Azerbaijan
[z] Also at Institute of Theoretical Physics, Ilia State University, Tbilisi, Georgia
[aa] Also at Lawrence Livermore National Laboratory, Livermore, United States of America
[ab] Also at National Institute of Physics, University of the Philippines Diliman (Philippines), Philippines
[ac] Also at Technical University of Munich, Munich, Germany
[ad] Also at The Collaborative Innovation Center of Quantum Matter (CICQM), Beijing, China
[ae] Also at TRIUMF, Vancouver BC, Canada
[af] Also at Università di Napoli Parthenope, Napoli, Italy
[ag] Also at University of Colorado Boulder, Department of Physics, Colorado, United States of America
[ah] Also at Washington College, Chestertown, MD, United States of America
[ai] Also at Yeditepe University, Physics Department, Istanbul, Türkiye
[*] Deceased

JHEP08(2024)223